ADVANCED ARRAY PROCESSING IN THE PRESENCE OF COMPLICATED SPATIO-TEMPORAL SOURCES

By

ABOULNASR HASSANIEN, B.Sc., M.Sc.

2005

A Thesis

Submitted to the Department of Electrical & Computer Engineering

and the School of Graduate Studies

in Partial Fulfilment of the Requirements

for the Degree of

Doctor of Philosophy

McMaster University

ADVANCED ARRAY PROCESSING IN THE PRESENCE OF COMPLICATED SPATIO-TEMPORAL SOURCES

DOCTOR OF PHILOSOPHY (2005) McMaster University

(Electrical & Computer Engineering) Hamilton, Ontario

TITLE:	Advanced Array Processing in the Presence of Complicated Spatio-Temporal Sources
AUTHOR:	Aboulnasr Hassanien B.Sc. (Communications and Electronics Engineering), M.Sc. (Communications Engineering) Assiut University, Assiut, Egypt
SUPERVISOR:	Alex B. Gershman, Professor
NUMBER OF PAGES:	xvii, 140

Dedications

To the soul of my father,

and to

my mother, my wife Mona,

and my children Basel and Hadeel.

Abstract

Array processing has been successfully applied in many areas such as radar, sonar and wireless communications. Most conventional array processing techniques are based on idealistic assumptions that are not valid in many practical situations. This thesis contributes to the development of novel array processing techniques for direction finding and parameter estimation in the presence of complicated spatio-temporal sources.

We address the problem of estimating the Directions-Of-Arrival (DOAs) of weak desired sources observed in the background of strong interference. We develop a new approach to beamspace preprocessing with improved robustness against out-of-sector interfering sources. Our techniques design the beamspace matrix filter based on proper tradeoffs between the in-sector (passband) source distortion and out-of-sector (stopband) source attenuation. We also introduce the novel concept of adaptive beamspace preprocessing that offers a significant improvement in the DOA estimation performance. Computationally efficient convex formulations for these beamspace matrix filter design problems are derived using second-order cone (SOC) programming.

We also develop a generalized Capon spatial spectrum estimator for localizing multiple incoherently distributed sources in sensor arrays. The proposed generalized Capon technique estimates the source central angles and angular spreads by means of a two-dimensional spectral search. The proposed method has a substantially improved

performance compared to several popular spread source localization techniques.

A new search-free ESPRIT-type algorithm for estimating the DOAs of multiple chirp signals using Spatial Time-Frequency Distributions (STFDs) is developed. An averaged STFD matrix (or multiple averaged STFD matrices) is used instead of the covariance matrix to estimate the signal and noise subspaces. The proposed algorithm is shown to provide significant performance improvement over the traditional ESPRIT algorithm for FM sources, specifically in situations with closely-spaced sources and low Signal-to-Noise Ratios (SNRs).

We also develop a new algorithm for estimating the parameters of multiple wideband polynomial-phase signals (PPSs) using sensor arrays. Our approach is based on extending the high-order instantaneous moment (HIM) concept by introducing a new nonlinear transformation called the spatial high-order instantaneous moment (SHIM). We apply this transformation to multiple wideband PPSs and employ the resulting SHIM to provide recursive estimates of the PPSs parameters. The data received at each sensor yields a different estimate of each frequency coefficient. Employing the multiple estimates simultaneously, the proposed algorithm removes the outliers and obtains a better final estimate. STFD-based methods are used in conjunction with the SHIM to estimate the DOAs of the observed signals. The proposed algorithm is shown to have an improved performance compared to the well-known chirp beamformer approach [31]. Furthermore, our algorithm is computationally more attractive as it requires multiple one-dimensional searches instead of a multi-dimensional search.

Acknowledgements

I would like to thank my supervisor, Prof. A. B. Gershman, for his continuous advice, encouragement and support on academic and non-academic matters. His enthusiasm, approachability and patience were essential to the completion of this dissertation. I am grateful to Prof. K. M. Wong for his insightful comments and for his valuable advice and suggestions. In addition, I would like to thank my supervisory committee members, Prof. N. Balakrishnan and Prof. T. Kirubarajan, for their precious comments and suggestions and for being helpful.

I would like to acknowledge Dr. S. Shahbazpanahi for his cooperation and contributive comments. In addition, I would like to thank Dr. M. Bakr and Mr. Amr ElKeyi for proof reading this thesis and for their useful comments. Moreover, I would like to give thanks to all my colleagues at McMaster University who have contributed greatly to provide a supportive and exciting research atmosphere. The assistance from other members and staff at the ECE Department at McMaster is also appreciated.

I would like to sincerely thank my parents and siblings for their endless support and continuous encouragement throughout my life. I am greatly indebted to my wife, Mona Zedan, for her support, understanding and patience. I would like to praise my son Basel and my daughter Hadeel; surely they have been a great source of energy.

I would like to acknowledge the "Department of Missions of the Egyptian Ministry

of Higher Education" for the financial support. I am greatly obligated to the "Bureau of Cultural and Educational Affairs of Egypt in Canada" for being supportive and conscientious. Finally, I would like to dedicate sincere feelings of devotion to my wonderful home country: Egypt — I really owe you a lot.

List of Acronyms

CBF	Chirp Beamformer
CD	Coherently Distributed
CRB	Cramér–Rao Bound
DML	Deterministic Maximum Likelihood
DOA	Direction–Of–Arrival
DPSS	Discrete Prolate Spheroidal Sequences
DPT	Discrete Polynomial–phase Transform
FIM	Fisher Information Matrix
FM	Frequency–Modulated
GC	Generalized Capon
HAF	High–order Ambiguity Function
HIM	High–order Instantaneous Moment
ID	Incoherently Distributed
INR	Interference–to–Noise Ratio
ISAR	Inverse Synthetis Aperture Radar
ISAS	Inverse Synthetis Aperture Sonar
LS	Least Square
ML	Maximum Likelihood
MVDR	Minimum Variance Distorionless

MUSIC	**MU**ltiple **SI**gnal **C**lassification
ODR	Optimal Dimension Reduction
pdf	Probability Density Function
PHAF	Product High−order Ambiguity Function
PPS	Polynomial−Phase Signal
RMSE	Root−Mean−Square Error
SML	Stochastic Maximum Likelihood
SAR	Synthetic Aperture Radar
SAS	Synthetic Aperture Sonar
SDS	Spatially Distributed Source
SHIM	Spatial High−order Instantaneous Moment
SNR	Signal−to−Noise Ratio
SOC	Second−Order Cone
SPWVD	Spatial Pseudo−Wigner−Ville Distribution
STFD	Spatial Time−Frequency Distribution
TLS	Total Least Square
ULA	Uniform Linear Array

List of Notations

Boldface lowercase letters are used to denote column vectors.

Boldface uppercase letters are used to denote matrices.

$(\cdot)^*$	the conjugate operator
$(\cdot)^T$	the transpose of a vector or a matrix
$(\cdot)^H$	the Hermitian transpose of a vector or a matrix
$(\cdot)^{-1}$	the inversion of a matrix
$(\cdot)^\dagger$	the pseudo inverse of a matrix
$(\cdot)_i$	the ith element of a vector
$[\cdot]_{ij}$	the ijth element of a matrix
$\lvert\cdot\rvert$	the determinant of a matrix
$\lVert\cdot\rVert$	the Euclidean norm of a vector
$\lVert\cdot\rVert_{\mathrm{F}}$	the Frobenius norm of a matrix
$\mathrm{E}\{\cdot\}$	the statistical expectation operator
$L\{\cdot\}$	the log−likelihood function
$\mathcal{N}(\cdot)$	the normal distribution
$\odot$	the Schur−Hadamard (elementwise) product of two matrices
$\otimes$	the Kronecker matrix product
M	the number of sensors
L	the number of source signals
N_s	the number of snapshots

$\mathbf{r}_s$	the position vector that describes the location of an emitting source
$\mathbf{r}_m$	the position vector that describes the location of the mth sensor
h_m	the spacing between the first and mth sensors
$\mathbf{u}$	the unit vector that describes the direction of wave propagation
τ_m	the time required for an incident wave to travel from the reference point to the mth sensor
θ_l	the DOA of the lth signal
$\mathbf{a}(\theta)$	the array steering vector
σ_s^2	the signal power
σ_n^2	the noise power
$\mathbf{I}$	the identity matrix
$\mathbf{A}$	the direction matrix
$\mathbf{R_x}$	the true convariance matrix
$\hat{\mathbf{R}}_\mathbf{x}$	the sample convariance matrix
$P_\mathbf{A}$	the projection matrix onto the space spanned by $\mathbf{A}$
$P_\mathbf{A}^\perp$	the projection matrix onto the nullspace of $\mathbf{A}$
$\text{diag}\{\mathbf{a}\}$	the diagonal matrix with the ith diagonal element $\mathbf{a}_i$
$\text{tr}\{\cdot\}$	the trace of a square matrix
$\text{vec}\{\cdot\}$	the vectorization operator stacking the columns of a matrix on top of each other
$\sigma_{\max}\{\cdot\}$	the maximal eigenvalue of a matrix
$\mathbf{B}$	the beamspace matrix
Θ	a continuum of all in−sector directions
$\bar{\Theta}$	a continuum of all out−of−sector directions
$\tilde{\mathbf{a}}(\theta)$	the array steering vector after beamspace transformation

Contents

List of Figures

Chapter 1

Introduction

"As far as the laws of mathematics refer to reality, they are not certain; and as far as they are certain, they do not refer to reality."

–Albert Einstein

The focus of this thesis is the development of advanced array processing algorithms for parameter estimation of complicated spatio-temporal sources. Sources with complicated spatio-temporal characteristics are frequently encountered in many practical situations. Modern array processing techniques are based on exploiting presumed array signal models. However, as far as the array signal models refer to practical situations, they are not certain, i.e., they do not exactly describe the actual characteristics of signal environments. The theme of this thesis is to approach the parameter estimation problem by considering more accurate signal models that best describe the characteristics of complicated spatio-temporal sources. Then, novel ideas and elegant manipulations that fully exploit the underlying signal model are used to solve that problem.

In this chapter, we give a brief introduction to the array signal processing topic

and highlight some of its applications. We also give an overview of the motivations and aims of the thesis. At the end of the chapter, we provide an outline of the thesis and point to our main contributions.

1.1 Array Signal Processing

Array signal processing finds applications in many different areas such as radar, sonar, wireless communications, tomography, seismology, radio astronomy and medical diagnosis. Historically, antenna arrays were first used in the radar area in the 1940s. Sensor array signal processing has received significant interest in the literature and has been the subject of numerous research papers and books (see [36], [45], [50], [99] and references therein). In what follows we briefly describe some of the array signal processing applications.

Radar

Antenna arrays are widely used in many radar systems such as airborne radars and air traffic control radars. They are also used in surface wave radars that can be used for low angle tracking [1], [25], [89], [106]. The use of adaptive arrays in airborne moving target indication (MTI) radars has been reported in [17]. Radar systems can either be active or passive [99]. In active radar systems, antenna arrays are used to transmit electromagnetic energy and to listen for the echo of the transmitted signal. When the radar works in passive mode, antenna arrays are used to receive the energy radiated by other sources. The signals captured by the antenna array enable the estimation of the spatial and temporal characteristics of the observed signal field. For example, the received data can be used for estimating parameters such as velocity, range and Directions-Of-Arrival (DOAs) of targets of interest. Antenna arrays are also used in

radars for interference/jamming cancellation and ground clutter suppression [50].

Sonar

The use of antenna arrays in sonar systems goes back to World War I when a towed/hull array sonar system was devised [55]. Similar to radar systems, sonar systems also work in one of two modes of operation; active or passive. In active sonar applications, arrays of hydrophones are used to transmit acoustic energy into the water and to listen for the returns. A major difference between active radar and active sonar is that the propagation of acoustic energy in the water is much more complicated than the propagation of electromagnetic waves in the atmosphere [99]. Due to complicated propagation characteristics, designing a sonar system may require more complex signal modeling [50]. On the other hand, passive sonar systems listen to incoming acoustic energy transmitted by other sources. The acoustic energy received by the sonar system can be used for estimating parameters such as range, bearings, and velocity of targets and for detecting and locating distant sources [97]. For example, Matched-field processing techniques typically exploit acoustic propagation models to perform range-depth localization (see [5], [51], [101] and references therein). The application of hydrophone array-based sonar to real data has been successfully reported in [32], [51], [61], and [84].

Wireless Communications

Antenna arrays are widely used in many communication systems, e.g., satellite communications [48], [56]. In this kind of communications, the antenna array can be used in either the earth terminal or onboard the satellite. This allows the satellite not only to communicate with the base station on earth, but also to communicate with

other satellites. This satellite-to-satellite communications is commonly referred to as inter-satellite communications. Inter-satellite communications are expected to play an important role in mobile communications, particularly with the use of low-orbit satellites [35], [48]. The relative positions between these low-orbit satellites change quickly. Hence, antenna arrays can be used to track the satellite of interest as well as to reject any interference that might arise due to the transmission of other satellites.

Another application that has received growing interest is the use of antenna arrays in mobile communication systems. The advantages of using antenna arrays in mobile communications include increasing the channel capacity, i.e., increasing the maximum data rate that can be reliably transferred between the mobile and the base station [35], [104]. In addition, the use of antenna arrays in mobile communications offers the ability to extend the range of coverage, combat fading and provide more robustness against co-channel interference [35], [79]. Antenna arrays are capable of reducing co-channel interference by focusing a beam in the direction of the desired signal [22]. However, reducing co-channel interference using this technique requires prior knowledge about the signals DOAs. When the DOAs are not known, they have to be estimated which motivates doing more research on this topic.

1.2 Overview of the Thesis

1.2.1 Motivations and Aims of the Thesis

Most conventional parameter estimation and direction finding techniques are based on one or more of the following assumptions [50], [62]

1. The signal and noise processes are stationary over the observation interval and are uncorrelated to each other.

2. The emitter is a point source which means that the source energy is concentrated at a distinct discrete angle.

3. The received signals are narrowband.

However, when applied to practical problems, these techniques may suffer from severe degradation in performance because of their high sensitivity to mismatches between the presumed assumptions and the actual characteristics of the environments and/or the sources. In this section, we will touch on three complicated spatio-temporal scenarios that are frequently encountered in practical situations. In subsequent chapters we will address the parameter estimation problem in the presence of these non-ideal environments.

Sources with Substantially Different Powers

In sensor arrays, interfering sources may take different forms and have widely varying impacts. Jamming is a typical interfering example that takes the form of high power transmission that might result in impairing the receiving system, e.g., in radar. Intentional jamming may be used to disrupt a guidance system, e.g., a guided missile, via obscuring the display of potential sources of interest at the front end of the receiving system.

On the other hand, friendly interfering signals can be used to protect certain targets from being located and tracked. This can be done by emitting false signals that make the receiver of the tracker take ineffective measures. Interfering problems can also arise in civilian applications. For instance, localized radiation sources may interfere with commercial aviation and landing systems.

For decades, the problem of DOA estimation of weak desired sources in the presence of severe interfernce/jamming has received much interest. It is known that the

performance of conventional array processing techniques degrades in the case of a mixture of high signal-to-noise ratio (SNR) and low SNR signals [99]. Hence, new efficient algorithms that can handle this case, in particular the case of weak signal sources observed in the background of strong interference, are of great interest.

Polynomial-Phase Signals

Polynomial-phase signals (PPSs) arise in many practical applications such as radar, sonar and wireless communications. For example, in communication systems that use continuous-phase modulation, the phase can be modeled as a finite-order polynomial within a finite duration in time [81]. Furthermore, frequency-modulated (FM) signals are intentionally transmitted in synthetic aperture radar (SAR), synthetic aperture sonar (SAS), Doppler radar and sonar imaging and mobile communications. PPSs can also arise as a result of the relative radar-target motion or the relative transmitter-receiver motion.

Much interest has been given to the problem of estimating the parameters of PPSs impinging on a sensor array (see for example [31] and references therein). PPSs are nonstationary signals and most of the time they can not be modeled as narrowband signals. Therefore, traditional array processing techniques can not efficiently handle the parameter estimation problem in this case. However, the rich structure of the PPS model can be exploited in developing new algorithms that can efficiently deal with the PPS parameter estimation problem.

Spatially Dispersed Signals

In practice, the source signal may be transmitted through a reflective medium. If this medium is dispersive, it can cause the reflected wave to be scattered in space. In wireless communication systems, for the information-bearing signals to reach physically distant receivers, the ionosphere is typically used as a reflector for the sky electromagnetic wave. However, due to the nonuniformity of the ionosphere, the travelling wave reaches the receiving array as a spatially distributed source.

Spatially distributed sources can also arise as a result of multipath propagation. Multipath propagation phenomena are very typical in practical applications such as radar, sonar and wireless communications. For example, in the case of a radar performing low angle tracking, the multipath propagation caused by the reflection from a rough sea surface usually results in a distributed source [63]. Distributed sources are also common in mobile communications, particularly in urban areas [68], [69] and in audio signals propagating in a reverberant room [62].

The problem of estimating the parameters of spatially distributed sources has received considerable attention in the literature; see for example [21], [49] and [54]. More efficient algorithms that can handle this problem are still of great demand.

1.2.2 Thesis Outline

In this thesis, we address the topic of direction finding and parameter estimation in complicated environments using sensor arrays. We develop advanced array processing algorithms for estimating the spatial and temporal characteristics of complicated spatio-temporal sources. The main body of the thesis consists of Chapters 3 through to 6. In each of these chapters we address one of the complicated spatio-temporal scenarios given in Section 1.2.1 and develop an approach that properly addresses

the parameter estimation problem in that scenario. In what follows, we give a brief overview of our work. Detailed definitions and background are given in individual chapters as appropriate.

In Chapter 2, we give a brief overview of conventional array processing and parameter estimation techniques. We briefly describe the array signal model that has been widely used in the array signal processing area over the last few decades. We also present a concise description of several optimal and suboptimal estimation techniques that have been widely used in array processing. At the end of the chapter, we present the Cramér-Rao Bound (CRB) which provides a lower bound on the performance of any unbiased estimator, i.e., it provides a baseline standard that can be used to assess the performance of suboptimal estimation techniques.

In Chapter 3, we address the DOA estimation problem in the presence of sources with substantially different powers where the general locations of the sources-of-interest are assumed to be located within a certain sector. We propose a novel approach to beamspace preprocessing with application to DOA estimation that offers improved robustness against out-of-sector sources. The beamspace matrix is designed as a matrix filter that satisfies a certain tradeoff between the in-sector (passband) and out-of-sector (stopband) requirements. Furthermore, the novel concept of *adaptive beamspace* preprocessing is introduced which extends the beamspace formulations by assuming that the beamspace matrix can be driven by the array data. Computationally efficient convex formulations for these problems are derived using second-order cone (SOC) programming. Simulation results are presented that illustrate the robustness of our techniques compared to traditional beamspace techniques.

In Chapter 4, we develop an algorithm for localizing multiple incoherently distributed (ID) sources[1]. The popular Capon spectral estimator is generalized to the

[1]For more information on ID sources see [85], [86] and [98].

case of multiple ID sources without imposing any approximation on the covariance matrix of the received data. The proposed generalized Capon technique estimates the central angles and the angular spreads by means of a two-dimensional parameter search. Simulation results are given, showing that the proposed method has a substantially improved performance compared to several popular spread source localization methods.

Chapter 5 presents a new time-frequency ESPRIT-type algorithm for DOA estimation of multiple narrowband chirp signals. Improved estimates of the signal and noise subspaces are obtained by using an averaged spatial time-frequency distribution (STFD) matrix (or multiple averaged STFD matrices) in lieu of the covariance matrix used in the conventional ESPRIT algorithm. The presented method enables separating the signals in different averaged STFD matrices prior to DOA estimation and, therefore, makes it possible to estimate the source DOAs in the case when the number of array sensors is less than the number of sources. Simulation results are used to validate the effectiveness of the proposed technique. It is shown that significant performance gains can be achieved by the proposed algorithm compared to the conventional ESPRIT technique.

Chapter 6 addresses the problem of parameter estimation of multiple wideband PPSs in sensor arrays. A nonlinear transformation called the spatial high-order instantaneous moment (SHIM) is introduced. The SHIM is used to transform the wideband PPSs data snapshots into a new set of snapshots, which have a rich structure that is easy to deal with. The SHIM is employed to provide estimates of the PPSs frequency parameters. The estimation process is done in a recursive manner starting with the highest order coefficients. STFD-based techniques and the SHIM are used jointly to provide estimates of the DOAs. The proposed technique is computationally attractive as it requires multiple one-dimensional searches instead of a

multi-dimensional search to estimate the required parameters. Simulation results are provided to validate the effectiveness of the proposed algorithm.

In Chapter 7, we draw some conclusions and point to possible extensions for future research work.

1.2.3 Contributions and Related Publications

The author has contributed substantially to the following original developments presented in this thesis:

1. A new approach to beamspace preprocessing with improved robustness against out-of-sector sources.

2. A generalized Capon spatial spectrum estimator for localization of multiple ID sources.

3. A new time-frequency ESPRIT-type algorithm for DOA estimation of multiple narrowband chirp signals.

4. A computationally efficient subspace-based approach for estimating the parameters of multiple wideband PPSs.

The contents of Chapter 3 have been published in the *IEEE Transactions on Signal Processing* [41]. An earlier exposition of some parts of Chapter 3 was also presented at the *IEEE Sensor Array and Multichannel Signal Processing Workshop (SAM'04)* [40]. The contents of Chapter 4 have been published in the *IEEE Transactions on Signal Processing* [44]. The contents of Chapter 5 have been presented at the *IEEE Sensor Array and Multichannel Signal Processing Workshop (SAM'02)* [43]. The contents of Chapter 6 have been summarized in [42] and will be submitted for journal publication.

Chapter 2

Conventional Array Processing and Parameter Estimation Techniques

2.1 Introduction

Sensor arrays have been widely used to solve the direction finding problem. In fact, array processing is mainly understood as direction finding. The most notable application of direction finding is source localization in radar and sonar. Emitting sources can be localized by finding their DOAs using two separate arrays followed by finding the intersection for the two lines of bearing of each emitting source.

The problem of estimating the DOAs of multiple signals impinging on sensor arrays has attracted much attention for several decades [35], [45], [50], [99]. It is remarkable that the DOA estimation area has links to the area of time-series analysis. Several parameter estimation techniques have originated in time-series analysis and then they were borrowed and applied in array processing. For instance, conventional beamformer, that dates back to the 1940s, is a mere application of Fourier-based spectral analysis to spatio-temporally sampled data.

As a result of intensive research during the last three decades, many high-resolution optimal and suboptimal DOA estimation techniques have been developed. For example, the **MU**ltiple **SI**gnal **C**lassification (MUSIC), proposed by Schmidt [82], is one of the most popular high-resolution approaches to the direction finding problem. A similar approach has been independently proposed by Beinvenu and Kopp [15]. Most of the developed high-resolution direction finding techniques are based on parametric modeling. However, most of these techniques make some idealistic assumptions that might not be valid in practice. Hence, more advanced techniques for the direction finding problem, especially in complicated environments, are of great interest.

In this chapter, we give a brief description of the conventional array signal model as well as a brief review of the most popular parameter estimation techniques that have been widely used in the array processing area. We classify these techniques into two main categories: *nonparametric* techniques and *parametric* (model-based) techniques. We further divide the parametric techniques into two sub-categories: subspace-based methods and maximum likelihood (ML) techniques. All these methods will be explained in the context of DOA estimation. At the end of the chapter, we briefly describe the CRB that provides a lower bound on the performance of any unbiased estimator. In subsequent chapters, the CRB will be used as a standard measure to assess the performance of suboptimal estimation techniques.

2.2 Array Signal Model

Consider an array of M sensors located in three-dimensional coordinate space. The sensors locations are defined by the position vectors

$$\mathbf{r}_m = [\mathrm{x}_m, \mathrm{y}_m, \mathrm{z}_m]^T, \quad m = 1, 2, \ldots, M,$$

where $(\cdot)^T$ stands for the transpose. The sensors spatially sample an external signal field that is assumed to be generated by a finite number of emitters. The generated waves are assumed to be travelling in a homogenous medium at a constant speed c. The signals received by the array sensors due to the incident wavefields are given by the $M \times 1$ vector

$$\mathbf{x}(t) = \Big[x(t, \mathbf{r}_1), \ldots, x(t, \mathbf{r}_M)\Big]^T, \tag{2.1}$$

where $x(t, \mathbf{r}_m)$ is the signal received by the mth sensor. In the following, we analyze the response of the array to the incident wavefields and provide the mathematical signal model that has been widely used in the array signal processing literature.

2.2.1 Near-Field and Far-Field Wave Scenarios

Propagating waves are classified into spherical waves and planar waves according to the ratio of the total aperture size of the array to the distance between the array and the location of the emitting source. The wavefield will be spherical in shape if the emitting source is located relatively close to the sensor array. This case is also termed as the near-field case. If the location of the emitting source in three-dimensional space is known, then the signal received by the array due to a spherical wavefield can be uniquely identified [18]. For example, if the signal emitted by a near-field source is denoted by $\bar{s}(t)$, then the signal received by the mth sensor of the array is given by

$$x(t, \mathbf{r}_m) = ß_m(t, \boldsymbol{\phi})\bar{s}(t - \tau_m) + n_m(t), \quad m = 1, 2, \ldots, M, \tag{2.2}$$

where $ß_m(t, \boldsymbol{\phi})$ is the direction pattern of the mth sensor, $\boldsymbol{\phi}$ is the parameter vector that can be associated with several scalar parameters such as frequency, azimuth angle, elevation angle and polarization of the wave impinging on the mth sensor, and $n_m(t)$ is an additive noise term that represents the background and/or thermal noise associated with the mth sensor. In (2.2), τ_m is the time required for the propagating

wave to travel from the location of the emitter to the location of the mth sensor. That is,

$$\tau_m \triangleq \frac{\|\mathbf{r}_m - \mathbf{r}_s\|}{c}, \tag{2.3}$$

where $\|\cdot\|$ denotes the Euclidean norm of a vector and $\mathbf{r}_s$ is the position vector that describes the location of the emitting source.

On the other hand, if the distance between the location of the emitting source and the array is large compared to the total aperture size of the array, then the wavefronts are modeled as plane-waves. This case is also referred to as the far-field case. Assume that the plane-wave is propagating with frequency ω in the direction $\mathbf{u}$, where $\mathbf{u}$ is a unit vector. Assume also that $\tilde{s}(t)$ is the signal that would be received by a virtual sensor located at the origin of the coordinate system. Then, the signal captured by the mth sensor of the array is given by [99]

$$x(t, \mathbf{r}_m) = ß_m(t, \phi)\tilde{s}(t - \tau_m) + n_m(t), \quad m = 1, 2, \ldots, M, \tag{2.4}$$

where

$$\tau_m = \frac{\mathbf{u}^T \mathbf{r}_m}{c} \tag{2.5}$$

is the time required for the plane-wave to travel from the origin of the coordinate system to the location of the mth sensor.

Usually, the direction pattern of the sensors is assumed to be constant over the observation interval. We also assume that the sensors are omnidirectional and identical and that the direction pattern is constant over the frequency range of the received signals. Hence, $ß_m(t, \phi)$ is a constant and will be omitted from the equations for the sake of mathematical convenience.

To give a simple illustrative example, consider the case of a far-field signal that impinges on a linear array as shown in Figure 2.1. Without loss of generality, we take the position of the first element of the array as the reference point and denote

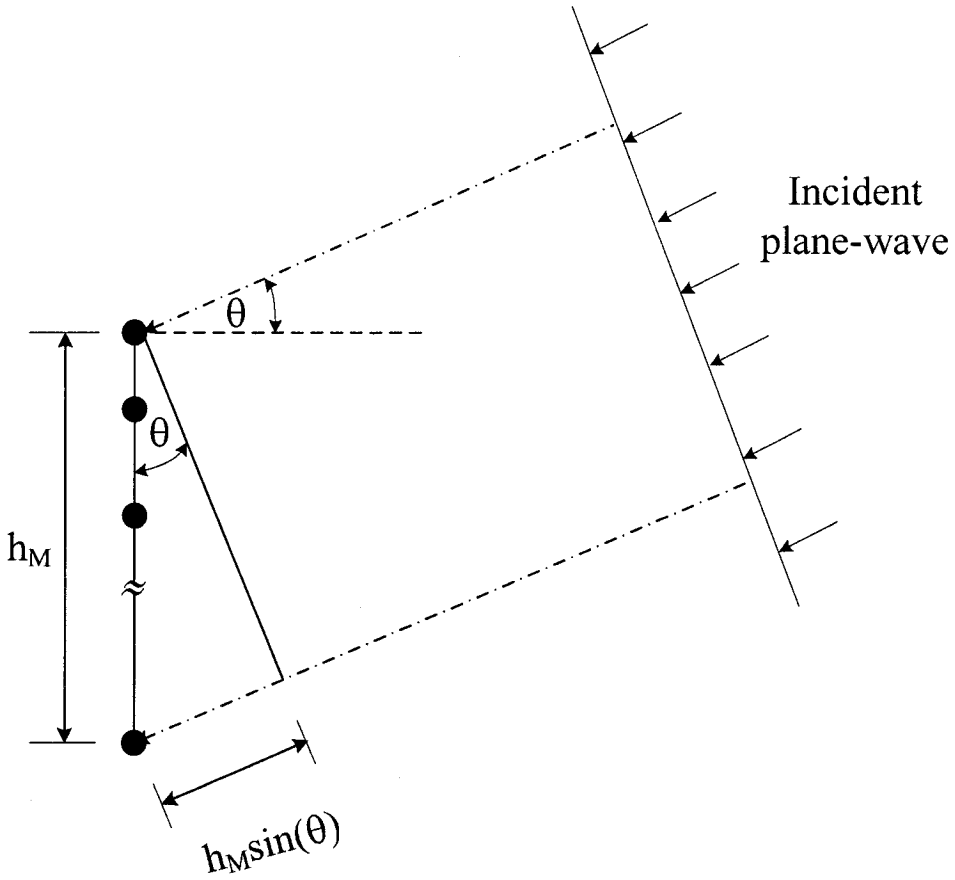

Figure 2.1: Linear array with plane-wave input.

the signal that impinges on that element as $\tilde{s}(t)$. We also assume that the emitting source and the receiving array are in the same plane. Therefore, the elevation angle can be assumed to be equal to 0° and the incident plane-wave will be characterized by its azimuth DOA, e.g. θ, where θ is measured relative to the broadside of the array. In this case, the position of the mth sensor with respect to the location of the first sensor can be described by the translation vector

$$\mathbf{r}_m \triangleq [0, 0, -h_m]^T, \tag{2.6}$$

where h_m is the spacing between the first and mth sensors of the array. The propagation direction of the incident plane-wave can be expressed as

$$\mathbf{u} \triangleq [0, -\cos(\theta), -\sin(\theta)]^T. \tag{2.7}$$

Substituting (2.6) and (2.7) into (2.5), we obtain that the time required for the incident wave to travel from the location of the first sensor to the location of the mth sensor is given by

$$\tau_m = \frac{h_m}{c}\sin(\theta). \tag{2.8}$$

Therefore, the signal received by the mth sensor is given by

$$x_m(t) = \tilde{s}\left(t - \frac{h_m}{c}\sin(\theta)\right) + n_m(t), \quad m = 1, \ldots, M. \tag{2.9}$$

2.2.2 Narrow-band Snapshot Model

The signal observed at the sensor array is modeled as a complex bandpass signal [99]

$$\tilde{s}(t) = s(t)\exp\{j\omega_o t\}, \tag{2.10}$$

where $s(t)$ is the informative (base-band) complex envelope signal and ω_o is the carrier frequency. Therefore, the noise free part of the signal received by the mth sensor is given by

$$\begin{aligned} \tilde{s}_m(t) &= s(t-\tau_m)\exp\{j\omega_o(t-\tau_m)\} \\ &= s(t-\tau_m)\exp\{j\omega_o t\}\exp\left\{-j\frac{h_m}{c}\omega_o\sin(\theta)\right\}. \end{aligned} \tag{2.11}$$

A typical underlying assumption in array signal processing is that the signals are narrowband which means that the spectrum of the signal is bandlimited and that the signal bandwidth is much smaller than the carrier frequency. In other words, we assume that the bandwidth of the base-band signal $s(t)$ is much less than $1/\tau_M$. The

narrowband assumption implies that the source signal $s(t)$ changes very slowly in the sense that it remains constant during the time required for the incident wave to travel across the entire aperture of the array. Hence, the approximation

$$s\left(t - \frac{h_m}{c}\sin(\theta)\right) \approx s(t), \quad m = 1, \ldots, M \tag{2.12}$$

is fairly accurate and it can be used to obtain a convenient signal model for the array output signal.

Making use of the above approximation, the pure signal part of the signal received by the mth sensor is given by

$$\tilde{s}_m(t) \approx s(t)\exp\{j\omega_o t\}\exp\left\{-j\frac{h_m}{c}\omega_o \sin(\theta)\right\}. \tag{2.13}$$

In practical array processing applications, the signal is usually down-converted to base-band before sampling [50], [99]. Dropping the term $\exp\{j\omega_o t\}$, the array output signal is modeled as

$$\mathbf{x}(t) \triangleq s(t)\begin{bmatrix} 1 \\ \exp\left\{-j\frac{h_2}{c}\omega_o \sin(\theta)\right\} \\ \vdots \\ \exp\left\{-j\frac{h_M}{c}\omega_o \sin(\theta)\right\} \end{bmatrix} + \mathbf{n}(t), \tag{2.14}$$

where

$$\mathbf{n}(t) \triangleq [n_1(t), \ldots, n_M(t)]^T \tag{2.15}$$

is the $M \times 1$ vector that represents the additive noise term.

In the general case, there are L different signals $\{s_l(t)\}_{l=1}^{L}$ that impinge on the array. By applying the principle of superposition, the array snapshot vector is simply a linear combination of the received vectors due to individual signals. That is,

$$\mathbf{x}(t) = \sum_{l=1}^{L} s_l(t)\mathbf{a}(\theta_l) + \mathbf{n}(t), \tag{2.16}$$

where θ_l is the DOA of the lth signal and

$$\mathbf{a}(\theta) \triangleq \left[1, \exp\left\{-j\frac{h_2}{c}\omega_o \sin(\theta)\right\}, \ldots, \exp\left\{-j\frac{h_M}{c}\omega_o \sin(\theta)\right\}\right]^T, \tag{2.17}$$

is the array manifold vector[1] associated with the direction θ.

For an algebraic characterization of the array snapshot model, we express (2.16) in a more compact form as follows

$$\mathbf{x}(t) = \mathbf{A}(\boldsymbol{\theta})\mathbf{s}(t) + \mathbf{n}(t), \tag{2.18}$$

where

$$\boldsymbol{\theta} = [\theta_1, \theta_2, \ldots, \theta_L]^T \tag{2.19}$$

is the $L \times 1$ vector that contains the DOAs of the received signals, and

$$\mathbf{s}(t) = [s_1(t), s_2(t), \ldots, s_L(t)]^T \tag{2.20}$$

is the $L \times 1$ vector that contains the signal waveforms. In (2.18), the matrix

$$\mathbf{A}(\boldsymbol{\theta}) \triangleq [\mathbf{a}(\theta_1), \ldots, \mathbf{a}(\theta_L)] \tag{2.21}$$

is the steering matrix which is assumed to be full rank, i.e., the columns of $\mathbf{A}(\boldsymbol{\theta})$ are assumed to be linearly independent.

2.2.3 Statistical Characterization of the Array Output Signal

Let us assume that the array output signal is temporally-sampled in time with sampling interval Δt and that N_s different snapshots are available. In this subsection, we describe the statistical characterization for both the signal and noise terms in

[1]The array response vector and the steering vector are other names that are commonly used to define the array manifold vector $\mathbf{a}(\theta)$.

(2.16) that has been commonly used in the array signal processing area. This statistical characterization allows us to express the signal model by means of its sufficient statistics.

The random noise term $\{\mathbf{n}(t)\}_{t=1}^{N_s}$ is modeled as a zero-mean circularly complex Gaussian process. We assume that the noise is temporally and spatially white, i.e., the noise covariance matrix is a scaled version of the identity matrix. That is,

$$\mathbf{R}_n = \mathrm{E}\{\mathbf{n}(t)\mathbf{n}^H(s)\} = \sigma_n^2 \mathbf{I}\,\delta_{t,s}, \tag{2.22}$$

where $\mathbf{I}$ is the identity matrix, σ_n^2 is the noise variance, $\delta_{t,s}$ is the Kronecker delta, and $(\cdot)^H$ stands for the Hermitian transpose. The above assumption means that the noise at different sensors is uncorrelated. It also means that the noise at different snapshots is uncorrelated. Another common assumption that has been widely used in the array signal processing literature is that the noise and the signal waveforms are uncorrelated.

Two different models are commonly used to statistically characterize the observed signals $\{s_l(t)\}_{l=1}^{L}$. These are the *stochastic signal model* and the *deterministic signal model* [94]. In the stochastic signal model, the received signals are sample functions of a zero-mean Gaussian random process. That is, the source signals are modeled as

$$\mathbf{s}(t) \sim \mathcal{N}(\mathbf{0},\ \mathbf{S}), \tag{2.23}$$

where $\mathcal{N}(\cdot)$ denotes the complex multivariate Gaussian distribution and $\mathbf{S}$ is the source covariance matrix that is given by

$$\mathbf{S} = \mathrm{E}\{\mathbf{s}(t)\mathbf{s}^H(t)\}. \tag{2.24}$$

In this case, the received signal snapshot is modeled as

$$\mathbf{x}(t) \sim \mathcal{N}(\mathbf{0},\ \mathbf{A}(\boldsymbol{\theta})\mathbf{S}\mathbf{A}^H(\boldsymbol{\theta}) + \sigma_n^2\mathbf{I}). \tag{2.25}$$

In the deterministic signal model, the received signals are assumed to be either deterministic or unknown random signals. We make no assumptions on the statistics of the waveforms. In this case, the signal snapshot model is written as

$$\mathbf{x}(t) \sim \mathcal{N}(\mathbf{A}(\boldsymbol{\theta})\mathbf{s}(t), \sigma_n^2\mathbf{I}). \tag{2.26}$$

There are many parameter estimation problems in the array processing area that can be of interest. For example, the objective of array signal processing might involve detecting the number of emitting sources, estimating the range of a target (in the near-field), source localization and DOA estimation, channel characterization, or estimating the optimal positions of the sensors in the array. In this thesis we assume that the number of signals L is known and that the emitting sources are located in the far-field. Hence, our main objective will be focussed on estimating the signal parameters, e.g. the DOAs, of the plane-waves arriving at the array.

2.3 Nonparametric Estimation Techniques

Nonparametric DOA estimation techniques do not make any assumptions on the properties of the covariance matrix of the received data snapshots. The basic idea behind these methods is to obtain a spatial spectrum and to estimate the parameters of interest, e.g. the DOAs, by searching for the locations of the highest peaks of this spatial spectrum. Consider the generic structure linear beamformer shown in Figure 2.2. The signal received at each sensor is multiplied by a complex weight. Then, the beamformer output is obtained by forming a linear combination of the weighted signals. That is,

$$y(t) = \mathbf{w}^H\mathbf{x}(t), \tag{2.27}$$

where

$$\mathbf{w} = [w_1, w_2, \ldots, w_M]^T \tag{2.28}$$

is the complex weight vector. For a given weight vector $\mathbf{w}$, the mean output power of the array is given by [36]

$$\begin{aligned} P(\mathbf{w}) &= \mathrm{E}\{y(t)y^*(t)\} \\ &= \mathbf{w}^H \mathrm{E}\{\mathbf{x}(t)\mathbf{x}^H(t)\}\mathbf{w} \\ &= \mathbf{w}^H \mathbf{R}_{\mathbf{x}} \mathbf{w}, \end{aligned} \tag{2.29}$$

where $\mathrm{E}\{\cdot\}$ is the expectation operator, and

$$\mathbf{R}_{\mathbf{x}} = \mathrm{E}\{\mathbf{x}(t)\mathbf{x}^H(t)\} \tag{2.30}$$

is the spatial correlation matrix of the received snapshots. In practical situations, the sample covariance matrix

$$\hat{\mathbf{R}}_{\mathbf{x}} = \frac{1}{N_s} \sum_{t=1}^{N_s} \mathbf{x}(t)\mathbf{x}^H(t) \tag{2.31}$$

is used instead of the true covariance matrix $\mathbf{R}_{\mathbf{x}}$. In the sequel we will give a brief description of two popular nonparametric estimation techniques.

2.3.1 Conventional Beamformer

Conventional beamformer is a classic ($\mathbf{w}$ does not depend on the input/output array signals) direction finding technique that scans the beam to evaluate the received power in each direction. It maximizes the output power received from a certain direction such that the norm of the weight vector is fixed [36], [50]. Let us consider the scenario of a single source signal observed in the background of white noise. That is,

$$\mathbf{x}(t) = s(t)\mathbf{a}(\theta) + \mathbf{n}(t). \tag{2.32}$$

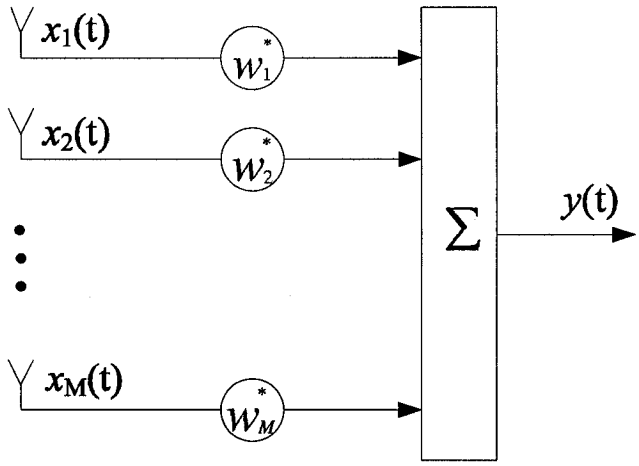

Figure 2.2: The generic structure of linear beamformer.

Using (2.29), the beamformer output power can be written as

$$\begin{aligned} P(\mathbf{w}) &= \mathbf{w}^H \mathrm{E}\{(s(t)\mathbf{a}(\theta) + \mathbf{n}(t))(s(t)\mathbf{a}(\theta) + \mathbf{n}(t))^H\}\mathbf{w} \\ &= \mathbf{w}^H \left\{\sigma_s^2 \mathbf{a}(\theta)\mathbf{a}^H(\theta) + \sigma_n^2 \mathbf{I}\right\} \mathbf{w} \\ &= \sigma_s^2 |\mathbf{w}^H \mathbf{a}(\theta)|^2 + \sigma_n^2 \|\mathbf{w}\|^2, \end{aligned} \tag{2.33}$$

where $\sigma_s^2 = \mathrm{E}\{s(t)s^*(t)\}$ is the signal power.

The unit norm weight vector $\mathbf{w}$ that maximizes the output power is obtained as the solution to the following optimization problem [50]

$$\begin{aligned} \underset{\mathbf{w}}{\text{maximize}} \quad & \sigma_s^2 |\mathbf{w}^H \mathbf{a}(\theta)|^2 + \sigma_n^2 \|\mathbf{w}\|^2 \\ \text{subject to} \quad & \|\mathbf{w}\|^2 = 1 \end{aligned} \tag{2.34}$$

The objective function in the above optimization problem will be maximum when $\mathbf{w}$ is a unit vector that has the same direction as the steering vector $\mathbf{a}(\theta)$, i.e.,

$$\mathbf{w} = \frac{\mathbf{a}(\theta)}{\|\mathbf{a}(\theta)\|}. \tag{2.35}$$

Substituting (2.35) in (2.29), we obtain the conventional beamformer spatial spectrum [36], [50]

$$P_{\text{CBF}}(\theta) = \frac{\mathbf{a}^H(\theta)\mathbf{R}_\mathbf{x}\mathbf{a}(\theta)}{\|\mathbf{a}(\theta)\|^2}. \tag{2.36}$$

Note that in practice, the sample covariance matrix $\hat{\mathbf{R}}_\mathbf{x}$ is used in lieu of the true covariance matrix $\mathbf{R}_\mathbf{x}$ in order to obtain the conventional beamformer spatial spectrum.

In addition to its simplicity, conventional beamformer provides good robustness against model mismatch. In the case of uniform linear array (ULA), conventional beamformer enjoys efficient implementation via FFT. However, in the presence of multiple sources, conventional beamformer is no longer optimal and has low resolution capabilities. Hence, its performance is limited by the aperture size of the array [73].

2.3.2 Minimum Variance Distortionless (MVDR) Beamformer

Based on point source modeling, the MVDR spatial spectrum estimator has been developed in [19]. This estimator can be considered as a spatial filter (beamformer) which passes the signal of a hypothetical point source arriving from the direction θ while maximally rejecting the signals coming from other directions. The $M \times 1$ beamformer coefficient vector $\mathbf{w}_{\text{opt}}$ is obtained as the solution to the following optimization problem [93], [99]

$$\begin{aligned} \underset{\mathbf{w}}{\text{minimize}} \quad & \mathbf{w}^H\mathbf{R}_\mathbf{x}\mathbf{w} \\ \text{subject to} \quad & \mathbf{w}^H\mathbf{a}(\theta) = 1. \end{aligned} \tag{2.37}$$

In adaptive beamforming, (2.37) is commonly referred to as the minimum variance distorionless (MVDR) beamforming problem, see [99].

The solution to (2.37) is given by [50], [99]

$$\mathbf{w}_{\text{opt}}(\theta) = \frac{\mathbf{R}_\mathbf{x}^{-1}\mathbf{a}(\theta)}{\mathbf{a}^H(\theta)\mathbf{R}_\mathbf{x}^{-1}\mathbf{a}(\theta)}. \tag{2.38}$$

For any direction θ, the spatial spectrum is defined through the output power of the MVDR beamformer as [93], [99]

$$\begin{aligned} P_{\mathrm{C}}(\theta) &\triangleq \mathbf{w}_{\mathrm{opt}}^{H}(\theta)\hat{\mathbf{R}}_{\mathbf{x}}\mathbf{w}_{\mathrm{opt}}(\theta) \\ &= \frac{1}{\mathbf{a}^{H}(\theta)\hat{\mathbf{R}}_{\mathbf{x}}^{-1}\mathbf{a}(\theta)}. \end{aligned} \tag{2.39}$$

Note that in (2.39), the sample covariance matrix $\hat{\mathbf{R}}_{\mathbf{x}}$ is used instead of the true covariance matrix $\mathbf{R}_{\mathbf{x}}$. It is clear that if the energy of the lth point source impinges on the array from a direction θ_l, then $P_{\mathrm{C}}(\theta)$ is expected to have a separate peak at $\theta = \theta_l$. Hence, the point source DOAs can be estimated from the L highest maxima of (2.39) which can be obtained by means of a one-dimensional spectral search.

2.4 Subspace-Based Methods

Subspace-based DOA estimation techniques have been studied extensively in the literature and were proven to have high-resolution capabilities (see [36], [50], [99] and references therein). These methods are based on the following properties [36]:

1. The space spanned by the received data vectors may be partitioned into two subspaces, namely, the signal subspace and the noise subspace.

2. The steering vectors associated with the DOAs are orthogonal to the noise subspace.

The array output signal is assumed to obey the stochastic signal model (c.f. 2.25). In this case, the array covariance matrix is written as

$$\mathbf{R}_{\mathbf{x}} = \mathbf{A}(\boldsymbol{\theta})\mathbf{S}\mathbf{A}^{H}(\boldsymbol{\theta}) + \sigma_n^2\mathbf{I}. \tag{2.40}$$

Eigen-analysis techniques have been widely used to obtain the signal and noise subspaces from the array covariance matrix. Let $\{\lambda_m\}_{m=1}^{M}$ be the eigenvalues of $\mathbf{R}_{\mathbf{x}}$

arranged in descending order, i.e.,

$$\lambda_1 \geq \lambda_2 \geq \ldots \geq \lambda_L > \lambda_{L+1} = \ldots = \lambda_M = \sigma_n^2. \tag{2.41}$$

The first L eigenvalues $\{\lambda_m\}_{m=1}^{L}$ are referred to as the signal subspace eigenvalues and the rest are referred to as the noise subspace eigenvalues. Hence, the array covariance matrix can be rewritten in the form

$$\mathbf{R_x} = \mathbf{U_s}\mathbf{\Lambda_s}\mathbf{U_s}^H + \mathbf{U_n}\mathbf{\Lambda_n}\mathbf{U_n}^H, \tag{2.42}$$

where the $L \times L$ diagonal matrix $\mathbf{\Lambda_s}$ contains the signal-subspace eigenvalues and the columns of the $M \times L$ matrix $\mathbf{U_s}$ are the corresponding eigenvectors. Similarly, the $(M-L) \times (M-L)$ diagonal matrix $\mathbf{\Lambda_n}$ contains the smallest (noise-subspace) eigenvalues while the $M \times (M-L)$ matrix $\mathbf{U_n}$ is built from the corresponding eigenvectors.

Multiplying equations (2.40) and (2.42) by $\mathbf{U_n}$ from the right and comparing the results we obtain

$$\mathbf{A}(\boldsymbol{\theta})\mathbf{S}\mathbf{A}^H(\boldsymbol{\theta})\mathbf{U_n} = \mathbf{0}. \tag{2.43}$$

Since $\mathbf{A}(\boldsymbol{\theta})\mathbf{S}$ is a full column rank matrix, it follows immediately that

$$\mathbf{A}^H(\boldsymbol{\theta})\mathbf{U_n} = \mathbf{0}. \tag{2.44}$$

The orthogonality between the steering matrix and the noise subspace in (2.44) is the basis for all subspace-based direction finding techniques.

2.4.1 Spectral-MUSIC DOA Estimator

The first developed parametric subspace-based method was Pisarenko's method which was derived in the context of time-series analysis [75]. However, the introduction of the MUSIC algorithm has inspired a tremendous interest in the subspace-based

approach to the direction finding problem [15], [50], [82], [83], [95]. In what follows, we provide a brief review of the spectral-MUSIC DOA estimator.

Equation (2.44) can be rewritten as [50], [82]

$$\mathbf{a}^H(\theta_l)\mathbf{U}_\mathrm{n}\mathbf{U}_\mathrm{n}^H\mathbf{a}(\theta_l) = 0, \qquad l = 1, \ldots, L. \tag{2.45}$$

Based on (2.45), the spectral-MUSIC spatial spectrum is defined as

$$f_{\mathrm{MUSIC}}(\theta) = \frac{1}{\mathbf{a}^H(\theta)\mathbf{U}_\mathrm{n}\mathbf{U}_\mathrm{n}^H\mathbf{a}(\theta)} = \frac{1}{\mathbf{a}^H(\theta)[\mathbf{I} - \mathbf{U}_\mathrm{s}\mathbf{U}_\mathrm{s}^H]\mathbf{a}(\theta)}. \tag{2.46}$$

Since the steering vectors $\{\mathbf{a}(\theta_l)\}_{l=1}^L$ are orthogonal to $\mathbf{U}_\mathrm{n}$, the spatial spectrum (2.46) is expected to have sharp peaks at values of θ that correspond to the DOAs $\{\theta_l\}_{l=1}^L$. In practice, the sample covariance matrix $\hat{\mathbf{R}}_\mathbf{x}$ (c.f. 2.31) is used instead of the true covariance matrix $\mathbf{R}_\mathbf{x}$. Using eigendecomposition we have

$$\hat{\mathbf{R}}_\mathbf{x} = \hat{\mathbf{U}}_\mathrm{s}\hat{\mathbf{\Lambda}}_\mathrm{s}\hat{\mathbf{U}}_\mathrm{s}^H + \hat{\mathbf{U}}_\mathrm{n}\hat{\mathbf{\Lambda}}_\mathrm{n}\hat{\mathbf{U}}_\mathrm{n}^H. \tag{2.47}$$

Hence, estimates of the DOAs can be obtained by searching for the L highest peaks in the spectral-MUSIC spatial spectrum [50], [82]

$$\hat{f}_{\mathrm{MUSIC}}(\theta) \triangleq \frac{1}{\mathbf{a}^H(\theta)\hat{\mathbf{U}}_\mathrm{n}\hat{\mathbf{U}}_\mathrm{n}^H\mathbf{a}(\theta)} = \frac{1}{\mathbf{a}^H(\theta)[\mathbf{I} - \hat{\mathbf{U}}_\mathrm{s}\hat{\mathbf{U}}_\mathrm{s}^H]\mathbf{a}(\theta)}. \tag{2.48}$$

It is worth mentioning that the spectral-MUSIC algorithm is a high-resolution DOA estimator that is applicable to any array with arbitrary geometry. However, the main disadvantage of this algorithm is that it requires a one-dimensional search that could be computationally expensive if the MUSIC estimate is evaluated on a fine angular grid.

2.4.2 Root-MUSIC DOA Estimator

Root-MUSIC is a computationally efficient search-free direction finding algorithm that was originally introduced in [6]. This algorithm is only applicable to ULAs. For

the case of a ULA, the steering vector is given by

$$\mathbf{a}(\theta) = \left[1,\ \exp\{-j\frac{\Delta}{c}\omega_{\mathrm{o}}\sin(\theta)\},\ldots,\exp\{-j\frac{\Delta}{c}(M-1)\omega_{\mathrm{o}}\sin(\theta)\}\right]^T, \tag{2.49}$$

where Δ is the interelement spacing of the array. Letting

$$z = \exp\{-j\frac{\Delta}{c}\omega_{\mathrm{o}}\sin(\theta)\}, \tag{2.50}$$

we can rewrite (2.49) as

$$\mathbf{a}(\theta) = [1,\ z,\ldots,z^{(M-1)}]^T. \tag{2.51}$$

Making use of (2.45) and (2.51), the root-MUSIC characteristic equation is defined as

$$\mathbf{a}^T(z^{-1})\mathbf{U}_{\mathrm{n}}\mathbf{U}_{\mathrm{n}}^H\mathbf{a}(z) = 0. \tag{2.52}$$

Note that the characteristic equation (2.52) is of order $2M-2$, hence there are $2M-2$ roots for it. The roots form $M-1$ pairs where one root is the conjugate reciprocal to another, i.e., if z is a root, then $1/z^*$ is also a root [6], [50], [99]. Among the roots that are located inside the unit circle there will be L roots that are exactly located on the unit circle. Each one of the roots that are located on the unit circle corresponds to one of the true DOAs.

In practice, the estimated noise subspace is used instead of the true one. Therefore, the root-MUSIC characteristic equation is given by

$$\mathbf{a}^T(z^{-1})\hat{\mathbf{U}}_{\mathrm{n}}\hat{\mathbf{U}}_{\mathrm{n}}^H\mathbf{a}(z) \simeq 0. \tag{2.53}$$

In this case, the locations of the roots that correspond to the true DOAs will deviate from the unit circle. Among the roots inside the unit circle, let $\{\hat{z}_l\}_{l=1}^L$ be the L closest roots to it. Then, the root-MUSIC algorithm estimates the DOAs as

$$\hat{\theta}_l = \arcsin\left\{-\frac{c}{\omega_{\mathrm{o}}\Delta}\arg\hat{z}_l\right\}, \quad l = 1,\ldots,L. \tag{2.54}$$

It is worth mentioning that the root-MUSIC algorithm is not only a search-free technique, but also it enjoys efficient implementation via any of the existing numerically efficient rooting algorithms [52].

2.4.3 ESPRIT DOA Estimator

Another search-free and computationally efficient direction finding technique is the ESPRIT algorithm [80]. This algorithm requires an array structure that consists of two identical subarrays separated in space by a known displacement vector[2]. The ESPRIT algorithm is based on the so-called shift structure of the steering matrix $\mathbf{A}$. This shift structure describes the relationship between the steering matrix of the first subarray and the steering matrix of the second subarray.

Without loss of generality, we consider the case of two linear subarrays aligned parallel to each other and separated by a displacement ζ as shown in Figure 2.3. We assume that L narrowband signals are impinging on the two subarrays from the DOAs $\{\theta_l\}_{l=1}^{L}$. Let $\mathbf{x}_l(t)$ be the signal received by the first subarray due to the lth narrowband signal that impinges on the array from direction θ_l. Then, the signal received by the second subarray due to the same signal is given by

$$\mathbf{r}_l(t) \triangleq \mathbf{x}_l(t) \exp\{-j\omega_o \tau_\zeta\}, \tag{2.55}$$

where

$$\tau_\zeta \triangleq \frac{\zeta \cos(\theta_l)}{c} \tag{2.56}$$

is the time delay required for the lth signal to travel from the first subarray to the second subarray. Let $\mathbf{x}(t)$ and $\mathbf{r}(t)$ be the array signals received by the first and the second subarrays respectively and assume that the location of the first sensor of the

[2]The two subarrays are allowed to overlap. For example, a ULA of M sensors can be thought of as two subarrays of $M-1$ sensors each.

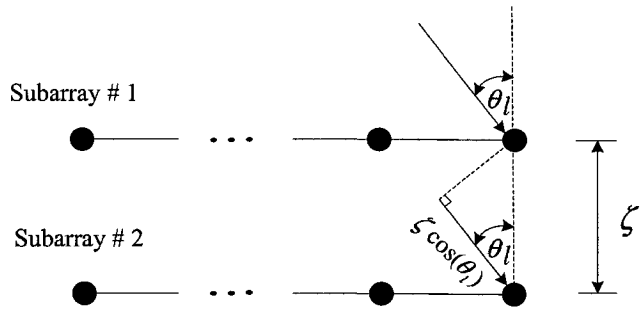

Figure 2.3: ESPRIT array structure.

first subarray is the reference point. Then, by making use of (2.55) it follows that

$$\mathbf{x}(t) = \mathbf{A}\mathbf{s}(t) + \mathbf{n}_{\mathrm{x}}(t), \tag{2.57}$$

and

$$\mathbf{r}(t) = \mathbf{A}\mathbf{\Phi}\mathbf{s}(t) + \mathbf{n}_{\mathrm{r}}(t), \tag{2.58}$$

where $\mathbf{n}_{\mathrm{x}}(t)$ and $\mathbf{n}_{\mathrm{r}}(t)$ are the additive noise terms associated with the first and the second subarrays respectively. In (2.58), $\mathbf{\Phi}$ is the $L \times L$ diagonal matrix that is defined as

$$\mathbf{\Phi} = \mathrm{diag}\left\{\exp\{-j\omega_{\mathrm{o}}\frac{\zeta\cos(\theta_1)}{c}\}, \ldots, \exp\{-j\omega_{\mathrm{o}}\frac{\zeta\cos(\theta_L)}{c}\}\right\}. \tag{2.59}$$

Let $\mathbf{U}_s$ be the $M \times L$ matrix whose columns span the signal subspace associated with the first subarray. Recall that $\mathbf{U}_s$ and $\mathbf{A}$ span the same signal subspace, and therefore, we have the relationship

$$\mathbf{U}_{\mathrm{s}} = \mathbf{A}\mathbf{T}, \tag{2.60}$$

where $\mathbf{T}$ is an $L \times L$ arbitrary full rank matrix. Similarly, if the $M \times L$ matrix $\mathbf{U}_{\mathrm{r}}$ spans the signal subspace associated with the second subarray, it follows that

$$\mathbf{U}_{\mathrm{r}} = \mathbf{A}\mathbf{\Phi}\mathbf{T}. \tag{2.61}$$

By substituting (2.60) in (2.61), we have

$$\begin{aligned} \mathbf{U}_{\mathrm{r}} &= \mathbf{U}_{\mathrm{s}}\mathbf{T}^{-1}\mathbf{\Phi}\mathbf{T} \\ &= \mathbf{U}_{\mathrm{s}}\mathbf{\Psi}, \end{aligned} \tag{2.62}$$

where

$$\mathbf{\Psi} = \mathbf{T}^{-1}\mathbf{\Phi}\mathbf{T}. \tag{2.63}$$

From (2.63), it follows that the diagonal elements of $\mathbf{\Phi}$ are the eigenvalues of $\mathbf{\Psi}$. Now let $\hat{\mathbf{U}}_{\mathrm{s}}$ and $\hat{\mathbf{U}}_{\mathrm{r}}$ be the estimates of the signal subspace matrices that can be obtained from the measurements $\mathbf{x}(t)$ and $\mathbf{r}(t)$. Then, we can obtain an estimate of $\mathbf{\Psi}$ from $\hat{\mathbf{U}}_{\mathrm{s}}$ and $\hat{\mathbf{U}}_{\mathrm{r}}$ by solving the following equation

$$\hat{\mathbf{U}}_{\mathrm{r}} = \hat{\mathbf{U}}_{\mathrm{s}}\hat{\mathbf{\Psi}}. \tag{2.64}$$

There are two criteria that can be used to solve (2.64), namely the least square (LS) approach and the total least square (TLS) approach [50], [99]. If the LS method is used, then $\mathbf{\Psi}$ can be estimated as [99]

$$\hat{\mathbf{\Psi}}_{\mathrm{LS}} = (\hat{\mathbf{U}}_{\mathrm{s}}^H\hat{\mathbf{U}}_{\mathrm{s}})^{-1}\hat{\mathbf{U}}_{\mathrm{s}}^H\hat{\mathbf{U}}_{\mathrm{r}}. \tag{2.65}$$

On the other hand, the TLS solution for $\mathbf{\Psi}$ is given by [37, Section 12.3], [99]

$$\hat{\mathbf{\Psi}}_{\mathrm{TLS}} = -\mathbf{V}_{12}\mathbf{V}_{22}^{-1}, \tag{2.66}$$

where $\mathbf{V}_{12}$ and $\mathbf{V}_{22}$ are $L \times L$ matrices defined by the eigendecomposition of the $2L \times 2L$ matrix

$$\hat{\mathbf{U}} \triangleq \begin{bmatrix} \hat{\mathbf{U}}_{\mathrm{s}}^H \\ \hat{\mathbf{U}}_{\mathrm{r}}^H \end{bmatrix} \begin{bmatrix} \hat{\mathbf{U}}_{\mathrm{s}} & \hat{\mathbf{U}}_{\mathrm{r}} \end{bmatrix} = \begin{bmatrix} \mathbf{V}_{11} & \mathbf{V}_{12} \\ \mathbf{V}_{21} & \mathbf{V}_{22} \end{bmatrix} \mathbf{\Lambda} \begin{bmatrix} \mathbf{V}_{11}^H & \mathbf{V}_{21}^H \\ \mathbf{V}_{12}^H & \mathbf{V}_{22}^H \end{bmatrix}. \tag{2.67}$$

Once $\hat{\mathbf{\Psi}}$ is obtained, the ESPRIT algorithm estimates the DOAs as

$$\hat{\theta}_l = \arccos\left\{ -\frac{c}{\zeta\omega_{\mathrm{o}}} \arg\hat{\mu}_l \right\}, \quad l = 1, \ldots, L, \tag{2.68}$$

where $\{\hat{\mu}_l\}_{l=1}^{L}$ are the eigenvalues of $\hat{\mathbf{\Psi}}$.

2.5 Maximum Likelihood Techniques

The ML technique is the most well known and widely studied approach to the problem of parameter estimation in array processing. Its importance arises because it fully exploits the underlying statistical signal model. Unlike subspace-based techniques, the ML technique is known to have an optimal performance for both uncorrelated and coherent sources but at the price of higher computational cost. In this section, we briefly describe the ML technique in the context of DOA estimation.

The general approach to obtain the ML estimates is to define the likelihood function which is the joint probability density function (pdf) of the sampled data under the assumption that the DOAs are given. Then, the approach involves maximizing the likelihood function with respect to the unknown parameters, e.g., the DOAs. Hence, the ML criterion signifies that the signals impinging on the array from these directions are most likely to cause the given samples to occur.

2.5.1 Stochastic Maximum Likelihood

The stochastic maximum likelihood (SML) algorithm is based on the assumption that the received data snapshots obey the stochastic data model given in (2.25). That is, the observation vector $\mathbf{x}(t)$ is a circularly symmetric zero-mean white Gaussian random process. Recall that the covariance matrix for this case is given by

$$\mathbf{R}_{\mathbf{x}} = \mathbf{A}(\boldsymbol{\theta})\mathbf{S}\mathbf{A}^H(\boldsymbol{\theta}) + \sigma_n^2\mathbf{I}.$$

The multivariate pdf for a single snapshot is expressed in terms of $\boldsymbol{\theta}$, $\mathbf{S}$, and σ_n^2 as follows

$$f(\boldsymbol{\theta}, \mathbf{S}, \sigma_n^2) = \frac{1}{\pi^M |\mathbf{R}_{\mathbf{x}}|} \exp\left\{-\mathbf{x}^H(t)\mathbf{R}_{\mathbf{x}}^{-1}\mathbf{x}(t)\right\}, \tag{2.69}$$

where $|\cdot|$ denotes the determinant of a matrix. Assuming that N_s successive statistically independent snapshots $\{\mathbf{x}(t)\}_{t=1}^{N_s}$ are available, the joint multivariate pdf is given by

$$f(\boldsymbol{\theta}, \mathbf{S}, \sigma_n^2) = \prod_{t=1}^{N_s} \frac{1}{\pi^M |\mathbf{R_x}|} \exp\left\{-\mathbf{x}^H(t)\mathbf{R_x}^{-1}\mathbf{x}(t)\right\}. \tag{2.70}$$

The negative log-likelihood function is given by

$$\begin{aligned} L(\boldsymbol{\theta}, \mathbf{S}, \sigma_n^2) &\triangleq -\log(f(\boldsymbol{\theta}, \mathbf{S}, \sigma_n^2)) \\ &= N_s M \log(\pi) + N_s \log(|\mathbf{R_x}|) + \sum_{t=1}^{N_s} \mathbf{x}^H(t)\mathbf{R_x}^{-1}\mathbf{x}(t). \end{aligned} \tag{2.71}$$

Since $L(\cdot)$ is monotonic, the negative log-likelihood function (2.71) can be minimized instead of maximizing the likelihood function (2.70) [73]. Ignoring the constant term and dividing through by N_s, we have

$$\begin{aligned} L(\boldsymbol{\theta}, \mathbf{S}, \sigma_n^2) &= \log(|\mathbf{R_x}|) + \mathrm{tr}\left\{\frac{1}{N_s}\sum_{t=1}^{N_s} \mathbf{x}^H(t)\mathbf{R_x}^{-1}\mathbf{x}(t)\right\} \\ &= \log(|\mathbf{R_x}|) + \mathrm{tr}\left\{\mathbf{R_x}^{-1}\sum_{t=1}^{N_s} \frac{1}{N_s}\mathbf{x}(t)\mathbf{x}^H(t)\right\} \\ &= \log(|\mathbf{R_x}|) + \mathrm{tr}\{\mathbf{R_x}^{-1}\hat{\mathbf{R}}_\mathbf{x}\}, \end{aligned} \tag{2.72}$$

where $\hat{\mathbf{R}}_\mathbf{x}$ is the sample covariance matrix given in (2.31) and $\mathrm{tr}\{\cdot\}$ denotes the matrix trace. Fortunately, the above problem is solvable for $\mathbf{S}$ and σ_n^2 so that we can obtain an explicit function in $\boldsymbol{\theta}$ [16] [47], [99].

The maximization of (2.71) over $\mathbf{S}$ yields [99]

$$\hat{\mathbf{S}} = \mathbf{A}^\dagger(\boldsymbol{\theta})(\hat{\mathbf{R}}_\mathbf{x} - \sigma_n^2\mathbf{I})(\mathbf{A}^\dagger(\boldsymbol{\theta}))^H, \tag{2.73}$$

where $\mathbf{A}^\dagger = (\mathbf{A}^H\mathbf{A})^{-1}\mathbf{A}^H$ is the pseudo-inverse of $\mathbf{A}$. Similarly, the maximization of (2.71) over σ_n^2 yields [99]

$$\hat{o}_n^2 = \frac{1}{N_s - L}\mathrm{tr}\{\mathbf{P}_\mathbf{A}^\perp \hat{\mathbf{R}}_\mathbf{x}\}, \tag{2.74}$$

where $\mathbf{P}_{\mathbf{A}}^{\perp} = \mathbf{I} - \mathbf{A}\mathbf{A}^{\dagger}$ is the projection matrix onto the nullspace of $\mathbf{A}$. Substituting (2.73) and (2.74) into (2.71), we obtain the SML estimator [16], [47], [99]

$$\hat{\boldsymbol{\theta}}_{\text{STOC}} = \arg\min_{\boldsymbol{\theta}} \log \left| \mathbf{P}_{\mathbf{A}} \hat{\mathbf{R}}_{\mathbf{x}} \mathbf{P}_{\mathbf{A}} + \frac{1}{N_s - L} \text{tr}\{\mathbf{P}_{\mathbf{A}}^{\perp} \hat{\mathbf{R}}_{\mathbf{x}}\} \mathbf{P}_{\mathbf{A}}^{\perp} \right|, \tag{2.75}$$

where $\mathbf{P}_{\mathbf{A}} = \mathbf{A}\mathbf{A}^{\dagger}$ is the projection matrix onto the space spanned by $\mathbf{A}$.

2.5.2 Deterministic Maximum Likelihood

The deterministic maximum likelihood (DML) algorithm is based on the assumption that the received data snapshots obey the deterministic signal model given in (2.26). That is, the observation vector $\mathbf{x}(t)$ is a circularly symmetric white Gaussian random process with mean $\mathbf{A}(\boldsymbol{\theta})\mathbf{s}(t)$ and covariance matrix

$$\mathbf{R}_{\mathbf{x}} = \sigma_n^2 \mathbf{I}. \tag{2.76}$$

Once more, we assume that N_s successive statistically independent snapshots $\{\mathbf{x}(t)\}_{t=1}^{N_s}$ are available. Then, the joint pdf is given by

$$f(\boldsymbol{\theta}, \mathbf{s}(t), \sigma_n^2) = \prod_{t=1}^{T} \frac{1}{(\pi\sigma_n^2)^M} \exp\left\{ -\frac{\|\mathbf{x}(t) - \mathbf{A}(\boldsymbol{\theta})\mathbf{s}(t)\|^2}{\sigma_n^2} \right\}. \tag{2.77}$$

Hence, the unknown parameters can be sought by looking for the values of the parameters that minimize the negative log-likelihood function[3]

$$L(\boldsymbol{\theta}, \mathbf{s}(t), \sigma_n^2) = M \log \sigma_n^2 + \frac{1}{\sigma_n^2} \sum_{t=1}^{N_s} \frac{1}{N_s} \|\mathbf{x}(t) - \mathbf{A}(\boldsymbol{\theta})\mathbf{s}(t)\|^2. \tag{2.78}$$

The number of parameters involved in the minimization of (2.78) can be reduced by finding the separate ML estimates of the nuisance parameters $\mathbf{s}(t)$ and σ_n^2. This can be done by fixing $\boldsymbol{\theta}$ and solving for σ_n^2 and $\mathbf{s}(t)$ which yields [50], [95]

$$\hat{\sigma}_n^2 = \frac{1}{M} \text{tr}\{\mathbf{P}_{\mathbf{A}}^{\perp} \hat{\mathbf{R}}_{\mathbf{x}}\}, \tag{2.79}$$

[3]Note that all constant terms are omitted as they do not affect the optimal solution.

and

$$\hat{\mathbf{s}}(t) = \mathbf{A}^{\dagger}\mathbf{x}(t). \tag{2.80}$$

By substituting (2.79) and (2.80) into (2.78), we obtain the DML DOA estimator [50]

$$\hat{\boldsymbol{\theta}}_{\mathrm{DET}} = \arg\max_{\boldsymbol{\theta}} \ \mathrm{tr}\{\mathbf{P}_{\mathbf{A}}\hat{\mathbf{R}}_{\mathbf{x}}\}. \tag{2.81}$$

It is worth noting that, for the single-source case, the DML simplifies to

$$\begin{aligned} \hat{\theta}_{\mathrm{DET}} &= \arg\max_{\theta} \mathrm{tr}\left\{\frac{\mathbf{a}(\theta)\mathbf{a}^{H}(\theta)}{\mathbf{a}^{H}(\theta)\mathbf{a}(\theta)}\hat{\mathbf{R}}_{\mathbf{x}}\right\} \\ &= \arg\max_{\theta} \frac{\mathbf{a}^{H}(\theta)\hat{\mathbf{R}}_{\mathbf{x}}\mathbf{a}(\theta)}{\|\mathbf{a}(\theta)\|^{2}}. \end{aligned} \tag{2.82}$$

From (2.82), it is interesting to note that the DML for the single-source case is equivalent to conventional beamformer (c.f. 2.36).

2.6 Cramér-Rao Bounds

In this Section, we will briefly describe the bounds on the performance of the DOA estimation techniques that are based on both the deterministic and the stochastic signal models. The CRB provides a lower bound on the performance of any unbiased estimator. Hence, it provides a baseline standard that can be used to assess the performance of suboptimal estimation techniques.

For any unbiased estimate of $\boldsymbol{\theta}$, the covariance matrix of the estimation errors is given by

$$\mathbf{E}(\boldsymbol{\theta}) \triangleq \mathrm{E}\left\{(\hat{\boldsymbol{\theta}} - \boldsymbol{\theta})(\hat{\boldsymbol{\theta}} - \boldsymbol{\theta})^{T}\right\}, \tag{2.83}$$

where $\hat{\boldsymbol{\theta}}$ is the estimate of $\boldsymbol{\theta}$. The CRB states that [99]

$$\mathbf{E}(\boldsymbol{\theta}) \geq \mathrm{CRB}(\boldsymbol{\theta}) \triangleq \mathbf{F}^{-1}, \tag{2.84}$$

where the matrix inequality means that $\mathbf{E}(\boldsymbol{\theta}) - \text{CRB}(\boldsymbol{\theta})$ is a positive semi-definite matrix, and $\mathbf{F}$ is the so-called Fisher Information Matrix (FIM). The (i,j)th element of $\mathbf{F}$ is given by [99]

$$[\mathbf{F}]_{i,j} = \text{E}\left\{\frac{\partial L(\boldsymbol{\theta})}{\partial \theta_i} \cdot \frac{\partial L(\boldsymbol{\theta})}{\partial \theta_j}\right\}, \tag{2.85}$$

where $L(\boldsymbol{\theta})$ is the log-likelihood function of the joint multivariate pdf. From (2.84), a bound on the variance of any unbiased estimate θ_l is given by

$$\text{var}\{\hat{\theta} - \theta\} \geq [\mathbf{F}^{-1}]_{i,i}. \tag{2.86}$$

The FIM for a circularly Gaussian process with mean $\mathbf{m}(\boldsymbol{\theta})$ and covariance $\mathbf{R}_\mathbf{x}$ is given by [99]

$$[\mathbf{F}]_{i,j} = N_s \cdot \text{tr}\left\{\mathbf{R}_\mathbf{x}^{-1}\frac{\partial \mathbf{R}_\mathbf{x}}{\partial \theta_i}\mathbf{R}_\mathbf{x}^{-1}\frac{\partial \mathbf{R}_\mathbf{x}}{\partial \theta_j}\right\} + 2\text{Re}\left\{\sum_{t=1}^{N_s}\frac{\partial \mathbf{m}^H(\boldsymbol{\theta})}{\partial \theta_i}\mathbf{R}_\mathbf{x}^{-1}\frac{\partial \mathbf{m}(\boldsymbol{\theta})}{\partial \theta_j}\right\}. \tag{2.87}$$

Stochastic CRB

If the array data vector $\mathbf{x}(t)$ is defined using the stochastic signal model (c.f. 2.25), then the CRB is given by [92], [95], [99]

$$\text{CRB}(\boldsymbol{\theta}) = \frac{\sigma_n^2}{2N_s}\left\{\text{Re}\left[(\mathbf{D}^H\mathbf{P}_\mathbf{A}^\perp\mathbf{D}) \odot (\mathbf{S}\mathbf{A}^H\mathbf{R}_\mathbf{x}^{-1}\mathbf{A}\mathbf{S})^T\right]\right\}^{-1}, \tag{2.88}$$

where $\odot$ is the Schur-Hadamard (elementwise) product of two matrices and

$$\mathbf{D} = \left[\frac{\partial \mathbf{a}(\theta_1)}{\partial \theta_1}, \frac{\partial \mathbf{a}(\theta_2)}{\partial \theta_2}, \ldots, \frac{\partial \mathbf{a}(\theta_L)}{\partial \theta_L}\right]. \tag{2.89}$$

Deterministic CRB

If the array data vector $\mathbf{x}(t)$ is defined using the deterministic signal model (c.f. 2.26), then the CRB is given by [94], [95], [99]

$$\text{CRB}(\boldsymbol{\theta}) = \frac{\sigma_n^2}{2N_s}\left\{\text{Re}\left[(\mathbf{D}^H\mathbf{P}_\mathbf{A}^\perp\mathbf{D}) \odot \hat{\mathbf{S}}^T\right]\right\}^{-1}. \tag{2.90}$$

2.7 Conclusions

In this chapter, the array signal models that are commonly used in array processing have been presented. The statistical characterizations of the signals observed by sensor arrays have been provided. Both the stochastic and the deterministic signal models have been described. A concise description of several well known array processing techniques has been provided. The CRB that provides a lower bound on the performance of unbiased estimation techniques has been presented.

Chapter 3

Robust Beamspace Preprocessing for Source Localization

3.1 Introduction

Beamspace preprocessing has been widely used to reduce the problem dimension in array processing and to lower the computational burden of high-resolution direction finding algorithms [3], [4], [26], [28], [39], [53], [88], [100], [107]–[109], [115], [116]. In addition to substantial computational improvements, beamspace preprocessing is able to offer visible performance improvements such as enhanced source resolution, reduced sensitivity to array calibration errors and reduced DOA estimation bias [28], [39], [53], [108], [109], [116]. However, a significant shortcoming of the existing beamspace transformation design approaches and criteria is that they essentially ignore interfering sources that are located outside the beamspace sectors-of-interest. As a result, the robustness of conventional beamspace preprocessing techniques against such out-of-sector sources may be insufficient.

In this chapter, we propose a novel approach to beamspace preprocessing with

application to DOA estimation that has improved robustness against out-of-sector sources. The beamspace matrix is designed as a matrix filter that satisfies a certain tradeoff between the in-sector (passband) and out-of-sector (stopband) requirements[1]. Several matrix filter optimization problems are proposed based on this approach and computationally efficient convex formulations for these problems are derived using SOC programming.

Furthermore, a novel concept of *adaptive beamspace* is introduced which extends these formulations by assuming that the beamspace matrix is not necessarily fixed but can be driven by the array data. Although the proposed adaptive beamspace approach does not lead to any substantial reduction of the computational burden of direction finding methods, it offers significant improvements of the DOA estimation performance in the presence of weak in-sector signal sources observed on the background of strong out-of-sector interferers.

To further reduce the complexity of the obtained SOC programming-based beamspace design problems, we propose to replace the conventional stopband constraints with a much smaller number of parsimonious constraints without losing the quality of beamspace matrix design. The latter constraints use the idea similar to that of the spheroidal sequences approach of [26], but apply it to characterize the out-of-sector angular areas rather than the sectors-of-interest.

At the end of the chapter we provide simulation results that illustrate the robustness improvements achieved by our techniques over the traditional beamspace methods.

[1]Related formulations for the array interpolation design problem were considered in [74].

3.2 Problem Formulation

3.2.1 Elementspace Array Signal Model

Let us consider a linear array of M sensors that receive the signals from L narrowband sources. The $M \times 1$ array snapshot vector can be modeled as

$$\mathbf{x}(t) = \mathbf{x}_{\mathrm{d}}(t) + \mathbf{x}_{\mathrm{i}}(t) + \mathbf{n}(t) \tag{3.1}$$

where $\mathbf{x}_{\mathrm{d}}(t)$ is in-sector desired signal component, $\mathbf{x}_{\mathrm{i}}(t)$ is out-of-sector interfering signal component, and $\mathbf{n}(t)$ is the additive noise term. The desired signal and the interfering signal components[2] are, respectively, modeled as

$$\mathbf{x}_{\mathrm{d}}(t) = \sum_{l=1}^{L} d_l(t)\mathbf{a}(\theta_l), \tag{3.2}$$

$$\mathbf{x}_{\mathrm{i}}(t) = \sum_{l=1}^{D-L} I_l(t)\mathbf{a}(\theta_{L+l}), \tag{3.3}$$

where $\{d_l(t)\}_{l=1}^{L}$ are the waveforms of the L in-sector desired signals, $\{I_l(t)\}_{l=1}^{D-L}$ are the waveforms of the $D-L$ out-of-sector interfering signals, and

$$\mathbf{a}(\theta) = \frac{1}{\sqrt{M}}\left[1, \exp\{j\frac{h_2}{c}\omega_{\mathrm{o}}\sin\theta\}, \ldots, \exp\{j\frac{h_M}{c}\omega_{\mathrm{o}}\sin\theta\}\right]^T \tag{3.4}$$

is the unit norm steering vector associated with the direction θ.

The signal model given in (3.1) can be expressed in a more compact form as follows

$$\mathbf{x}(t) = \mathbf{A}(\boldsymbol{\theta})\mathbf{s}(t) + \mathbf{n}(t), \tag{3.5}$$

where the $D \times 1$ vector

$$\boldsymbol{\theta} \triangleq [\theta_1, \ldots, \theta_L, \theta_{L+1}, \ldots, \theta_D]^T \tag{3.6}$$

[2]Note that we assume that all desired sources are located inside the sector-of-interest while all interfering sources are located outside the sector-of-interest.

is the vector that contains the source DOAs $\{\theta_l\}_{l=1}^{D}$ and the $D \times 1$ vector

$$\mathbf{s}(t) \triangleq [d_1(t), \ldots, d_L(t), I_1(t), \ldots, I_{D-L}(t)]^T \tag{3.7}$$

is the vector that contains the signal waveforms. In (3.5), the matrix

$$\mathbf{A}(\boldsymbol{\theta}) = [\mathbf{a}(\theta_1), \ldots, \mathbf{a}(\theta_L), \mathbf{a}(\theta_{L+1}), \ldots, \mathbf{a}(\theta_D)]\,. \tag{3.8}$$

is the $M \times D$ direction matrix. The $M \times M$ array covariance matrix can be written in the familiar form (2.40), which is repeated here for convenience

$$\mathbf{R}_{\mathbf{x}} \triangleq \mathrm{E}\{\mathbf{x}(t)\mathbf{x}^H(t)\} = \mathbf{A}(\boldsymbol{\theta})\mathbf{S}\mathbf{A}^H(\boldsymbol{\theta}) + \sigma_n^2\mathbf{I},$$

where $\mathbf{S}$ is defined in (2.24).

3.2.2 Beamspace Array Signal Model

The $M' \times 1$ beamspace snapshot vector $\mathbf{z}(t)$ of a reduced dimension ($M' < M$) is defined as a linear transformation of the original (elementspace) data snapshot $\mathbf{x}(t)$ as

$$\mathbf{z}(t) = \mathbf{B}^H\mathbf{x}(t), \tag{3.9}$$

where $\mathbf{B}$ is the $M \times M'$ beamspace matrix. If $\mathbf{B}$ is not orthonormal, an additional noise prewhitening operation is required and (3.9) should be modified as

$$\mathbf{z}(t) = (\mathbf{B}^H\mathbf{B})^{-1/2}\mathbf{B}^H\mathbf{x}(t). \tag{3.10}$$

As such a noise prewhitening can be done straightforwardly after the matrix $\mathbf{B}$ is designed, this operation will be ignored in our subsequent formulations of the beamspace matrix design problem.

The $M' \times M'$ beamspace array covariance matrix is given by [28], [53], [116]

$$\begin{aligned} \mathbf{R}_{\mathbf{z}} &\triangleq \mathrm{E}\{\mathbf{z}(t)\mathbf{z}^H(t)\} \\ &= (\mathbf{B}^H\mathbf{B})^{-1/2}\mathbf{B}^H\mathbf{R}_{\mathbf{x}}\mathbf{B}(\mathbf{B}^H\mathbf{B})^{-1/2} \\ &= (\mathbf{B}^H\mathbf{B})^{-1/2}\mathbf{B}^H\mathbf{A}(\boldsymbol{\theta})\mathbf{S}\mathbf{A}^H(\boldsymbol{\theta})\mathbf{B}(\mathbf{B}^H\mathbf{B})^{-1/2} + \sigma_n^2\mathbf{I}. \end{aligned} \tag{3.11}$$

From (3.11), it can be seen that the beamspace transformation changes the array manifold as

$$\tilde{\mathbf{a}}(\theta) = (\mathbf{B}^H\mathbf{B})^{-1/2}\mathbf{B}^H\mathbf{a}(\theta), \tag{3.12}$$

where $\tilde{\mathbf{a}}(\theta)$ is the new steering vector after the beamspace transformation.

The sample estimate of (3.11) takes the following form

$$\hat{\mathbf{R}}_{\mathbf{z}} = \frac{1}{N_s}\sum_{t=1}^{N_s}\mathbf{z}(t)\mathbf{z}^H(t) = (\mathbf{B}^H\mathbf{B})^{-1/2}\mathbf{B}^H\hat{\mathbf{R}}_{\mathbf{x}}\mathbf{B}(\mathbf{B}^H\mathbf{B})^{-1/2}. \tag{3.13}$$

Note that the dimension of the matrix $\hat{\mathbf{R}}_{\mathbf{z}}$ is less than that of $\hat{\mathbf{R}}_{\mathbf{x}}$. This fact is exploited in all beamspace high-resolution direction finding methods to obtain substantial computational savings relative to the conventional (elementspace) algorithms.

3.2.3 DOA Estimation in Beamspace

Let us assume, for the time being, that the beamspace transformation given in (3.9) is ideal in the sense that the interfering signal component is completely attenuated during the transformation process. In other words, we assume that the transformed data contains only the in-sector desired signal component as well as the additive noise term. Then, the eigendecomposition of (3.11) can be written as

$$\mathbf{R}_{\mathbf{z}} = \mathbf{U}_{\mathrm{s}}\boldsymbol{\Lambda}_{\mathrm{s}}\mathbf{U}_{\mathrm{s}}^H + \mathbf{U}_{\mathrm{n}}\boldsymbol{\Lambda}_{\mathrm{n}}\mathbf{U}_{\mathrm{n}}^H, \tag{3.14}$$

where the $L \times L$ diagonal matrix $\mathbf{\Lambda}_s$ contains the largest (signal-subspace) eigenvalues and the columns of the $M' \times L$ matrix $\mathbf{U}_s$ are the corresponding eigenvectors. Similarly, the $(M'-L) \times (M'-L)$ diagonal matrix $\mathbf{\Lambda}_n$ contains the smallest (noise-subspace) eigenvalues while the $M' \times (M'-L)$ matrix $\mathbf{U}_n$ is built from the corresponding eigenvectors.

Using (3.12) and applying the principle of the elementspace MUSIC estimator [82], we obtain that the beamspace spectral-MUSIC estimator[3] can be expressed as [26], [53], [108], [109]

$$f(\theta) = \frac{\tilde{\mathbf{a}}^H(\theta)\tilde{\mathbf{a}}(\theta)}{\tilde{\mathbf{a}}^H(\theta)\mathbf{P}\tilde{\mathbf{a}}(\theta)} = \frac{\mathbf{a}^H(\theta)\mathbf{B}(\mathbf{B}^H\mathbf{B})^{-1}\mathbf{B}^H\mathbf{a}(\theta)}{\mathbf{a}^H(\theta)\mathbf{B}(\mathbf{B}^H\mathbf{B})^{-1/2}\mathbf{P}(\mathbf{B}^H\mathbf{B})^{-1/2}\mathbf{B}^H\mathbf{a}(\theta)}, \tag{3.15}$$

where

$$\begin{aligned} \mathbf{P} &\triangleq \mathbf{U}_n(\mathbf{U}_n^H\mathbf{U}_n)^{-1}\mathbf{U}_n^H \\ &= \mathbf{I} - \mathbf{U}_s(\mathbf{U}_s^H\mathbf{U}_s)^{-1}\mathbf{U}_s^H \end{aligned} \tag{3.16}$$

is the projection matrix onto the noise subspace.

3.3 Conventional Approaches to Beamspace Design

Given the beamspace angular sectors-of-interest Θ, several powerful techniques have been proposed to design the beamspace matrix $\mathbf{B}$. In this section we briefly describe two of these conventional beamspace design techniques.

[3]Throughout this chapter, we assume that the number of signals observed within the sector-of-interest is less than the dimension of the beamspace vector. That is, $L < M'$.

3.3.1 Spheroidal Sequences-Based Beamspace Preprocessing

Let $\{\mathbf{b}_m\}_{m=1}^{M'}$ be the columns of the beamspace matrix $\mathbf{B}$ that is supposed to be orthonormal. We define the energy of the mth beam within the sector-of-interest Θ as

$$\begin{aligned} \mathcal{E}_m &= \int_{\Theta} |\mathbf{b}_m^H \mathbf{a}(\theta)|^2 d\theta \\ &= \mathbf{b}_m^H \mathbf{C} \mathbf{b}_m, \quad m = 1, \ldots, M', \end{aligned} \tag{3.17}$$

where

$$\mathbf{C} = \int_{\Theta} \mathbf{a}(\theta)\mathbf{a}^H(\theta)\, d\theta. \tag{3.18}$$

The principle of the discrete prolate spheroidal sequences-based (DPSS) approach [26], [99], [100] is to maximize the ratio of the beamspace energy within Θ to the energy within $[-\pi,\ \pi]$. That is, the DPSS approach is based on maximizing

$$\Xi_m \triangleq \frac{\mathbf{b}_m^H \mathbf{C} \mathbf{b}_m}{\int_{-\pi}^{\pi} |\mathbf{b}_m^H \mathbf{a}(\theta)|^2 d\theta}, \quad m = 1, \ldots, M', \tag{3.19}$$

subject to the orthonormality constraint

$$\mathbf{B}^H \mathbf{B} = \mathbf{I}. \tag{3.20}$$

It can easily be shown that [99]

$$\int_{-\pi}^{\pi} |\mathbf{b}_m^H \mathbf{a}(\theta)|^2 d\theta = 2\pi \mathbf{b}_m^H \mathbf{b}_m. \tag{3.21}$$

Substituting (3.21) in (3.19), we have

$$\Xi_m = \frac{\mathbf{b}_m^H \mathbf{C} \mathbf{b}_m}{2\pi \mathbf{b}_m^H \mathbf{b}_m}, \quad m = 1, \ldots, M'. \tag{3.22}$$

The maximization of $\{\Xi_m\}_{m=1}^{M'}$ subject to the orthonormality constraint (3.20) corresponds to finding the eigenvectors of $\mathbf{C}$ that are associated with the largest M' eigenvectors [99].

Hence, the DPSS-based method for beamspace design can be stated as follows:

1) Build the positive definite matrix $\mathbf{C}$ as given in (3.18).

2) Form the beamspace matrix as

$$\mathbf{B} = [\mathbf{u}_1, \mathbf{u}_2, \ldots, \mathbf{u}_{M'}], \tag{3.23}$$

where $\{\mathbf{u}_i\}_{i=1}^{M'}$ are the M' principal eigenvectors of $\mathbf{C}$.

3.3.2 Optimal Dimension Reduction-Based Beamspace Preprocessing

The optimal dimension reduction (ODR) approach to the beamspace matrix design was proposed in [3]. It was shown in this paper that the element- and beamspace DOA estimation CRBs coincide if

$$\text{range}\{[\mathbf{A}(\boldsymbol{\theta}), \mathbf{D}(\boldsymbol{\theta})]\} \subseteq \text{range}\{\mathbf{B}\}, \tag{3.24}$$

where

$$\mathbf{D}(\boldsymbol{\theta}) = [\mathbf{d}(\theta_1), \ldots, \mathbf{d}(\theta_L)], \tag{3.25}$$

and

$$\mathbf{d}(\theta_l) = \frac{\partial}{\partial \theta}\mathbf{a}(\theta)|_{\theta=\theta_l} . \tag{3.26}$$

Based on this result, it was proposed in [3] to design the beamspace matrix as $\mathbf{B} = \mathbf{U}$ where $\mathbf{U\Gamma V}^H$ is the SVD of the matrix $[\mathbf{A}(\tilde{\boldsymbol{\theta}}), \mathbf{D}(\tilde{\boldsymbol{\theta}})]$. Here, the $M'/2 \times 1$ vector $\tilde{\boldsymbol{\theta}}$ captures the $M'/2$ different angles $\{\tilde{\theta}_l\}_{l=1}^{M'/2}$ which properly represent the sectors-of-interest Θ and the $M \times M'/2$ matrices $\mathbf{A}(\tilde{\boldsymbol{\theta}})$ and $\mathbf{D}(\tilde{\boldsymbol{\theta}})$ contain, respectively, the corresponding steering vectors and their derivatives.

Unfortunately, both techniques considered in this section ignore interfering sources located outside the beamspace sectors-of-interest (such sources can frequently occur in practical scenarios because not all sectors of potential interference may be known).

Therefore, the robustness of these techniques against such out-of-sector sources may be insufficient.

3.4 Beamspace Preprocessing with Stopband Constraints

To provide robustness against out-of-sector sources, let us approach the problem of beamspace matrix design as a matrix filter optimization problem.

One meaningful formulation of this problem is to upper-bound the acceptable difference between the actual and quiescent responses of the beamspace transformation within the beamspace sectors-of-interest while maximizing the worst-case out-of-sector (stopband) attenuation. The corresponding optimization problem can be written as

$$\begin{aligned} \underset{\mathbf{B}}{\text{minimize}} \quad & \max_{\bar{\theta}} \|\mathbf{B}^H \mathbf{a}(\bar{\theta})\|, \quad \forall\, \bar{\theta} \in \bar{\Theta} \\ \text{subject to} \quad & \|(\mathbf{B} - \mathbf{B}_q)^H \mathbf{a}(\theta)\| \leq \varepsilon, \quad \forall\, \theta \in \Theta, \end{aligned} \tag{3.27}$$

where $\bar{\Theta}$ combines a continuum of all out-of-sector directions (i.e., directions lying outside the sectors-of-interest Θ), $\mathbf{B}_q$ is the quiescent response beamspace matrix, and $\varepsilon > 0$ is the parameter which bounds the passband distortion of the designed beamspace matrix $\mathbf{B}$ with respect to $\mathbf{B}_q$. The choice of the parameter ε in (3.29) is determined by the required accuracy of the approximation of the quiescent response in the sector-of-interest region, and is conceptually similar to the choice of passband parameters in the classic bandpass filter design problem.

The concept of quiescent response has originally emerged in adaptive beamforming, see [99] and references therein. According to it, the matrix $\mathbf{B}_q$ corresponds to a properly designed beamspace matrix without taking into account out-of-sector

sources. For example, proper choices of the quiescent response matrix $\mathbf{B}_q$ are the matrices obtained via the conventional beamspace designs described in the previous section. In particular, the matrix (3.23) can be used as a proper choice of $\mathbf{B}_q$.

Another alternative robust approach to the beamspace matrix design is to minimize the worst-case difference between the actual and quiescent responses of the beamspace transformation within the beamspace sectors-of-interest while keeping the stopband attenuation bounded by some constant. This gives us the following optimization problem:

$$\begin{aligned} \underset{\mathbf{B}}{\text{minimize}} \quad & \max_{\theta} \|(\mathbf{B}-\mathbf{B}_q)^H \mathbf{a}(\theta)\|, \quad \forall\, \theta \in \Theta \\ \text{subject to} \quad & \|\mathbf{B}^H \mathbf{a}(\bar{\theta})\| \le \gamma, \quad \forall\, \bar{\theta} \in \bar{\Theta} \end{aligned} \tag{3.28}$$

where $\gamma > 0$ is the parameter of the user choice that characterizes the worst acceptable stopband attenuation. The choice of this parameter is conceptually similar to the choice of stopband attenuation parameters in the classic bandpass filter design problem.

Examining the optimization problem (3.27), the objective function is the maximum of an infinite set of quadratic functions in $\mathbf{B}$; one for each direction $\bar{\theta} \in \bar{\Theta}$. Also, the constraint set contains an infinite number of inequality constraints imposed at each direction $\theta \in \Theta$. The problem of representing the infinite number of quadratic functions and/or the infinite number of inequality constraints in a finite manner can be handled through direction discretization. For this purpose, several discretization techniques are available, see for example [46], [64].

Let $\bar{\theta}_k \in \bar{\Theta},\ k = 1, \ldots, K$ be the angular grid chosen (uniform or nonuniform) which approximates the stopband region $\bar{\Theta}$ by a finite number K of directions and $\theta_n \in \Theta,\ n = 1, \ldots, N$ be the angular grid chosen which approximates the sector-of-interest region Θ by a finite number N of directions. Then, the optimization problem

(3.27) can be rewritten as

$$\begin{aligned} \underset{\mathbf{B}}{\text{minimize}} \quad & \max_{k} \|\mathbf{B}^H \mathbf{a}(\bar{\theta}_k)\|, \quad \bar{\theta}_k \in \bar{\Theta}, \quad k = 1, \ldots, K \\ \text{subject to} \quad & \|(\mathbf{B} - \mathbf{B}_q)^H \mathbf{a}(\theta_n)\| \leq \varepsilon, \quad \theta_n \in \Theta, \quad n = 1, \ldots, N. \end{aligned} \tag{3.29}$$

Similarly, the optimization problem (3.28) can be expressed as

$$\begin{aligned} \underset{\mathbf{B}}{\text{minimize}} \quad & \max_{n} \|(\mathbf{B} - \mathbf{B}_q)^H \mathbf{a}(\theta_n)\|, \quad \theta_n \in \Theta, \quad n = 1, \ldots, N \\ \text{subject to} \quad & \|\mathbf{B}^H \mathbf{a}(\bar{\theta}_k)\| \leq \gamma, \quad \bar{\theta}_k \in \bar{\Theta}, \quad k = 1, \ldots, K. \end{aligned} \tag{3.30}$$

Note that, the choice of K and N is determined by the required accuracy of approximation of $\bar{\Theta}$ and Θ via the sets of discrete angles $\bar{\theta}_k$ and θ_n respectively.

3.5 Adaptive Beamspace Preprocessing

Traditional formulations of the beamspace preprocessing design problem assume that the beamspace matrix $\mathbf{B}$ does not depend on the array snapshot data (this is also true for all the approaches considered above). An obvious reason for such a convention is to make the beamspace matrix design an off-line problem. Indeed, if $\mathbf{B}$ does not depend on the array snapshot data, it can be designed in advance and does not require any updating when the new data arrive.

However, if more computationally demanding *on-line* beamspace operations are acceptable, it becomes meaningful to consider *data-adaptive* beamspace techniques because they can be designed to include additional adaptive out-of-sector interference cancellation features and, therefore, can potentially provide better performance than the off-line beamspace techniques.

Let us develop a data-adaptive formulation for the beamspace matrix design problem based on minimizing the output power of the transformed data. This power can

be written as

$$\begin{aligned} \mathrm{E}\{\mathbf{z}^H(t)\mathbf{z}(t)\} &= \mathrm{tr}\{\mathrm{E}\{\mathbf{z}(t)\mathbf{z}^H(t)\}\} \\ &= \mathrm{tr}\{\mathbf{B}^H\mathbf{R}_\mathbf{x}\mathbf{B}\}, \end{aligned} \tag{3.31}$$

where $\mathrm{tr}\{\cdot\}$ denotes the trace of a square matrix. Using (3.31), the data-adaptive beamspace matrix design problem can be formulated as

$$\begin{aligned} \underset{\mathbf{B}}{\text{minimize}} \quad & \mathrm{tr}\{\mathbf{B}^H\mathbf{R}_\mathbf{x}\mathbf{B}\} \\ \text{subject to} \quad & \|(\mathbf{B}-\mathbf{B}_\mathrm{q})^H\mathbf{a}(\theta_n)\| \le \varepsilon, \quad \theta_n \in \Theta, \quad n = 1,\ldots,N. \end{aligned} \tag{3.32}$$

In (3.32), the matrix $\mathbf{B}$ is designed by minimizing the array output power in the beamspace domain while bounding the allowable difference between the actual and quiescent beamspace response by ε. Solving this problem will cancel the out-of-sector sources while preserving (up to a small distortion characterized by ε) the sources located within the sectors-of-interest. However, the stopband attenuation in the out-of-sector areas $\bar{\Theta}$ is not controlled in (3.32) and this can lead to a severe performance degradation in the case of unexpected (i.e., suddenly appearing) interferers [9], [58]. If we additionally control the stopband attenuation, the problem (3.32) can be further modified as

$$\begin{aligned} \underset{\mathbf{B}}{\text{minimize}} \quad & \mathrm{tr}\{\mathbf{B}^H\mathbf{R}_\mathbf{x}\mathbf{B}\} \\ \text{subject to} \quad & \|(\mathbf{B}-\mathbf{B}_\mathrm{q})^H\mathbf{a}(\theta_n)\| \le \varepsilon, \quad \theta_n \in \Theta, \quad n = 1,\ldots,N \\ & \|\mathbf{B}^H\mathbf{a}(\bar{\theta}_k)\| \le \gamma, \quad \bar{\theta}_k \in \bar{\Theta}, \quad k = 1,\ldots,K. \end{aligned} \tag{3.33}$$

In practical applications, the true covariance matrix $\mathbf{R}_\mathbf{x}$ should be replaced in (3.32) and (3.33) by the sample matrix $\hat{\mathbf{R}}_\mathbf{x}$ (where $\hat{\mathbf{R}}_\mathbf{x}$ may be updated whenever a new snapshot is received).

Although the parameters ε and γ in (3.33) have the same meaning as in (3.29) and (3.30), an important difference is that the problems in (3.29) and (3.30) remain

feasible for any choice of ε and γ , respectively, whereas not any choice of these parameters leads to a feasible problem in (3.33). Therefore, the values of ε and γ should be jointly adjusted off-line to warrant feasibility, and, at the same time, to obtain an acceptable tradeoff between the stopband and passband requirements.

Although the formulations (3.29), (3.30), (3.32) and (3.33) all lead to the beamspace designs that are expected to provide an improved robustness against out-of-sector interferers, the question that remains is whether these optimization problems can be efficiently solved. This question is answered in the next section where we show that (3.29), (3.30), (3.32) and (3.33) can be reformulated as convex SOC programming problems that can be efficiently solved using interior point algorithms [96].

3.6 SOC Programming-Based Implementations

In this section, we will derive the SOC formulations of the optimization problems (3.29), (3.30), (3.32) and (3.33). Note that (3.32) is a specific case of (3.33) and, therefore, the problem (3.32) is not considered in the sequel.

Preliminaries

The dual standard form of the convex SOC program can be written as [96]

$$\begin{aligned} \underset{\mathbf{y}}{\text{maximize}} \quad & \mathbf{p}^T\mathbf{y} \\ \text{subject to} \quad & \mathbf{c}_i - \mathbf{F}_i^T\mathbf{y} \in \text{SOC}^{q_i}, \quad i = 1, \ldots, J, \end{aligned} \tag{3.34}$$

where $\mathbf{F}_i$ are arbitrary real-valued matrices, $\mathbf{p}$ and $\mathbf{c}_i$ are arbitrary real-valued vectors, the real-valued vector $\mathbf{y}$ contains the design variables, J is the number of SOC constraints, and q_i is the dimension of the ith SOC that is defined as

$$\text{SOC}^{q_i} = \{\boldsymbol{\xi} \in \mathbb{R} \times \mathbb{R}^{(q_i-1)} \mid \xi \geq \|\tilde{\boldsymbol{\xi}}\|\},$$

where

$$\begin{aligned} \boldsymbol{\xi} &= [\xi, \tilde{\boldsymbol{\xi}}^T]^T \\ &= \mathbf{c}_i - \mathbf{F}_i^T \mathbf{y}, \\ \tilde{\boldsymbol{\xi}} &= [\xi_2, \xi_3, \ldots, \xi_{q_i}]^T. \end{aligned} \tag{3.35}$$

Let us introduce the notations

$$\mathbf{b} = \text{vec}\{\mathbf{B}^H\},$$

where vec$\{\cdot\}$ denotes the vectorization operator stacking the columns of a matrix on top of each other. The following property for arbitrary matrices $\mathbf{X}$, $\mathbf{Y}$ and $\mathbf{Z}$ of matching dimensions will be frequently used throughout the text:

$$\text{vec}\{\mathbf{XYZ}\} = (\mathbf{Z}^T \otimes \mathbf{X})\text{vec}\{\mathbf{Y}\}, \tag{3.36}$$

where $\otimes$ denotes the Kronecker matrix product.

SOC Formulation of Problem (3.29)

Making use of (3.36) we obtain

$$\mathbf{B}^H \mathbf{a}(\bar{\theta}_k) = (\mathbf{a}^T(\bar{\theta}_k) \otimes \mathbf{I})\mathbf{b} \tag{3.37}$$

and

$$(\mathbf{B} - \mathbf{B}_q)^H \mathbf{a}(\theta_n) = (\mathbf{a}^T(\bar{\theta}_n) \otimes \mathbf{I})\mathbf{b} - \tilde{\mathbf{a}}(\theta_n), \tag{3.38}$$

where

$$\tilde{\mathbf{a}}(\theta_n) = \mathbf{B}_q^H \mathbf{a}(\theta_n). \tag{3.39}$$

Using (3.37) and (3.38), we can reformulate (3.29) as

$$\begin{aligned} \underset{\mathbf{b}}{\text{minimize}} \quad & \max_k \|(\mathbf{a}^T(\bar{\theta}_k) \otimes \mathbf{I})\mathbf{b}\|, \quad \bar{\theta}_k \in \bar{\Theta}, \quad k = 1, \ldots, K \\ \text{subject to} \quad & \|(\mathbf{a}^T(\theta_n) \otimes \mathbf{I})\mathbf{b} - \tilde{\mathbf{a}}(\theta_n)\| \leq \varepsilon, \quad \theta_n \in \Theta, \quad n = 1, \ldots, N. \end{aligned} \tag{3.40}$$

Introducing a new auxiliary variable τ, we can rewrite (3.40) as

$$\begin{aligned} \underset{\tau,\mathbf{b}}{\text{maximize}} \quad & \tau \\ \text{subject to} \quad & \|(\mathbf{a}^T(\bar{\theta}_k) \otimes \mathbf{I})\mathbf{b}\| \leq -\tau, \quad \bar{\theta}_k \in \bar{\Theta}, \quad k = 1, \ldots, K \\ & \|(\mathbf{a}^T(\theta_n) \otimes \mathbf{I})\mathbf{b} - \tilde{\mathbf{a}}(\theta_n)\| \leq \varepsilon, \quad \theta_n \in \Theta, \quad n = 1, \ldots, N. \end{aligned} \tag{3.41}$$

This problem can be further reformulated in terms of real-valued variables. Let $(\cdot)_r$ and $(\cdot)_i$ hereafter denote the real and imaginary parts of a matrix/vector, respectively. Defining the vectors

$$\mathbf{p} \triangleq [1, 0, \ldots, 0]^T, \tag{3.42}$$

$$\mathbf{y} \triangleq [\tau, (\mathbf{b}^T)_r, (\mathbf{b}^T)_i]^T, \tag{3.43}$$

$$\mathbf{c}_k \triangleq [0, 0, \ldots, 0]^T, \quad k = 1, \ldots, K, \tag{3.44}$$

$$\mathbf{c}_n \triangleq [\varepsilon, (\tilde{\mathbf{a}}^T(\theta_n))_r, (\tilde{\mathbf{a}}^T(\theta_n))_i]^T, \quad n = 1, \ldots, N, \tag{3.45}$$

and the matrices

$$\mathbf{F}_k^T \triangleq \begin{bmatrix} 1 & \mathbf{0}^T & \mathbf{0}^T \\ \mathbf{0} & (\mathbf{a}^T(\bar{\theta}_k) \otimes \mathbf{I})_r & -(\mathbf{a}^T(\bar{\theta}_k) \otimes \mathbf{I})_i \\ \mathbf{0} & (\mathbf{a}^T(\bar{\theta}_k) \otimes \mathbf{I})_i & (\mathbf{a}^T(\bar{\theta}_k) \otimes \mathbf{I})_r \end{bmatrix}, \quad k = 1, \ldots, K, \tag{3.46}$$

$$\mathbf{F}_n^T \triangleq \begin{bmatrix} 0 & \mathbf{0}^T & \mathbf{0}^T \\ \mathbf{0} & (\mathbf{a}^T(\theta_n) \otimes \mathbf{I})_r & -(\mathbf{a}^T(\theta_n) \otimes \mathbf{I})_i \\ \mathbf{0} & (\mathbf{a}^T(\theta_n) \otimes \mathbf{I})_i & (\mathbf{a}^T(\theta_n) \otimes \mathbf{I})_r \end{bmatrix}, \quad n = 1, \ldots, N, \tag{3.47}$$

we can rewrite (3.41) as the following SOC programming problem:

$$\begin{aligned} \underset{\mathbf{y}}{\text{maximize}} \quad & \mathbf{p}^T\mathbf{y} \\ \text{subject to} \quad & \mathbf{c}_k - \mathbf{F}_k^T\mathbf{y} \in \text{SOC}^{2M'+1}, \quad k = 1, \ldots, K \\ & \mathbf{c}_n - \mathbf{F}_n^T\mathbf{y} \in \text{SOC}^{2M'+1}, \quad n = 1, \ldots, N. \end{aligned} \tag{3.48}$$

SOC Formulation of Problem (3.30)

Making use of (3.37) and (3.38), we can reformulate (3.30) as

$$\begin{aligned} \underset{\tau,\mathbf{b}}{\text{maximize}} \quad & \tau \\ \text{subject to} \quad & \|(\mathbf{a}^T(\bar{\theta}_k)\otimes\mathbf{I})\mathbf{b}\| \le \gamma, \quad \forall\,\bar{\theta}_k \in \bar{\Theta}, \quad k=1,\ldots,K \\ & \|(\mathbf{a}^T(\theta_n)\otimes\mathbf{I})\mathbf{b} - \tilde{\mathbf{a}}(\theta_n)\| \le -\tau, \quad \forall\,\theta_n \in \Theta, \quad n=1,\ldots,N. \end{aligned} \tag{3.49}$$

Redefining the vectors $\mathbf{c}_k$ $(k=1,\ldots,K)$ and $\mathbf{c}_n$ $(n=1,\ldots,N)$ as

$$\mathbf{c}_k \triangleq [\gamma, 0, \ldots, 0]^T, \quad k=1,\ldots,K, \tag{3.50}$$

$$\mathbf{c}_n \triangleq [0, (\tilde{\mathbf{a}}^T(\theta_n))_r, (\tilde{\mathbf{a}}^T(\theta_n))_i]^T, \quad n=1,\ldots,N, \tag{3.51}$$

and the matrices $\mathbf{F}_k$ $(k=1,\ldots,K)$ and $\mathbf{F}_n$ $(n=1,\ldots,N)$ as

$$\mathbf{F}_k^T \triangleq \begin{bmatrix} 0 & \mathbf{0}^T & \mathbf{0}^T \\ \mathbf{0} & (\mathbf{a}^T(\bar{\theta}_k)\otimes\mathbf{I})_r & -(\mathbf{a}^T(\bar{\theta}_k)\otimes\mathbf{I})_i \\ \mathbf{0} & (\mathbf{a}^T(\bar{\theta}_k)\otimes\mathbf{I})_i & (\mathbf{a}^T(\bar{\theta}_k)\otimes\mathbf{I})_r \end{bmatrix}, \quad k=1,\ldots,K, \tag{3.52}$$

$$\mathbf{F}_n^T \triangleq \begin{bmatrix} 1 & \mathbf{0}^T & \mathbf{0}^T \\ \mathbf{0} & (\mathbf{a}^T(\theta_n)\otimes\mathbf{I})_r & -(\mathbf{a}^T(\theta_n)\otimes\mathbf{I})_i \\ \mathbf{0} & (\mathbf{a}^T(\theta_n)\otimes\mathbf{I})_i & (\mathbf{a}^T(\theta_n)\otimes\mathbf{I})_r \end{bmatrix}, \quad n=1,\ldots,N, \tag{3.53}$$

we can rewrite (3.49) as the following SOC programming problem

$$\begin{aligned} \underset{\mathbf{y}}{\text{maximize}} \quad & \mathbf{p}^T\mathbf{y} \\ \text{subject to} \quad & \mathbf{c}_k - \mathbf{F}_k^T\mathbf{y} \in \text{SOC}^{2M'+1}, \quad k=1,\ldots,K \\ & \mathbf{c}_n - \mathbf{F}_n^T\mathbf{y} \in \text{SOC}^{2M'+1}, \quad n=1,\ldots,N. \end{aligned} \tag{3.54}$$

SOC Formulation of Problem (3.33)

Using (3.36) and the properties of the Frobenius norm, we can reformulate the objective function in (3.33) as

$$\begin{aligned} \mathrm{tr}\{\mathbf{B}^H\mathbf{R}_x\mathbf{B}\} &= \mathrm{tr}\{\mathbf{B}^H\mathbf{G}\mathbf{G}\mathbf{B}\} \\ &= \|\mathbf{B}^H\mathbf{G}\|_{\mathrm{F}}^2 \\ &= \|\mathrm{vec}\{\mathbf{I}\mathbf{B}^H\mathbf{G}\}\|^2 \\ &= \|(\mathbf{G}^T \otimes \mathbf{I})\mathbf{b}\|^2, \end{aligned} \tag{3.55}$$

where $\mathbf{G} \triangleq \mathbf{R}_x^{1/2}$. Noting that minimizing $\|(\mathbf{G}^T \otimes \mathbf{I})\mathbf{b}\|^2$ is equivalent to minimizing $\|(\mathbf{G}^T \otimes \mathbf{I})\mathbf{b}\|$ and making use of (3.37) and (3.38), we can reformulate (3.33) as

$$\begin{aligned} \underset{\tau,\mathbf{b}}{\text{maximize}} \quad & \tau \\ \text{subject to} \quad & \|(\mathbf{a}^T(\theta_n) \otimes \mathbf{I})\mathbf{b} - \tilde{\mathbf{a}}(\theta_n)\| \le \varepsilon, \quad \forall \theta_n \in \Theta, \quad n = 1, \ldots, N \\ & \|(\mathbf{a}^T(\bar{\theta}_k) \otimes \mathbf{I})\mathbf{b}\| \le \gamma, \quad \forall \bar{\theta}_k \in \bar{\Theta}, \quad k = 1, \ldots, K \\ & \|(\mathbf{G}^T \otimes \mathbf{I})\mathbf{b}\| \le -\tau. \end{aligned} \tag{3.56}$$

Redefine the vectors $\mathbf{c}_n$ $(n = 1, \ldots, N)$ and $\mathbf{c}_k$ $(k = 1, \ldots, K+1)$ as

$$\mathbf{c}_n \triangleq [\varepsilon, (\tilde{\mathbf{a}}^T(\theta_n))_r, (\tilde{\mathbf{a}}^T(\theta_n))_i]^T, \quad n = 1, \ldots, N, \tag{3.57}$$

$$\mathbf{c}_k \triangleq [\gamma, 0, \ldots, 0]^T, \quad k = 1, \ldots, K, \tag{3.58}$$

$$\mathbf{c}_{K+1} \triangleq [0, 0, \ldots, 0]^T. \tag{3.59}$$

We also redefine the matrices $\mathbf{F}_n$ $(n = 1, \ldots, N)$ as

$$\mathbf{F}_n^T \triangleq \begin{bmatrix} 0 & \mathbf{0}^T & \mathbf{0}^T \\ \mathbf{0} & (\mathbf{a}^T(\theta_n) \otimes \mathbf{I})_r & -(\mathbf{a}^T(\theta_n) \otimes \mathbf{I})_i \\ \mathbf{0} & (\mathbf{a}^T(\theta_n) \otimes \mathbf{I})_i & (\mathbf{a}^T(\theta_n) \otimes \mathbf{I})_r \end{bmatrix}, \quad n = 1, \ldots, N, \tag{3.60}$$

and the matrices $\mathbf{F}_k$ $(k = 1, \ldots, K+1)$ as

$$\mathbf{F}_k^T \triangleq \begin{bmatrix} 0 & \mathbf{0}^T & \mathbf{0}^T \\ \mathbf{0} & (\mathbf{a}^T(\bar{\theta}_k) \otimes \mathbf{I})_r & -(\mathbf{a}^T(\bar{\theta}_k) \otimes \mathbf{I})_i \\ \mathbf{0} & (\mathbf{a}^T(\bar{\theta}_k) \otimes \mathbf{I})_i & (\mathbf{a}^T(\bar{\theta}_k) \otimes \mathbf{I})_r \end{bmatrix}, \quad k = 1, \ldots, K, \tag{3.61}$$

$$\mathbf{F}_{K+1}^T \triangleq \begin{bmatrix} 1 & \mathbf{0}^T & \mathbf{0}^T \\ \mathbf{0} & (\mathbf{G}^T \otimes \mathbf{I})_r & -(\mathbf{G}^T \otimes \mathbf{I})_i \\ \mathbf{0} & (\mathbf{G}^T \otimes \mathbf{I})_i & (\mathbf{G}^T \otimes \mathbf{I})_r \end{bmatrix}, \tag{3.62}$$

we can rewrite (3.56) as the following SOC programming problem

$$\begin{aligned} \underset{\mathbf{y}}{\text{maximize}} \quad & \mathbf{p}^T\mathbf{y} \\ \text{subject to} \quad & \mathbf{c}_n - \mathbf{F}_n^T\mathbf{y} \in \text{SOC}^{2M'+1}, \quad n = 1, \ldots, N \\ & \mathbf{c}_k - \mathbf{F}_k^T\mathbf{y} \in \text{SOC}^{2M'+1}, \quad k = 1, \ldots, K \\ & \mathbf{c}_{K+1} - \mathbf{F}_{K+1}^T\mathbf{y} \in \text{SOC}^{2MM'+1}. \end{aligned} \tag{3.63}$$

The derived SOC problems (3.48), (3.54), and (3.63) can be efficiently solved using modern interior point algorithms [96].

Computational Complexity

The number of iterations required to solve the SOC problem (3.34) using the interior-point method is bounded by $O(\sqrt{J})$ [65]. The computational complexity associated with each iteration is of $O(n^2 \sum_{i=1}^{J} q_i)$ [59], [65], where n is the number of design variables contained in $\mathbf{y}$. For each of the SOC programming problems (3.48), (3.54), and (3.63), the number of design variables is $n = M'M$. Hence, the worst-case computational load will be of $O((M'\zeta)^{3.5})$, where $\zeta = \max\{M, (K+N)\}$.

It is worth mentioning that the optimization problems (3.48), (3.54), and (3.63) involve sparse matrices. Obviously, this sparsity can be further exploited to reduce

the computational burden of solving these problems.

3.7 Parsimonious Formulations of Quadratic Inequality Constraints

In the interest of better stopband attenuation accuracy, the number of inequality constraints K in (3.29), (3.30) and (3.33) should be as large as possible. At the same time, in the interest of low computational complexity of the resulting SOC programs, K should be reduced as much as possible. Therefore, in practice the parameter K should be obtained by finding some desired tradeoff between the complexity and accuracy. In this section, we propose an approach that allows us to reduce the number of inequality constraints (the complexity) substantially without greatly affecting the accuracy of stopband attenuation in the obtained SOC programming-based matrix filter design problems. We use the idea similar to that of the spheroidal sequences approach [26] but apply it to characterize the out-of-sector angular areas rather than the sectors-of-interest. Towards this end, let us introduce a Hermitian positive definite matrix

$$\bar{\mathbf{C}} = \int_{\bar{\Theta}} \mathbf{a}(\theta)\mathbf{a}^H(\theta)\, d\theta. \tag{3.64}$$

The eigendecomposition of (3.64) can be written as

$$\bar{\mathbf{C}} = \mathbf{Q}\boldsymbol{\Delta}\mathbf{Q}^H, \tag{3.65}$$

where $\boldsymbol{\Delta} = \text{diag}\{\delta_1, \delta_2, \ldots, \delta_M\}$ is the $M \times M$ diagonal matrix of the eigenvalues of $\bar{\mathbf{C}}$ (which are positive and assumed to be sorted in the descending order as $\delta_1 \geq \delta_2 \cdots \geq \delta_M$) and $\mathbf{Q} = [\mathbf{q}_1, \ldots, \mathbf{q}_M]$ is the $M \times M$ matrix of the corresponding unit-norm eigenvectors.

We propose to replace the K inequality constraints

$$\|\mathbf{B}^H\mathbf{a}(\bar{\theta}_k)\| \leq \gamma, \quad k = 1, \ldots, K \tag{3.66}$$

by a substantially smaller number P ($P \leq M$) of the spheroidal sequences-based constraints

$$\|\mathbf{B}^H\mathbf{q}_p\| \leq \gamma, \quad p = 1, \ldots, P. \tag{3.67}$$

We also propose to replace the N inequality constraints

$$\|(\mathbf{B} - \mathbf{B}_\mathrm{q})^H\mathbf{a}(\theta_n)\| \leq \varepsilon, \quad n = 1, \ldots, N \tag{3.68}$$

by a single constraint that is given by

$$\|\mathbf{B} - \mathbf{B}_\mathrm{q}\|_\mathrm{F} \leq \varepsilon. \tag{3.69}$$

With such new set of constraints, we can rewrite the problems (3.29) and (3.30) as

$$\begin{aligned} \underset{\mathbf{B}}{\text{minimize}} \quad & \max_p \|\mathbf{B}^H\mathbf{q}_p\|, \quad p = 1, \ldots, P \\ \text{subject to} \quad & \|\mathbf{B} - \mathbf{B}_\mathrm{q}\|_\mathrm{F} \leq \varepsilon, \end{aligned} \tag{3.70}$$

and

$$\begin{aligned} \underset{\mathbf{B}}{\text{minimize}} \quad & \|\mathbf{B} - \mathbf{B}_\mathrm{q}\|_\mathrm{F} \\ \text{subject to} \quad & \|\mathbf{B}^H\mathbf{q}_p\| \leq \gamma, \quad p = 1, \ldots, P \end{aligned} \tag{3.71}$$

respectively. Similarly, the problems (3.32) and (3.33) can be rewritten as

$$\begin{aligned} \underset{\mathbf{B}}{\text{minimize}} \quad & \mathrm{tr}\{\mathbf{B}^H\mathbf{R}_\mathbf{x}\mathbf{B}\} \\ \text{subject to} \quad & \|\mathbf{B} - \mathbf{B}_\mathrm{q}\|_\mathrm{F} \leq \varepsilon, \end{aligned} \tag{3.72}$$

and

$$\begin{aligned} \underset{\mathbf{B}}{\text{minimize}} \quad & \mathrm{tr}\{\mathbf{B}^H\mathbf{R}_\mathbf{x}\mathbf{B}\} \\ \text{subject to} \quad & \|\mathbf{B} - \mathbf{B}_\mathrm{q}\|_\mathrm{F} \leq \varepsilon, \\ & \|\mathbf{B}^H\mathbf{q}_p\| \leq \gamma, \quad p = 1, \ldots, P, \end{aligned} \tag{3.73}$$

respectively.

Note that the forms of SOC programming implementations of the problems (3.70)-(3.73) are similar to that of the problems (3.29), (3.30),(3.32), and (3.33), respectively. However, provided that $P \ll K$ is chosen, the SOC programs corresponding to (3.70), (3.71), and (3.73) have much lower computational burden than the SOC programs (3.48), (3.54), and (3.63).

3.8 Simulation Results

Throughout our simulations, we assume a ULA of $M = 16$ omnidirectional sensors spaced half a wavelength apart. The beamspace dimension $M' = 4$ and the number of snapshots $N_s = 400$ are taken. The conventional beamspace design approaches described in Section 3.3 are compared with the robust techniques based on (3.29), (3.30), (3.32), and (3.33) (and in some examples, with their parsimonious modifications (3.70)-(3.73)). All robust techniques have been implemented using the SOC programs derived in Section 3.6. In all examples, the matrix $\mathbf{B}_q$ is calculated using the spheroidal sequences-based method (3.23). That is, the matrix $\mathbf{B}_q$ is orthonormal and $\|\mathbf{B}_q\|_F^2 = M'$. The SeDuMi convex optimization MATLAB toolbox (e.g. [96]) has been used to solve the corresponding convex SOC programming problems.

3.8.1 Example 1: Beamspace Attenuation Gain

In the first example, we assume that there are two signals-of-interest with the DOAs $\theta_1 = 16°$ and $\theta_2 = 18°$ and two out-of-sector (interfering) sources located at $\theta_3 = -20°$ and $\theta_4 = -5°$. The signal and interfering sources have the SNR equal to -10 dB and the interference-to-noise ratio (INR) equal to 40 dB, respectively. In this example, the sector-of-interest area is $\Theta = [10°, 25°]$ while the out-of-sector area is

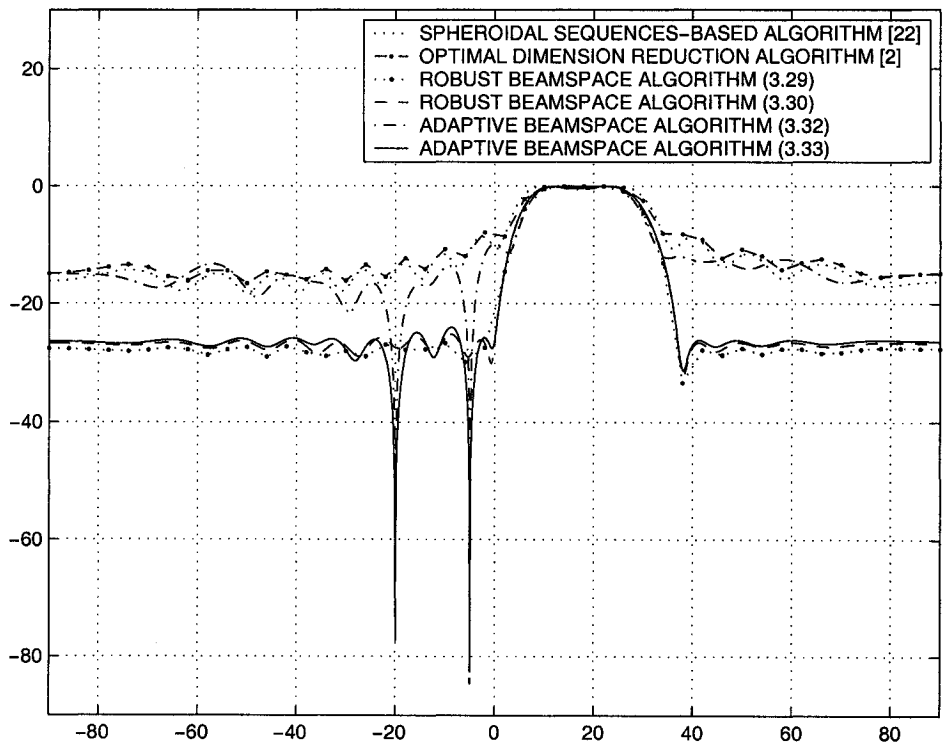

Figure 3.1: Beamspace attenuation versus angle; first example.

$\bar{\Theta} = [-90°, 0°] \cup [35°, 90°]$. A uniform grid is used to obtain the angles $\{\theta_n\}_{n=1}^{N}$ with $N = 100$ and $\{\bar{\theta}_k\}_{k=1}^{K}$ with $K = 100$. The parameters $\varepsilon = 1.0$ and $\gamma = 0.166$ have been chosen to warrant feasibility[4] of the problem (3.33). Figure 3.1 displays the beamspace attenuation

$$g(\theta) \triangleq \frac{\|\mathbf{B}^H\mathbf{a}(\theta)\|^2}{\|\mathbf{a}(\theta)\|^2} = \frac{\mathbf{a}^H(\theta)\mathbf{B}\mathbf{B}^H\mathbf{a}(\theta)}{\mathbf{a}^H(\theta)\mathbf{a}(\theta)} \tag{3.74}$$

for different beamspace design methods. In this figure, the function (3.74) is normalized to its maximal value. From this figure, it can be clearly seen that the proposed robust beamspace design methods provide better out-of-sector attenuation than the

[4]Note that the optimization problems (3.29) and (3.30) are always feasible regardless of the choice of the values of ε and γ.

conventional beamspace design methods. Moreover, it can be seen that the adaptive beamspace method further attenuates the interfering sources by means of providing deep nulls towards their directions. In particular, the adaptive beamspace method with stopband constraints (3.33) is not only robust against out-of-sector interfering sources but also robust against sensor noise as it provides deep nulls towards the interfering sources directions while at the mean time it provides low sidelobe levels over the whole out-of-sector areas.

3.8.2 Example 2: DOA Estimation RMSEs Versus INR

In the second example, we have chosen the same scenario as before but fix the SNR at 0 dB and vary the INR and compare the performance of the elementspace MUSIC estimator [82] and the beamspace MUSIC DOA estimator (3.15) that is computed using different conventional and robust beamspace matrix designs[5]. The root-mean-square errors (RMSEs) of these algorithms versus the INR are shown in Figure 3.2. In this figure, the RMSE curves are averaged over the signal sources and over 1000 independent simulation runs. For all beamspace MUSIC algorithms, the dimension of the signal subspace is assumed to be equal to two (unless otherwise is noted). As beamspace MUSIC makes use of the information about the signal source sectors and elementspace MUSIC does not, we make our comparison of these two techniques more fair by taking the dimension of the elementspace signal subspace equal to four, while restricting the elementspace MUSIC search to the sector-of-interest, provided that there is a sufficient number of maxima in this sector. Otherwise, the search in the whole field-of-view ([-90, 90]) is used.

Figure 3.3 displays the probabilities of source resolution versus INR for the same

[5]As all the compared beamspace approaches apply to the general (nonuniform) linear array case, spectral-MUSIC is used for comparisons rather then root-MUSIC.

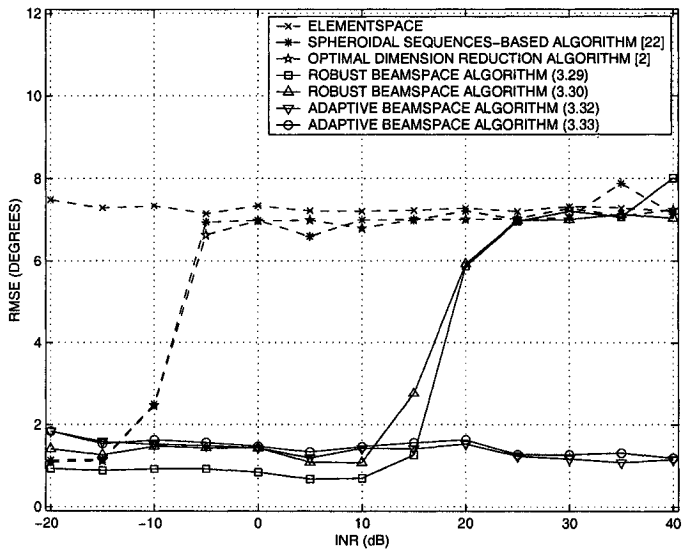

Figure 3.2: DOA estimation RMSEs versus INR; second example.

example and the same methods tested. Similar to Figure 3.2, all curves are averaged over both signal sources and 1000 simulation runs. The signal sources are said to be resolved in the lth run if [28]

$$\sum_{i=1}^{2} |\hat{\theta}_i(l) - \theta_i| < |\theta_1 - \theta_2|,$$

where $\hat{\theta}_i(l)$ is the DOA estimate of the ith source in the lth run. From Figures 3.2 and 3.3 it can be seen that in the example tested, the beamspace MUSIC algorithms using the proposed robust beamspace designs have much better robustness against out-of-sector interference than the conventional beamspace MUSIC methods. They also perform much better than the elementspace MUSIC which in this scenario has quite poor performance at any INR simply because the value of SNR = 0 dB is below the elementspace SNR threshold. Among the robust beamspace design-based algorithms, MUSIC based on the data-adaptive beamspace matrix design has the best performance. Indeed, the performance of the latter algorithm is similar to that

without any interferers for all the values of INR tested. Such a high robustness against strong out-of-sector sources is due to the adaptive interference cancellation feature of this approach.

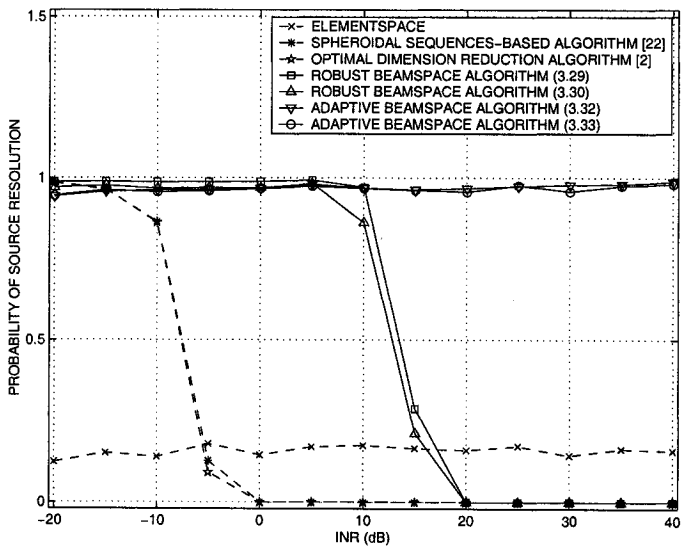

Figure 3.3: Probabilities of source resolution versus INR; second example.

3.8.3 Example 3: DOA Estimation RMSEs Versus SNR

In our third example, the INR is fixed to 20 dB while the SNR varies. All other parameters of the scenario tested are the same as in the previous example. The experimental RMSEs and probabilities of source resolution are displayed versus the SNR in Figures 3.4 and 3.5, respectively. From these figures, we observe that, similar to the previous example, the MUSIC DOA estimators based on the proposed robust beamspace designs have much better robustness against out-of-sector sources than the MUSIC estimators based on the conventional beamspace designs. Interestingly,

in this example the elementspace MUSIC has better asymptotic and threshold performance than all non-adaptive beamspace methods. This fact can be explained by a relatively high value of INR taken in this example. However, it is noteworthy that the data-adaptive beamspace design-based MUSIC estimator has substantially lower SNR threshold than the elementspace MUSIC technique. Furthermore, it can be seen from Figure 3.4 that the asymptotic (high SNR) performances of these two estimators are nearly identical. This fact provides a strong motivation to use and further develop data-adaptive methods of beamspace design.

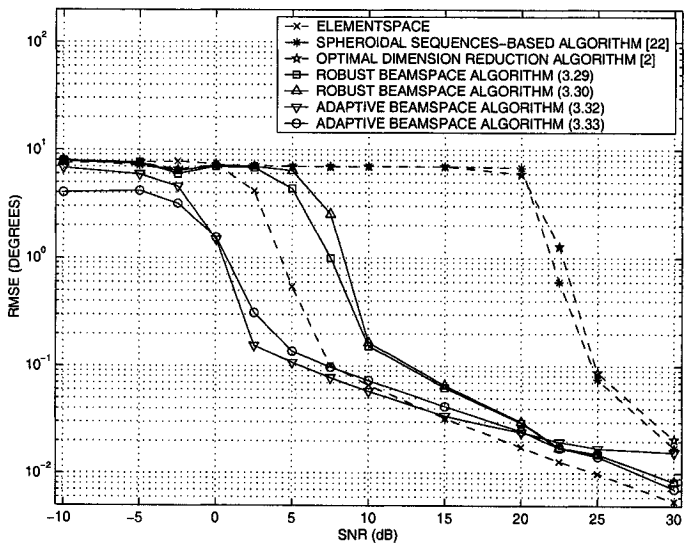

Figure 3.4: DOA estimation RMSEs versus SNR; third example.

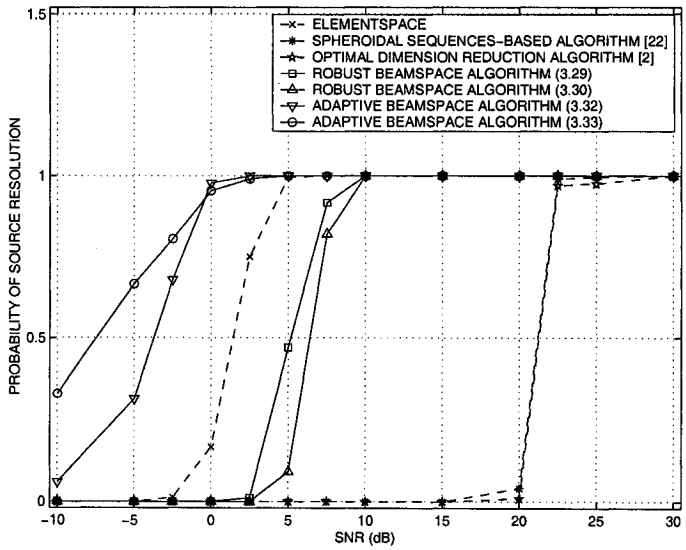

Figure 3.5: Probabilities of source resolution versus SNR; third example.

3.8.4 Example 4: Parsimonious Versus Non-parsimonious Beamspace Methods

In our fourth example, we compare the performances of the non-parsimonious (equations (3.29)-(3.30) and (3.32)-(3.33)) and parsimonious (equations (3.70)-(3.73)) approaches to robust beamspace design. In this example, we assume that the sectors-of-interest area is $\Theta = [-10^\circ\ 10^\circ]$ and the out-of-sectors area is $\bar{\Theta} = [-90^\circ, -20^\circ] \cup [20^\circ, 90^\circ]$. We assume that there is one interfering source that impinges on the array from the DOA $\theta = -40^\circ$ with INR = 40 dB. The sources of interest are assumed to be absent. The parameters $\varepsilon = 1.0$ and $\gamma = 0.0866$ are used for all methods.

Figure 3.6 shows the beamspace attenuation (3.74) of the robust beamspace design methods tested with the non-parsimonious type of constraints. In that figure, a total of $N = 16$ and $K = 16$ inequality constraints are used to control the pass-band distortion and the out-of-sector attenuation level respectively. Figure 3.7 shows

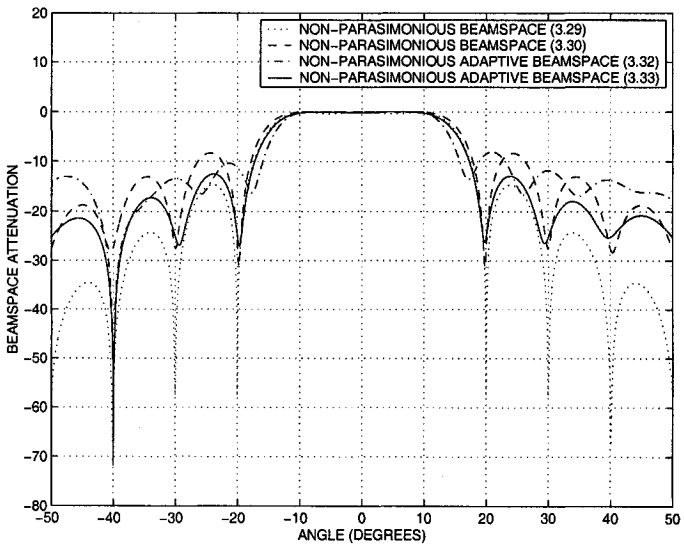

Figure 3.6: Beamspace attenuation versus angle non-parsimonious robust beamspace design methods ($K = 16$ and $N = 16$); fourth example.

the beamspace attenuation of the robust beamspace design methods tested with the parsimonious type of constraints where only a total of $P = 12$ inequality constraints are used to control the out-of-sector attenuation level. Note that the computational complexities required to produce Figures 3.6 and 3.7 are of the same order. It can be observed from these figures that the methods with parsimonious constraints perform much better than that with non-parsimonious constraints in having more firm out-of-sector attenuation control[6]. Therefore, the parsimonious constraints-based beamspace methods should be preferred to the non-parsimonious ones.

[6]Note that the out-of-sector attenuation of the methods with non-parsimonious constraints can be improved by increasing the value of the parameters K and N. However, this improvement will be at the price of increased computational complexity.

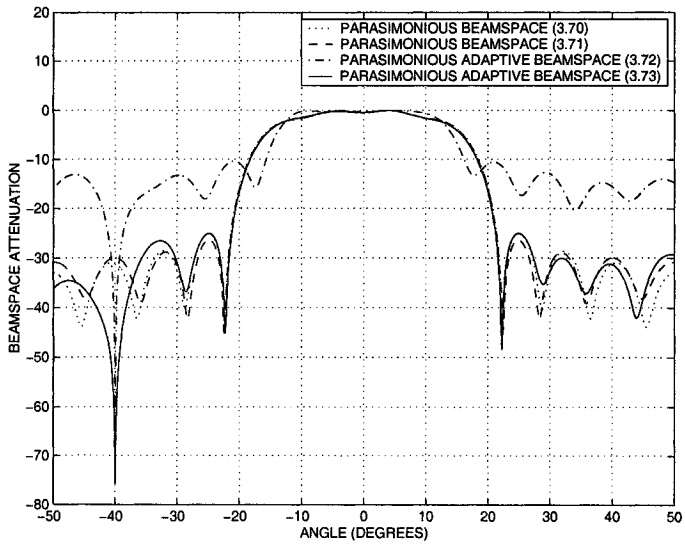

Figure 3.7: Beamspace attenuation versus angle for parsimonious robust beamspace design methods ($P = 12$); fourth example.

3.9 Conclusions

In this chapter, a new approach to beamspace preprocessing with a substantially improved robustness against out-of-sector sources has been developed. Our techniques design the beamspace matrix filter based on proper tradeoffs between the in-sector (passband) source distortion and out-of-sector (stopband) source attenuation. Moreover, the novel concept of adaptive beamspace preprocessing that offers a significant improvement in the DOA estimation performance has been introduced. Convex optimization formulations of such robust beamspace matrix filter design problems have been proposed using SOC programming. Simulation results have been provided to validate robustness of the proposed techniques.

Chapter 4

Localization of Spatially Spread Sources

4.1 Introduction

Most of conventional direction finding techniques are based on the assumption that the source energy is concentrated at discrete angles which are referred to as the source DOAs. However, in several applications such as sonar, radar and wireless communications, such a point source assumption can be irrelevant because signal scattering phenomena may result in angular spreading of the source energy [11], [13], [14], [63], [68], [69], [77], [85], [90], [98], [112]. In such cases, a *distributed source model* is more realistic than the point source one.

In wireless communication systems with antenna arrays at base stations, one of the central problems is the fast fading due to a local scattering in the vicinity of the mobile [68], [69], [112]. In the presence of such fading, the source can no longer be modeled using the point assumption. In particular, depending on the environment of the mobile, the base-mobile distance and the base station height, angular spreads up

to 10° can be commonly observed in practice [68], [69]. Depending on the relationship between the channel coherency time and the observation period, the sources can be viewed either as coherently distributed (CD) or incoherently distributed (ID) sources. A source is called CD if the signal components arriving from different directions are replicas of the same signal, while in the ID source case, all signals coming from different directions are assumed to be uncorrelated [85], [86], [98]. Indeed, if the channel coherency time is much smaller than the observation period, then the ID model is relevant [85]. In the opposite case, if the channel coherency time is comparable to the observation period, then the CD model or a partially coherent model can be used [77].

Furthermore, source localization in the presence of angular spreading (or, equivalently multiplicative noise) is one of the main problems in SAR interferometry (see [34], [60], [78] and references therein). This problem arises when different height contributions collapse in the same range-azimuth resolution cell, due to the presence of strong terrain slopes or discontinuities in the sensed scene [34]. Again, in such cases, the *distributed source* model is more appropriate than the point source one.

Recently, ID source localization has been a focus of intensive research. Many techniques have been developed for scenarios with a single source, e.g. [13], [14], [77], [90]. Several other techniques have been presented to estimate the angular parameters of multiple ID sources [11], [33], [63], [85], [86], [98]. Unfortunately, all techniques developed for multiple source localization are based on certain approximations of the array covariance matrix, and hence, the resulting parameter estimates are biased.

In the present chapter, we develop a new algorithm for ID source localization which does not use any approximation of the covariance matrix. The popular Capon spectral estimator [19], [93], [99] is generalized to the case of multiple ID sources. The proposed generalized Capon technique estimates the central angles and the angular spreads by means of a two-dimensional parameter search. The proposed technique is

shown to substantially outperform the popular DISPARE algorithm [63] as well as the root-MUSIC based estimator for spread sources [11], [85].

4.2 Problem Formulation

Assume that the signals of L narrowband stationary sources impinge on an array of M sensors. The complex envelope of the array output can be written as

$$\mathbf{x}(t) = \sum_{l=1}^{L} \mathbf{s}_l(t) + \mathbf{n}(t), \qquad t = 0, \ldots, N_s - 1, \tag{4.1}$$

where $\mathbf{x}(t)$ is the $M \times 1$ array snapshot vector, $\mathbf{s}_l(t)$ is the $M \times 1$ vector which describes the contribution of the lth signal source to the array output, $\mathbf{n}(t)$ is the $M \times 1$ vector of sensor noise, and N_s is the number of snapshots available.

In point source modeling, the baseband signal of the lth source is modeled as

$$\mathbf{s}_l(t) = s_l(t)\mathbf{a}(\theta_l), \tag{4.2}$$

where $s_l(t)$ is the complex envelope of the lth source signal, θ_l is its DOA, and $\mathbf{a}(\theta_l)$ is the corresponding steering vector.

In distributed source modeling, the source energy is considered to be spread over some angular volume. Hence, $\mathbf{s}_l(t)$ is written as [85], [98]

$$\mathbf{s}_l(t) = \int_{\theta \in \Theta} \tilde{s}_l(\theta, \boldsymbol{\psi}_l, t)\mathbf{a}(\theta)\, d\theta, \tag{4.3}$$

where $\tilde{s}_l(\theta, \boldsymbol{\psi}_l, t)$ is the angular signal density of the lth source, $\boldsymbol{\psi}_l$ is the vector of its location parameters, and Θ is the angular field-of-view. Examples of the parameter vector $\boldsymbol{\psi}_l$ are the two angular bounds of a uniformly distributed source, or the mean and standard deviation of a source with Gaussian angular distribution [85].

Throughout the chapter, we will consider the ID source model[1]. For the lth ID source, we have [85]

$$\mathrm{E}\{\tilde{s}_l(\theta,\boldsymbol{\psi}_l,t)\tilde{s}_l^*(\theta',\boldsymbol{\psi}_l,t)\} = \sigma_l^2\,\rho(\theta,\boldsymbol{\psi}_l)\,\delta(\theta-\theta'), \tag{4.4}$$

where $\mathrm{E}\{\cdot\}$ denotes the statistical expectation, $\delta(\theta-\theta')$ is the Dirac delta-function, σ_l^2 is the power of the lth source, and $\rho(\theta,\boldsymbol{\psi}_l)$ is its *normalized angular power density*

$$\int \rho(\theta,\boldsymbol{\psi}_l)d\theta = 1. \tag{4.5}$$

We assume that different sources have the same (known) shape of the angular power density but different (unknown) vectors of location parameters.

4.3 DISPARE Algorithm: A Review

The covariance matrix of a spatially distributed source (SDS) is theoretically full rank, i.e., the signal subspace occupies the whole observation space. However, it has been shown in the literature that most of the energy of an SDS is concentrated in the first few eigenvectors of the source covariance matrix [14], [62], [63]. The essence of the DISPARE algorithm is to decompose the received signal covariance matrix into a quasi-signal subspace of dimension L_{e} ($L_{\mathrm{e}} \geq L$) and a quasi-noise subspace of dimension $M - L_{\mathrm{e}}$. The effective dimension of the quasi-signal subspace is characterized by the number of significant eigenvalues in a noise-free environment. Heuristic methods that can be used to determine the value of L_{e} can be found in [63]

[1]The assumption of ID sources has been theoretically and experimentally shown to be relevant in wireless communications in the case of rural and suburban environments with a high base station [68], [69], [112].

and [98]. Hence, the array covariance matrix can be written as

$$\begin{aligned} \mathbf{R}_{\mathrm{x}} &\triangleq \mathrm{E}\{\mathbf{x}(t)\mathbf{x}^H(t)\} \\ &= \mathbf{U}_{\mathrm{s}}\mathbf{\Lambda}_{\mathrm{s}}\mathbf{U}_{\mathrm{s}}^H + \mathbf{U}_{\mathrm{n}}\mathbf{\Lambda}_{\mathrm{n}}\mathbf{U}_{\mathrm{n}}^H, \end{aligned} \tag{4.6}$$

where $\mathbf{\Lambda}_{\mathrm{s}}$ is the $L_{\mathrm{e}} \times L_{\mathrm{e}}$ diagonal matrix that contains the largest (quasi-signal subspace) eigenvalues and the columns of the $M \times L_{\mathrm{e}}$ matrix $\mathbf{U}_{\mathrm{s}}$ are the corresponding eigenvectors. Similarly, the $(M - L_{\mathrm{e}}) \times (M - L_{\mathrm{e}})$ diagonal matrix $\mathbf{\Lambda}_{\mathrm{n}}$ contains the smallest (quasi-noise subspace) eigenvalues and the columns of the $M \times (M - L_{\mathrm{e}})$ matrix $\mathbf{U}_{\mathrm{n}}$ are the corresponding eigenvectors.

Let $\mathbf{R}_l = \sigma_l^2 \mathbf{R}_{\mathrm{s}}(\boldsymbol{\psi}_l)$ be the covariance matrix of the lth ID source, where

$$\mathbf{R}_{\mathrm{s}}(\boldsymbol{\psi}) = \int_{\theta \in \Theta} \rho(\theta, \boldsymbol{\psi}) \mathbf{a}(\theta)\mathbf{a}^H(\theta) d\theta \tag{4.7}$$

is the covariance matrix of the ID source with the parameter vector $\boldsymbol{\psi}$ [85]. Then, using the fact that the quasi-signal subspace $\mathbf{U}_{\mathrm{s}}$ is orthogonal to the quasi-noise subspace $\mathbf{U}_{\mathrm{n}}$ and the fact that the space of $\mathbf{R}_l$ is approximately spanned by the quasi-signal subspace $\mathbf{U}_{\mathrm{s}}$, we can say that [63]

$$\mathbf{R}_l \mathbf{U}_{\mathrm{n}} \simeq \mathbf{0}. \tag{4.8}$$

In practical situations, the statistically expected covariance $\mathbf{R}_{\mathrm{x}}$ is replaced by the sample covariance matrix

$$\begin{aligned} \hat{\mathbf{R}}_{\mathrm{x}} &= \frac{1}{N_s} \sum_{t=0}^{N_s-1} \mathbf{x}(t)\mathbf{x}^H(t) \\ &\triangleq \hat{\mathbf{U}}_{\mathrm{s}}\hat{\mathbf{\Lambda}}_{\mathrm{s}}\hat{\mathbf{U}}_{\mathrm{s}}^H + \hat{\mathbf{U}}_{\mathrm{n}}\hat{\mathbf{\Lambda}}_{\mathrm{n}}\hat{\mathbf{U}}_{\mathrm{n}}^H. \end{aligned} \tag{4.9}$$

Using (4.8) and (4.9), the unknown parameters of the lth distributed source can be estimated as [63]

$$\hat{\boldsymbol{\psi}}_l = \arg \min_{\boldsymbol{\psi}_l} \|\mathbf{R}_{\mathrm{s}}(\boldsymbol{\psi}_l)\hat{\mathbf{U}}_{\mathrm{n}}\|_{\mathrm{F}}^2. \tag{4.10}$$

Based on (4.10) the DISPARE multi-dimensional spectrum is defined as [63]

$$P(\boldsymbol{\psi}) = \frac{1}{\mathrm{tr}\{\hat{\mathbf{U}}_{\mathrm{n}}^H \mathbf{R}_{\mathrm{s}}^H(\boldsymbol{\psi}) \mathbf{R}_{\mathrm{s}}(\boldsymbol{\psi}) \hat{\mathbf{U}}_{\mathrm{n}}\}}, \tag{4.11}$$

where the fact that

$$\|\mathbf{R}_{\mathrm{s}}(\boldsymbol{\psi}_l)\hat{\mathbf{U}}_{\mathrm{n}}\|_{\mathrm{F}}^2 = \mathrm{tr}\{\hat{\mathbf{U}}_{\mathrm{n}}^H \mathbf{R}_{\mathrm{s}}^H(\boldsymbol{\psi}) \mathbf{R}_{\mathrm{s}}(\boldsymbol{\psi}) \hat{\mathbf{U}}_{\mathrm{n}}\} \tag{4.12}$$

has been used. Hence, the DISPARE algorithm [63] estimates the unknown parameters contained in the unknown vectors $\{\boldsymbol{\psi}_l\}_{l=1}^L$ by searching for the L main maxima of the d-dimensional spectrum (4.11) where d is the number of the unknown parameters contained in the vector $\boldsymbol{\psi}$.

4.4 Generalized Capon Parameter Estimator

The essence of the conventional Capon DOA estimator that was briefly described in Section 2.3.2 is to maintain a distorionless response to a hypothetical point source arriving from the direction θ while maximally rejecting any other sources. That is, the Capon estimator is based on solving the constrained optimization problem (2.37) which is repeated here for convenience

$$\begin{aligned} \underset{\mathbf{w}}{\text{minimize}} \quad & \mathbf{w}^H \mathbf{R}_{\mathrm{x}} \mathbf{w} \\ \text{subject to} \quad & \mathbf{w}^H \mathbf{a}(\theta) = 1. \end{aligned} \tag{4.13}$$

From the solution of the above optimization problem, the Capon pseudo-spectrum is given by (2.39) which is also repeated here for convenience

$$P_{\mathrm{C}}(\theta) = \frac{1}{\mathbf{a}^H(\theta) \mathbf{R}_{\mathrm{x}}^{-1} \mathbf{a}(\theta)}. \tag{4.14}$$

Hence, the point source DOAs can be estimated from the L highest maxima of (4.14) which can be obtained by means of a one-dimensional spectral search.

In order to estimate the parameters of ID sources, the conventional Capon DOA estimator can be generalized by generalizing the problem (4.13) as

$$\begin{aligned} \underset{\mathbf{w}}{\text{minimize}} \quad & \mathbf{w}^H \mathbf{R}_x \mathbf{w} \\ \text{subject to} \quad & \mathbf{w}^H \mathbf{R}_s(\psi) \mathbf{w} = 1. \end{aligned} \tag{4.15}$$

According to (4.15), the generalized Capon spatial filter maintains distortionless spatial response to a hypothetical source with the vector parameter ψ while maximally rejecting the contribution of any other sources. Such a response is now represented by means of the covariance matrix $\mathbf{R}_s(\psi)$ (which can be full rank in the general case) rather than the steering vector $\mathbf{a}(\theta)$. In other words, in contrast to (4.13), the distortionless response is maintained in (4.15) in the mean power sense rather than in the deterministic sense. The solution to (4.15) can be found by means of minimization of the Lagrangian function

$$L(\mathbf{w}, \lambda) = \mathbf{w}^H \mathbf{R}_x \mathbf{w} + \lambda(1 - \mathbf{w}^H \mathbf{R}_s(\psi) \mathbf{w}), \tag{4.16}$$

where λ is the Lagrange multiplier. Taking the gradient of (4.16) and equating it to zero, we obtain that the solution to (4.15) is given by the following generalized eigenvalue problem

$$\mathbf{R}_x \mathbf{w} = \lambda \mathbf{R}_s(\psi) \mathbf{w}, \tag{4.17}$$

where the Lagrange multiplier λ plays the role of the corresponding generalized eigenvalue of the matrix pencil $\{\mathbf{R}_x, \mathbf{R}_s(\psi)\}$. Note that the matrices $\mathbf{R}_x$ and $\mathbf{R}_s(\psi)$ are both positive semidefinite and, therefore, all generalized eigenvalues of the matrix pencil $\{\mathbf{R}_x, \mathbf{R}_s(\psi)\}$ are nonnegative real numbers.

Multiplying (4.17) by $\mathbf{w}^H$ from left and using the constraint

$$\mathbf{w}^H \mathbf{R}_s(\psi) \mathbf{w} = 1 \tag{4.18}$$

we obtain that

$$\lambda = \mathbf{w}^H \mathbf{R}_x \mathbf{w}. \tag{4.19}$$

Therefore, the minimal value of the objective function $\mathbf{w}^H \mathbf{R}_x \mathbf{w}$ is equal to the smallest generalized eigenvalue of the matrix pencil $\{\mathbf{R}_x, \mathbf{R}_s(\psi)\}$. Mathematically, this means that if $\mathbf{w}^H \mathbf{R}_s(\psi)\mathbf{w} = 1$ then

$$\min_{\mathbf{w}} \mathbf{w}^H \mathbf{R}_x \mathbf{w} = \lambda_{\min}\{\mathbf{R}_x, \mathbf{R}_s(\psi)\}, \tag{4.20}$$

where $\lambda_{\min}\{\cdot,\cdot\}$ denotes the minimal generalized eigenvalue of a matrix pencil.

Similar to the point source case, we define the generalized Capon pseudo-spectrum as the beamformer output power when the beamformer is "steered" to an ID source with the parameter vector ψ. Hence, using (4.20), the generalized Capon (GC) estimator can be written as

$$P_{\mathrm{GC}}(\psi) = \lambda_{\min}\{\mathbf{R}_x, \mathbf{R}_s(\psi)\}. \tag{4.21}$$

Let us rewrite (4.17) as follows

$$(\mathbf{R}_x^{-1}\mathbf{R}_s(\psi))\mathbf{w} = \frac{1}{\lambda}\mathbf{w}. \tag{4.22}$$

Using (4.22), the generalized Capon estimator can be redefined as

$$P_{\mathrm{GC}}(\psi) = \frac{1}{\sigma_{\max}\{\mathbf{R}_x^{-1}\mathbf{R}_s(\psi)\}}, \tag{4.23}$$

where $\sigma_{\max}\{\cdot\}$ stands for the maximal eigenvalue of a matrix. The parameter vector estimates $\hat{\psi}_l$ $(l = 1, 2, \ldots, L)$ can be obtained by searching for the L main maxima of (4.23). Generally, a d-dimensional search, where d is the length of the vector ψ, is required. However, it is common to characterize spread sources by two parameters only (the central angle and the angular spread, see [63], [85], [98]). In this case, a two-dimensional search is required in (4.23) to estimate the source parameters.

It is worth noting that the conventional Capon estimator (4.14) is a *nonparametric* estimator, whereas the generalized Capon technique (4.23) is a *parametric* (model-based) one.

In a point source case, the vector $\boldsymbol{\psi}$ reduces to the scalar θ and $\mathbf{R}_s(\boldsymbol{\psi})$ transforms to the rank one matrix $\mathbf{a}(\theta)\mathbf{a}^H(\theta)$. In this case, the generalized Capon estimator (4.23) can be simplified as follows

$$\begin{aligned} P_{\mathrm{GC}}(\boldsymbol{\psi}) &= \frac{1}{\sigma_{\max}\{\mathbf{R}_x^{-1}\mathbf{a}(\theta)\mathbf{a}(\theta)^H\}} \\ &= \frac{1}{\mathrm{tr}\{\mathbf{R}_x^{-1}\mathbf{a}(\theta)\mathbf{a}(\theta)^H\}} \\ &= \frac{1}{\mathbf{a}(\theta)^H\mathbf{R}_x^{-1}\mathbf{a}(\theta)}. \end{aligned} \tag{4.24}$$

Therefore, in the point source case (4.23) simplifies to the conventional Capon estimator (c.f. 4.14).

4.5 Simulation Results

In our simulation examples, we consider a ULA of $M = 10$ sensors spaced half a wavelength apart. The number of snapshots used to estimate the sample array covariance matrix $\hat{\mathbf{R}}_x$ is $N_s = 500$. Each simulated point is obtained as an average over 100 independent simulation runs. The performance of the proposed method is compared with that of the DISPARE method [63] and the root-MUSIC based technique [11] with additional improvements introduced in [85].

4.5.1 Example 1: Uniformly Distributed Spread Sources

In the first example, we consider two equipower uniform ID sources with central angles 0° and 10° and the corresponding angular spreads 4° and 5°, respectively. The

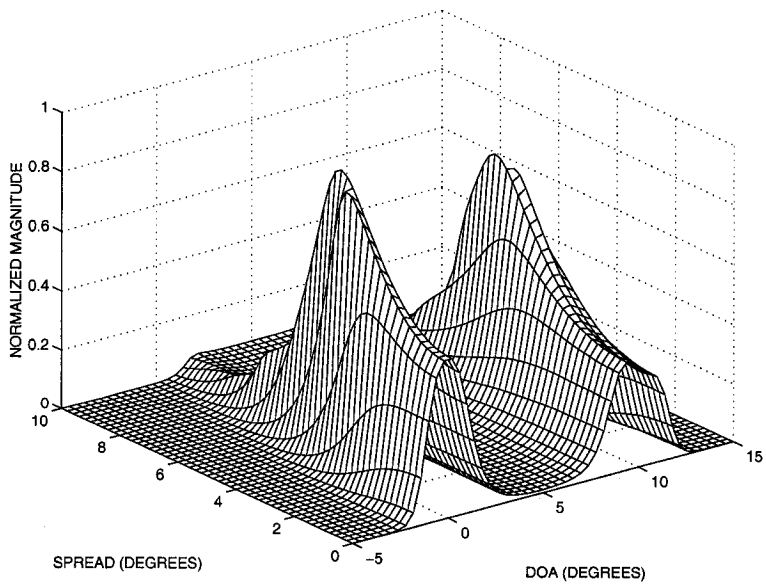

Figure 4.1: Two-dimensional spectrum of the proposed generalized Capon estimator for uniformly distributed sources; first example.

angular spread of a uniform source is defined as the total width (support interval) of its angular power density. The two-dimensional pseudo-spectrum of the generalized Capon estimator for SNR = 35 dB is shown in Figure 4.1. The RMSEs of the central angle estimates are shown versus the source SNR in Figure 4.2. The RMSEs of the angular spread estimates are displayed versus the SNR in Figure 4.3. As it can be seen from these figures, the proposed generalized Capon estimator has a substantially better estimation performance as compared with the other two methods tested. It is worth mentioning that both the proposed algorithm and the DISPARE algorithm involve performing a two-dimensional search over the parameter space. However, the proposed algorithm is computationally more expensive than the DISPARE algorithm as it requires to perform eigen-decomposition at each point on the two-dimensional search grid.

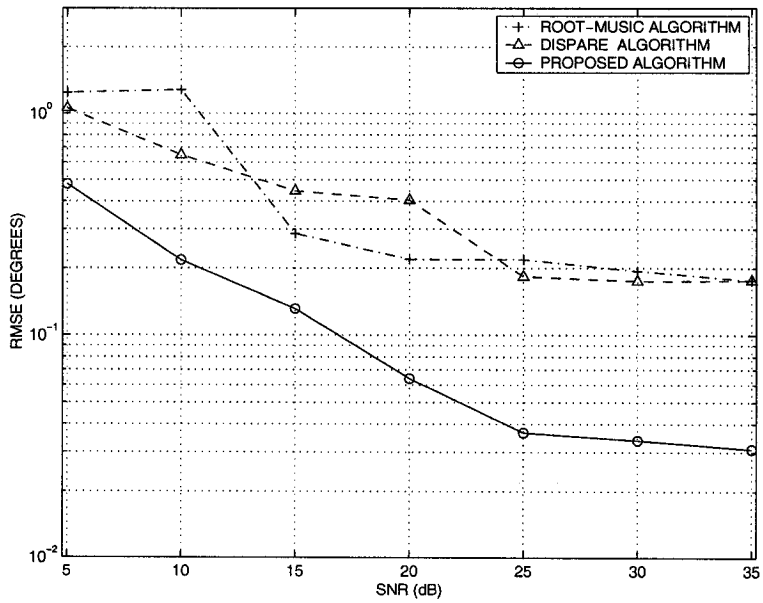

Figure 4.2: RMSEs versus SNR for the central angle estimates; first example.

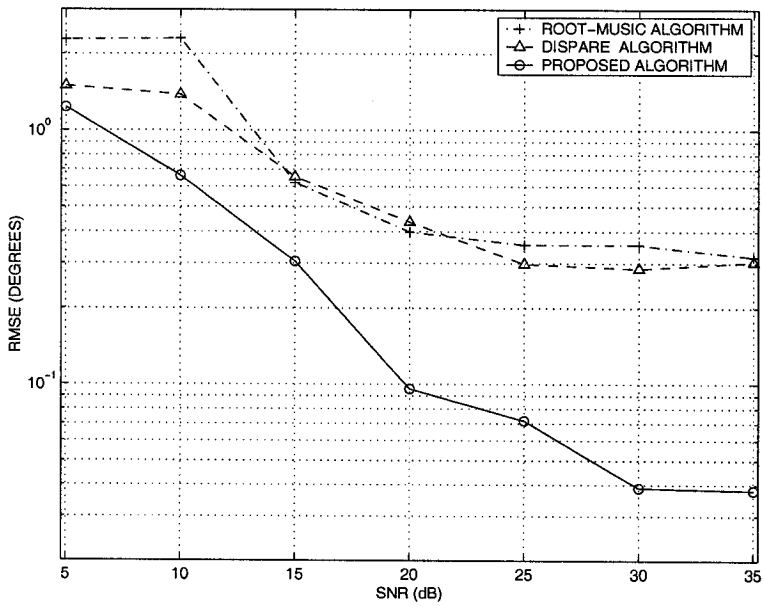

Figure 4.3: RMSEs versus SNR for the angular spread estimates; first example.

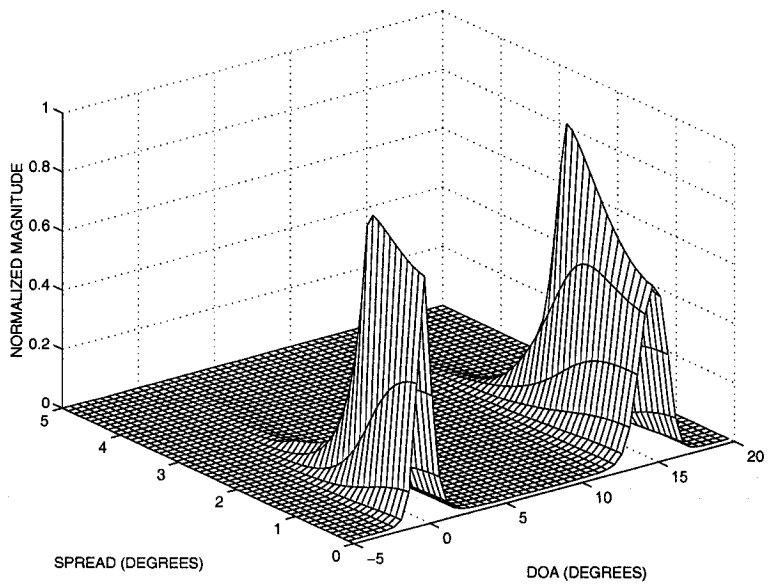

Figure 4.4: Two-dimensional spectrum of the proposed generalized Capon estimator for Gaussian distributed spread sources; second example.

4.5.2 Example 2: Gaussian Distributed Spread Sources

In our second example, we assume two equipower Gaussian ID sources with central angles 0° and 15° and the angular spreads (standard deviations) 2° and 3°, respectively. The two-dimensional pseudo-spectrum of the generalized Capon estimator for SNR = 35 dB is shown in Figure 4.4. Figures 4.5 and 4.6 show the RMSEs of the central angle and angular spread estimates, respectively, versus the SNR. Similar to the previous example, the proposed generalized Capon estimator can be seen to substantially outperform the other two techniques tested.

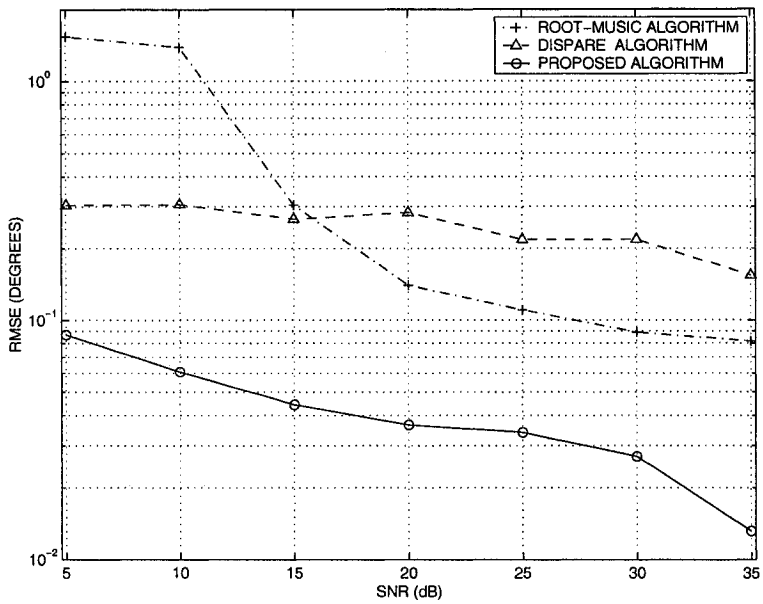

Figure 4.5: RMSEs versus SNR for the central angle estimates; second example.

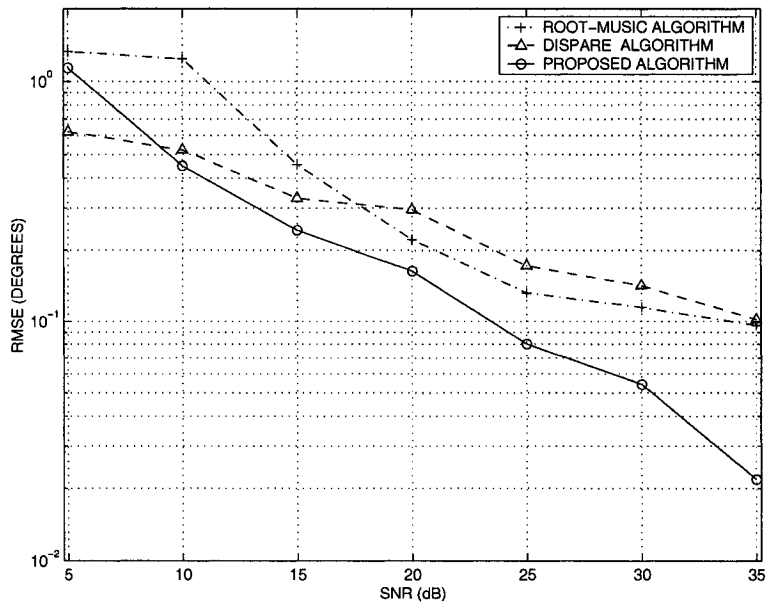

Figure 4.6: RMSEs versus SNR for the angular spread estimates; second example.

4.6 Conclusions

In this chapter, we have developed a new method for estimating the angular parameters of ID sources. The proposed technique is based on the generalization of the well-known Capon estimator. Our method involves a two-dimensional search over the parameter space and shows a substantially improved performance relative to several popular spread source localization techniques.

Chapter 5

Time-Frequency Subspace-Based Localization of Chirp Signals Using the ESPRIT Estimator

5.1 Introduction

The problem of DOA estimation in the presence of chirp and FM signal sources in sensor arrays arises in SAR, SAS, inverse SAR and SAS (ISAR and ISAS), Doppler radar and sonar imaging, as well as in mobile communications, where FM signal waveforms can be intentionally transmitted [8], [12], [20], [24], [27], [31], [72], [87], [105]. In conventional array processing, subspace methods (for example, MUSIC and ESPRIT) are commonly applied and achieve excellent performance at a moderate computational cost. However, conventional subspace methods are based on the assumption that the received signals are stationary. As a result, the performance of conventional subspace-based DOA estimation techniques can degrade when dealing with nonstationary chirp signals.

Recently, STFDs have emerged as an efficient means of array processing in the case of multiple FM signals [2], [10], [30], [113], [114]. Spreading the noise power while localizing the sources in the time-frequency domain helps to improve the DOA estimation performance and enhance robustness against sensor noise. However, the existing narrowband STFD-based DOA estimation techniques [2], [10], [113], [114] are based on a spectral search and, as a result, have high computational costs.

In this chapter, a search-free STFD-based (time-frequency) ESPRIT algorithm is developed. In order to obtain improved estimates of the signal and noise subspaces, we use an averaged STFD matrix (or multiple averaged STFD matrices) in place of the covariance matrix which is used in the conventional ESPRIT algorithm. This averaging involves time-frequency points that correspond to source signatures with a maximal energy. The source DOAs are then estimated using either the LS or the TLS ESPRIT approach [38], [67], [80].

The proposed technique enables to separate the signals in different averaged STFD matrices prior to DOA estimation and, therefore, makes it possible to estimate the source DOAs in the case when the number of array sensors is less than the number of sources. Moreover, closely spaced sources with well separated time-frequency signatures can be efficiently resolved by separating them in different averaged STFD matrices and applying the ESPRIT algorithm to each of them independently.

To validate the effectiveness of the proposed technique and compare its performance with the conventional array processing methods, simulation results for chirp sources are presented. It is shown that significant performance gains can be achieved by the proposed algorithm compared to the conventional LS- and TLS-based ESPRIT techniques.

5.2 Signal Model

Consider L chirp signals impinging on a ULA of M sensors. The array output (data snapshot) vector $\mathbf{x}(t) \in \mathbb{C}^{M\times 1}$ is modeled as

$$\mathbf{x}(t) = \mathbf{A}(\boldsymbol{\theta})\mathbf{s}(t) + \mathbf{n}(t)\ , \quad t = 1, \ldots, N_s, \tag{5.1}$$

where $\mathbf{s}(t) \in \mathbb{C}^{L\times 1}$ and $\mathbf{n}(t) \in \mathbb{C}^{M\times 1}$ are the vectors of signal waveforms and sensor noise, respectively. Recall that, for point source modeling the direction matrix can be expressed as

$$\mathbf{A} = [\mathbf{a}(\theta_1), \ldots, \mathbf{a}(\theta_L)]\,, \tag{5.2}$$

where $\mathbf{a}(\theta)$ is the steering vector that is given in (2.49). Note that this model corresponds to the assumption of *narrowband* chirp signals where changes of the central frequency within the observation interval are negligibly small (i.e., the matrix $\mathbf{A}$ is time independent) [2], [10], [113], [114]. The case of wideband chirp signals is addressed in [30] and [102].

The sample Spatial Pseudo-Wigner-Ville Distribution (SPWVD) matrix is given by [2], [10], [113], [114]

$$\hat{\mathbf{D}}_{\mathbf{xx}}(t,f) = \sum_{\tau=-(K-1)/2}^{(K-1)/2} \mathbf{x}(t+\tau)\mathbf{x}^H(t-\tau)e^{-j4\pi f\tau}, \tag{5.3}$$

where K is the odd window length. Taking the expectation, and assuming that the source waveforms and sensor noise are statistically independent, we have that [10], [30]

$$\begin{aligned} \mathbf{D}_{\mathbf{xx}}(t,f) &= \mathrm{E}\{\hat{\mathbf{D}}_{\mathbf{xx}}(t,f)\} \\ &= \mathbf{A}\mathbf{D}_{\mathbf{dd}}(t,f)\mathbf{A}^H + \sigma^2\mathbf{I}, \end{aligned} \tag{5.4}$$

where

$$\mathbf{D_{dd}}(t,f) = \mathrm{E}\{\hat{\mathbf{D}}_{\mathbf{dd}}(t,f)\}, \tag{5.5}$$

$$\hat{\mathbf{D}}_{\mathbf{dd}}(t,f) = \sum_{\tau=-(K-1)/2}^{(K-1)/2} \mathbf{d}(t+\tau)\mathbf{d}^H(t-\tau)e^{-j4\pi f\tau}. \tag{5.6}$$

The relationship (5.4) holds true for each (t,f) point. However, the STFD matrix at a single (t,f) point may be low rank. In order to make sure that the STFD matrix is full rank and to reduce the effect of the sensor noise, an averaging over multiple (t,f) points (corresponding to the autoterms of the STFD) can be used. The eigenstructure properties of the averaged STFD matrix can be exploited to estimate the signal DOAs in a similar way as in the conventional subspace-based array processing techniques [2], [10], [30], [113], [114].

In practical situations, the sample STFD matrices (5.3) are used instead of the exact (statistically expected) matrices (5.4). In the case of sources with distinct time-frequency signatures, it is possible to construct the averaged STFD matrices over time-frequency points belonging to a subset of the sources in the field-of-view. Using this approach, sources with close angular spacing can be efficiently resolved by separating them in different averaged STFD matrices and applying a DOA estimation algorithm to each matrix independently.

5.3 Time-Frequency ESPRIT

Let the averaged STFD matrix $\tilde{\mathbf{D}}_{\mathbf{xx}}$ be formed by averaging of multiple SPWVD matrices computed at PJ different time-frequency points $\{t_p, f_i\}$ $(p = 1,\ldots,P;$ $i = 1,\ldots,J)$ that belong to the time-frequency signatures of L_0 source signals ($L_0 \leq$

$L < M$):

$$\tilde{\mathbf{D}}_{\mathbf{xx}} = \sum_{p=1}^{P} \sum_{i=1}^{J} \hat{\mathbf{D}}_{\mathbf{xx}}(t_p, f_i). \tag{5.7}$$

Note that the values of P and J may vary with time and can be determined by means of detection of the source time-frequency signatures, see [23] and [30]. Let us divide a ULA of M sensors into two identical subarrays of $M-1$ sensors shifted by the interelement spacing Δ, as shown in Figure 5.1. As in the conventional ESPRIT case, define the sub-matrices $\mathbf{A}_1$ and $\mathbf{A}_2$ by deleting the last and first rows from $\mathbf{A}$ respectively, i.e. let

$$\mathbf{A} = \begin{bmatrix} \mathbf{A}_1 \\ \text{last row} \end{bmatrix} = \begin{bmatrix} \text{first row} \\ \mathbf{A}_2 \end{bmatrix}. \tag{5.8}$$

Then, $\mathbf{A}_1$ and $\mathbf{A}_2$ are related as

$$\mathbf{A}_2 = \mathbf{A}_1 \mathbf{\Phi}, \tag{5.9}$$

where

$$\mathbf{\Phi} = \text{diag}\{\exp\{j\mu_1\}, \ldots, \exp\{j\mu_{L_0}\}\} \tag{5.10}$$

and

$$\mu_l = (\omega_o/c)\Delta \sin\theta_l \tag{5.11}$$

are the source spatial frequencies.

Let $\mathbf{U}_S$ be the matrix formed from the eigenvectors of $\tilde{\mathbf{D}}_{\mathbf{xx}}$ that correspond to the L_0 eigenvalues with the largest magnitude. As the columns of the steering matrix $\mathbf{A}$ and the matrix $\tilde{\mathbf{U}}_S$ span approximately[1] the same (signal) subspace of the dimension L_0, there exists a nonsingular $L_0 \times L_0$ matrix $\mathbf{T}$ such that

$$\mathbf{U}_S \simeq \mathbf{AT}. \tag{5.12}$$

[1]Note that $\mathbf{U}_S$ is obtained from the eigendecomposition of the *sample* STFD matrix $\tilde{\mathbf{D}}_{\mathbf{xx}}$.

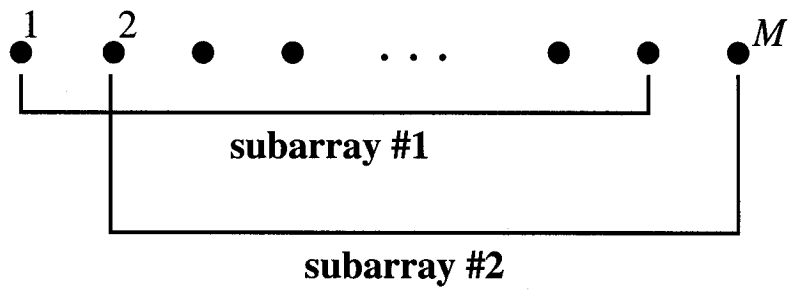

Figure 5.1: Array structure for ESPRIT; two subarrays with maximum overlap.

Applying this transformation to the sub-matrices $\mathbf{A}_1$ and $\mathbf{A}_2$, we obtain

$$\mathbf{U}_{S,1} \simeq \mathbf{A}_1\mathbf{T}, \tag{5.13}$$

$$\mathbf{U}_{S,2} \simeq \mathbf{A}_2\mathbf{T}, \tag{5.14}$$

where $\mathbf{U}_{S,1}$ and $\mathbf{U}_{S,2}$ are formed by deleting the last and first rows of $\mathbf{U}_S$, respectively. That is,

$$\mathbf{U}_S = \begin{bmatrix} \mathbf{U}_{S,1} \\ \text{last row} \end{bmatrix} = \begin{bmatrix} \text{first row} \\ \mathbf{U}_{S,2} \end{bmatrix}. \tag{5.15}$$

Using (5.9) and (5.13)-(5.14) yields

$$\mathbf{U}_{S,2} \simeq \mathbf{U}_{S,1}\mathbf{\Psi}, \tag{5.16}$$

where the matrices $\mathbf{\Psi}$ and $\mathbf{\Phi}$ are related as

$$\mathbf{\Psi} = \mathbf{T}^{-1}\mathbf{\Phi}\mathbf{T}. \tag{5.17}$$

This means that $\{\exp\{j\mu_l\}\}_{l=1}^{L_0}$ are the eigenvalues of the matrix $\mathbf{\Psi}$ [38], [67], [80].

Now, we can formulate our time-frequency ESPRIT algorithm as follows:

- *Step 1:* Compute the sample SPWVD matrices $\hat{\mathbf{D}}_{\mathbf{xx}}(t,f)$ for all time-frequency points of interest and select the maximal energy points that belong to the source signatures.

- *Step 2:* Compute the averaged STFD matrix $\tilde{\mathbf{D}}_{\mathbf{xx}}$ for a previously selected part of sources (for $L_0 \leq L$ sources) by means of involving in the averaging process only the time-frequency points that belong to the spatial signatures of these L_0 sources.

- *Step 3:* Compute the eigendecomposition of $\tilde{\mathbf{D}}_{\mathbf{xx}}$ and obtain $\mathbf{U}_S$.

- *Step 4:* Obtain an estimate $\hat{\mathbf{\Psi}}$ of the matrix $\mathbf{\Psi}$ by solving (5.16) using either LS or TLS approaches.

- *Step 5:* Obtain estimates of the spatial frequencies μ_i from the eigenvalues of $\hat{\mathbf{\Psi}}$ and use them to find the estimates of the source DOAs θ_i.

- *Step 6:* Repeat Steps 2-5 for other (selected) parts of sources.

Note that algorithms are available to classify auto- and cross-terms in STFDs [23]. These techniques can be used in Step 2.

The possibility of separating sources in different averaged STFD matrices prior to DOA estimation can essentially improve the performance of the ESPRIT algorithm, especially in the low SNR case and in the presence of closely spaced sources which are well separated in the time-frequency domain. However, this will increase the computational costs relative to the conventional ESPRIT algorithm because in this case ESPRIT should be applied simultaneously to several averaged STFD matrices.

5.4 Simulation Results

We assume a ULA with omnidirectional sensors spaced half a wavelength apart. This array is divided into two subarrays with half a wavelength inter-subarray displacement as shown in Figure 5.1. Two narrowband chirp signals impinge on the array from the

sources located at $\theta_1 = 3°$ and $\theta_2 = 6°$. After downconversion, the source waveforms are modeled as

$$\begin{aligned} d_1(t) &= \exp\{j(\omega_1 t + \beta_1 t^2/2)\}, \\ d_2(t) &= \exp\{j(\omega_2 t + \beta_2 t^2/2)\}. \end{aligned}$$

The initial discrete-time frequencies of the source signals are chosen to be $\omega_1 = 0$ and $\omega_2 = \pi$ while their chirp rates are assumed to be $\beta_1 = 0.002$ and $\beta_2 = -0.002$, respectively. An observation interval of $N_s = 255$ snapshots is considered. Figure 5.2 shows the pseudo-Wigner-Ville distribution of the signals in the first array sensor. The noise is modeled as a complex Gaussian zero-mean spatially and temporally white process. A total of 300 independent Monte-Carlo simulation runs have been used to obtain each simulated point. The averaged STFD matrix $\tilde{\mathbf{D}}_{\mathbf{xx}}$ is computed for each source signal separately by averaging the sample STFD matrices computed at 150 different time-frequency points that belong to the source signatures.

5.4.1 Example 1: DOA Estimation RMSEs Versus SNR

In the first example, we use an array of $M = 10$ sensors. Figure 5.3 displays the DOA estimation RMSEs versus the SNR for the conventional LS- and TLS-ESPRIT algorithms, as well as for the proposed time-frequency modification of the LS- and TLS-ESPRIT techniques. Additionally, the so-called deterministic CRB [94] is shown in this figure (the latter bound is computed under the assumption that the source waveforms are unknown deterministic sequences). From Figure 5.3, it is clear that the time-frequency ESPRIT algorithm has a substantial improvement over conventional ESPRIT. This is especially true in the low SNR case. Note that neither time-frequency ESPRIT nor conventional ESPRIT approaches the deterministic CRB.

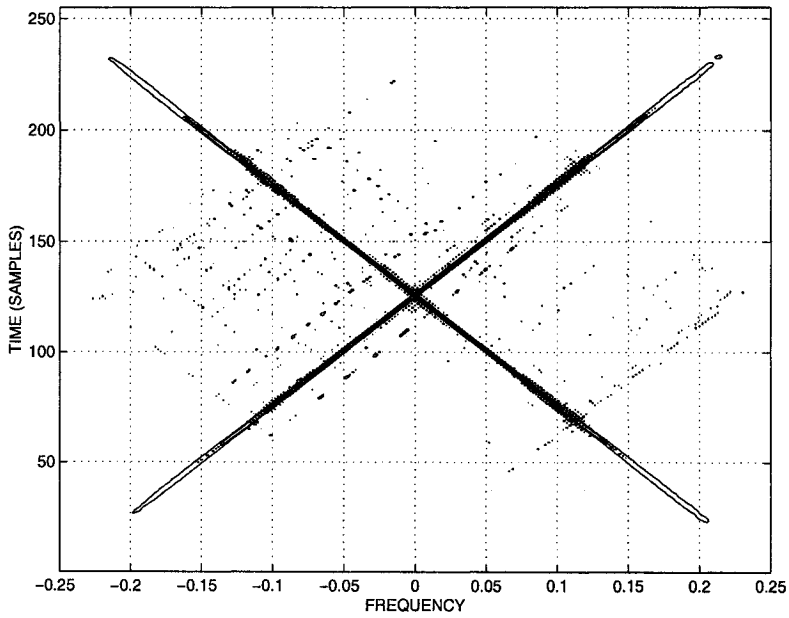

Figure 5.2: Pseudo-Wigner-Ville distribution of the source waveforms.

5.4.2 Example 2: DOA Estimation RMSEs Versus Number of Sensors

In the second example, the source SNR is fixed and equal to 4 dB, while the number of array sensors is varied. Figure 5.4 shows the RMSEs of the same four methods as in the previous example versus the number of sensors M. It is evident from this figure that the time-frequency ESPRIT algorithm has substantially better performance than the convectional ESPRIT technique.

5.5 Conclusions

A time-frequency ESPRIT algorithm is introduced for DOA estimation of narrow-band chirp signals in sensor arrays. The proposed algorithm is based on the concept

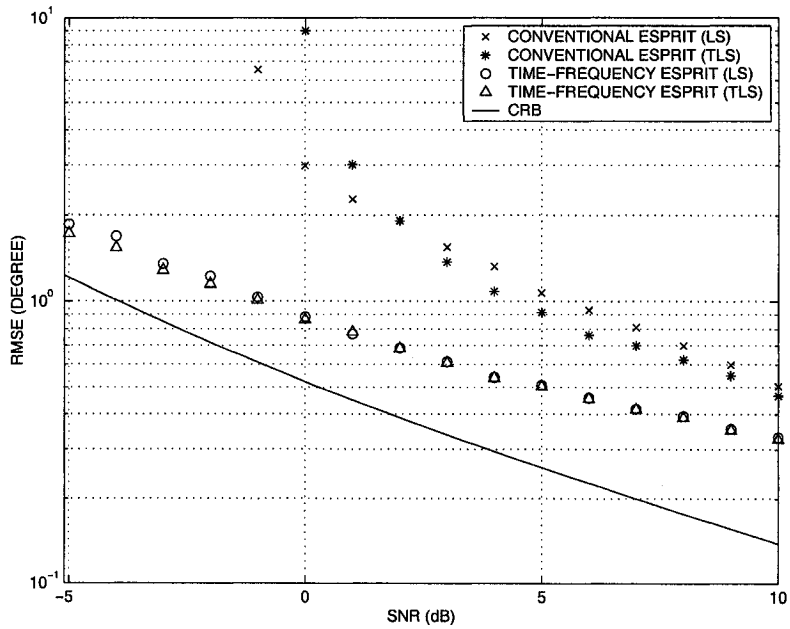

Figure 5.3: The DOA estimation RMSEs versus the SNR; first example: $\theta_1 = 3°$, $\theta_2 = 6°$, and $M = 10$.

of STFDs and employs multiple averaged STFD matrices, instead of the covariance matrix (used in conventional array processing methods), to obtain the estimates of the signal DOAs. Computer simulations show that in scenarios with chirp signals, the proposed technique outperforms the conventional ESPRIT algorithm. The performance improvement is especially high in the case when the SNR is low or the sources are closely spaced.

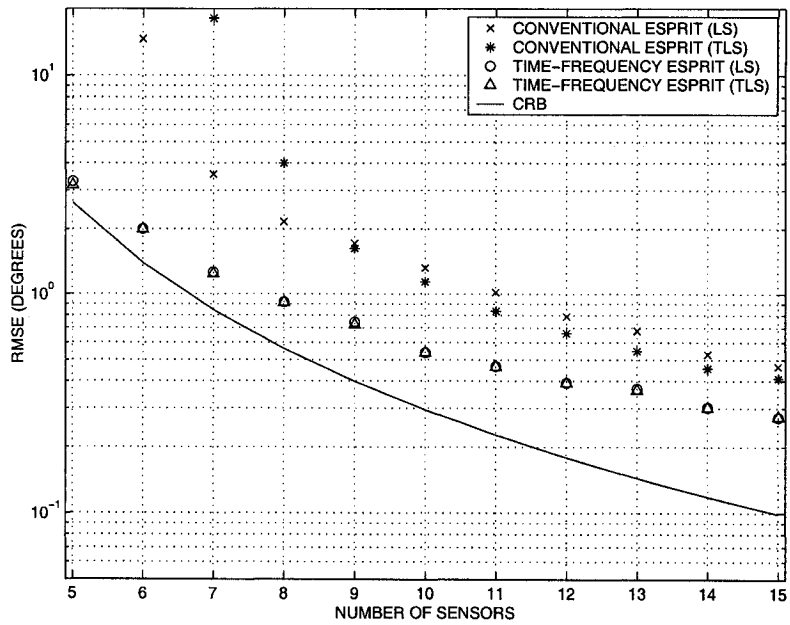

Figure 5.4: The DOA estimation RMSEs versus the number of sensors M; second example: $\theta_1 = 3°$, $\theta_2 = 6°$, and SNR $= 4$ dB.

Chapter 6

Estimating the Parameters of Multiple Wideband Polynomial-Phase Sources: A Computationally Efficient Approach

6.1 Introduction

Parameter estimation of PPSs is an important problem because they are encountered in many practical applications such as in radar, sonar and mobile communications. In these applications, the received signals within a finite duration of time can be modeled as PPSs [8], [20], [27], [31], [81], [105]. Furthermore, FM signals can be intentionally transmitted in SAR, SAS, ISAR, ISAS, Doppler radar and sonar imaging, and mobile communications. There is an extensive literature review on the problem of parameter estimation of PPSs in the single antenna case [7], [8], [66], [70], [71], [76], [81]. In particular, the high-order instantaneous moment (HIM) and its Fourier transform which is called the high-order ambiguity function (HAF) have provided a simple order-recursive and computationally attractive algorithm for estimating the phase

coefficients of PPSs [70], [71], [76]. The HAF-based algorithm suffers from an identifiability problem when dealing with multi-component PPSs having the same highest order phase coefficients, however this problem was solved by introducing the product high-order ambiguity function (PHAF) [8], [81].

In recent years, the parameter estimation of multiple PPS sources in sensor arrays has received considerable attention [2], [10], [30], [31], [43], [57], [103], [110], [111], [114]. Several methods that solve this problem using narrowband assumptions have been reported in the literature. For example, several exact and approximate ML estimators for estimating the parameters of narrowband PPSs have been given in [110], [111]. Also, subspace-based methods that employ STFD matrices have been effectively used for estimating the DOAs of multiple narrowband FM signals [10], [30]. STFD-based methods provide robustness against sensor noise and they can resolve closely spaced sources with well separated time-frequency signatures by separating them in different STFD matrices.

The case of multiple wideband PPSs impinging on a multi-sensor array has also received a considerable attention. Several approaches have been reported in the literature for solving this problem [30], [31], [103], [57]. In particular, an exact ML estimator that takes an advantage of the specific PPS structure has been proposed for estimating the parameters of multiple wideband constant-amplitude PPSs [31]. The chirp beamformer (CBF) is a suboptimal estimator that has originated from the analysis of the log-likelihood function in the single linear FM source case [31]. Although the CBF enjoys a simpler implementation than the exact ML estimator, it is still computationally expensive as it requires solving a three-dimensional optimization problem. Moreover, the CBF suffers from large bias even at high SNR. A simpler approach for estimating the parameters of multiple wideband chirp signals that requires multiple one-dimensional searches was proposed in [57]. This approach

employs the discrete polynomial-phase transform (DPT) in order to obtain a non-parametric estimate of each signal component. Then it exploits these nonparametric estimates in estimating the DOAs using the CBF. However, this method is restricted to ULA geometry and suffers from an ambiguity problem when the chirp signals are subject to aliasing in the time-domain. Moreover, it can not be used for estimating the parameters of higher-order wideband PPSs, i.e., PPSs of order greater than two.

In this chapter we introduce a new algorithm for estimating the parameters of multiple wideband PPSs using an array of sensors. We first introduce the SHIM which is a nonlinear transformation that can be applied to the data snapshots. We also give a detailed description of the output of the SHIM when applied to multiple wideband PPSs. The HAF concept is employed to obtain multiple estimates of the frequency parameters in a recursive manner starting with the highest-order frequency coefficients. Also, multiple different estimates of the sources DOAs are obtained from the transformed data using STFD subspace-based methods. The multiple different estimates of the frequency parameters and the multiple different estimates of the DOAs are employed simultaneously in order to remove the outliers and to obtain a better final estimate. Our approach is computationally attractive as it requires multiple one-dimensional searches to estimate the frequency parameters as well as the DOAs. Moreover, the DOAs can be obtained using search free techniques (e.g. root-MUSIC) if a ULA is used. Compared to the CBF, our estimation technique has better performance at lower computational complexity. Simulation results are provided to validate the effectiveness of the proposed algorithm.

6.2 Problem Formulation

6.2.1 Array Signal Model

We consider L wideband constant-amplitude PPSs impinging on a linear array of M omnidirectional sensors. The vector array output is assumed to obey the following model

$$\mathbf{x}(t) = \mathbf{A}(t)\mathbf{d}(t) + \mathbf{n}(t), \quad t = 0, 1, \ldots, N_s - 1, \tag{6.1}$$

where $\mathbf{A}(t)$ is the $M \times L$ time-varying direction matrix, $\mathbf{d}(t)$ is the $L \times 1$ vector of wideband nonstationary source waveforms.

The lth polynomial-phase source waveform can be modeled as

$$d_l(t) = \alpha_l \exp\left\{j\phi(\boldsymbol{\omega}_l, t)\right\}, \tag{6.2}$$

where

$$\boldsymbol{\omega}_l \triangleq [\omega_{l,1}, \omega_{l,2}, \ldots, \omega_{l,K}]^T \tag{6.3}$$

is the $K \times 1$ vector that contains the unknown discrete-time frequency parameters, α_l is the initial amplitude and

$$\phi(\boldsymbol{\omega}_l, t) \triangleq \omega_{l,0} + \sum_{k=1}^{K} \frac{1}{k}\omega_{l,k}t^k \tag{6.4}$$

is the instantaneous phase of the lth signal. In (6.4), $\omega_{l,0}$ is the initial phase (constant term), $\omega_{l,k}$ $(l = 1, 2, \ldots, L;\ k = 1, 2, \ldots, K)$ are the unknown discrete-time frequency parameters of the lth waveform, K is the order of the polynomial-phase model[1]. Let $\tilde{\omega}_l(t)$ be the discrete-time instantaneous frequency of the lth waveform defined as

$$\begin{aligned} \tilde{\omega}_l(t) &= \sum_{k=1}^{K} \omega_{l,k}t^{k-1} \\ &= \Delta t\, \tilde{\omega}_l^{\mathrm{ct}}(t), \end{aligned} \tag{6.5}$$

[1]In what follows, the order K is assumed to be known.

where Δt is the sampling interval and $\tilde{\omega}_l^{\mathrm{ct}}(t)$ is the continuous-time (physical) instantaneous frequency of the lth PPS. The direction matrix

$$\begin{aligned}\mathbf{A}(\boldsymbol{\theta},\boldsymbol{\omega},t) &\triangleq [\mathbf{a}(\theta_1,\tilde{\omega}_1(t)),\ldots,\mathbf{a}(\theta_L,\tilde{\omega}_L(t))] \\ &= [\mathbf{a}(\theta_1,\boldsymbol{\omega}_1,t),\ldots,\mathbf{a}(\theta_L,\boldsymbol{\omega}_L,t)] \end{aligned} \tag{6.6}$$

consists of the time-varying steering vectors

$$\mathbf{a}(\theta_l,\boldsymbol{\omega}_l,t) = \left[1, \exp\left\{j\,\frac{\tilde{\omega}_l(t)}{c\,\Delta t}h_1\sin\theta_l\right\},\ \ldots, \exp\left\{j\,\frac{\tilde{\omega}_l(t)}{c\,\Delta t}h_{M-1}\sin\theta_l\right\}\right]^T, \tag{6.7}$$

where

$$\boldsymbol{\omega} \triangleq \left[\boldsymbol{\omega}_1^T,\boldsymbol{\omega}_2^T,\ldots,\boldsymbol{\omega}_L^T\right]^T, \tag{6.8}$$

$$\boldsymbol{\theta} \triangleq [\theta_1,\theta_2,\ldots,\theta_L]^T. \tag{6.9}$$

The relationship (6.5) is used in (6.7) to express the steering vector as a function of the discrete-time frequency parameters. Note that in (6.7) it is assumed that the instantaneous signal frequencies $\tilde{\omega}_l(t)$ $(l = 1,\ldots,L)$ do not change during the time necessary for a wave to travel across the array aperture, i.e., the signals remain narrowband in each snapshot, whereas the signals are assumed to be wideband at the full observation interval of N_s samples.

The pure signal part in (6.1) can be rewritten as

$$\begin{aligned}\mathbf{x}(t) &= \mathbf{A}(\boldsymbol{\theta},\boldsymbol{\omega},t)\boldsymbol{G}(\boldsymbol{\omega},t)\boldsymbol{\alpha} \\ &= \tilde{\mathbf{A}}(\boldsymbol{\theta},\boldsymbol{\omega},t)\boldsymbol{\alpha}, \end{aligned} \tag{6.10}$$

where

$$\boldsymbol{\alpha} \triangleq \left[\alpha_1 e^{j\omega_{1,0}},\ldots,\alpha_L e^{j\omega_{L,0}}\right]^T, \tag{6.11}$$

$$\boldsymbol{G}(\boldsymbol{\omega},t) \triangleq \mathrm{diag}\left\{e^{j\phi(\boldsymbol{\omega}_1,t)},\ldots,e^{j\phi(\boldsymbol{\omega}_L,t)}\right\}, \tag{6.12}$$

$$\tilde{\mathbf{A}}(\boldsymbol{\theta},\boldsymbol{\omega},t) \triangleq \mathbf{A}(\boldsymbol{\theta},\boldsymbol{\omega},t)\boldsymbol{G}(\boldsymbol{\omega},t). \tag{6.13}$$

Note that all initial source amplitudes and initial source phases are now included in the vector $\boldsymbol{\alpha}$.

6.2.2 ML Estimator: A Review

The ML estimator that was derived in [31] is based on the assumption that the initial signal amplitudes are constant (deterministic) values. The negative log-likelihood function is given by

$$\begin{aligned} L_N(\boldsymbol{\theta}, \boldsymbol{\omega}, \boldsymbol{\alpha}) &= \sum_{t=0}^{N_s-1} ||\mathbf{x}(t) - \mathbf{A}(\boldsymbol{\theta}, \boldsymbol{\omega}, t)\boldsymbol{G}(\boldsymbol{\omega}, t)\boldsymbol{\alpha}||^2 \\ &= \sum_{t=0}^{N_s-1} ||\mathbf{x}(t) - \tilde{\mathbf{A}}(\boldsymbol{\theta}, \boldsymbol{\omega}, t)\boldsymbol{\alpha}||^2. \end{aligned} \tag{6.14}$$

By minimizing L_N over $\boldsymbol{\alpha}$ and substituting back in (6.14), the concentrated negative log-likelihood function is obtained [31]

$$\begin{aligned} L_N(\boldsymbol{\theta}, \boldsymbol{\omega}) &= \sum_{t=0}^{N_s-1} \mathbf{x}^H(t)\mathbf{x}(t) - \left\{ \sum_{t=0}^{N_s-1} \mathbf{x}^H(t)\tilde{\mathbf{A}}(\boldsymbol{\theta}, \boldsymbol{\omega}, t) \right\} \\ &\quad \cdot \left\{ \sum_{t=0}^{N_s-1} \tilde{\mathbf{A}}^H(\boldsymbol{\theta}, \boldsymbol{\omega}, t)\tilde{\mathbf{A}}(\boldsymbol{\theta}, \boldsymbol{\omega}, t) \right\}^{-1} \cdot \left\{ \sum_{t=0}^{N_s-1} \tilde{\mathbf{A}}^H(\boldsymbol{\theta}, \boldsymbol{\omega}, t)\mathbf{x}(t) \right\} \\ &= \sum_{t=0}^{N_s-1} \mathbf{x}^H(t)\mathbf{x}(t) - L_P(\boldsymbol{\theta}, \boldsymbol{\omega}), \end{aligned} \tag{6.15}$$

where $L_P(\cdot)$ is the concentrated positive log-likelihood function. Ignoring the constant term, the ML estimator is given by [31]

$$[\hat{\boldsymbol{\theta}}, \hat{\boldsymbol{\omega}}] = \arg \max_{\boldsymbol{\theta}, \boldsymbol{\omega}} L_P(\boldsymbol{\theta}, \boldsymbol{\omega}). \tag{6.16}$$

The above estimator is highly nonlinear and difficult to optimize. However, it is easy to evaluate the value of L_P for a given set of parameters $\{\boldsymbol{\theta}, \boldsymbol{\omega}\}$. This means that if more than one set of estimates of the parameter set $\{\boldsymbol{\theta}, \boldsymbol{\omega}\}$ are available, then one

can use the ML estimator (c.f. (6.16)) to select the set that yields the highest ML value as the final estimate. This ML-based selection criterion will be used in Section 6.4.

6.3 Spatial High-Order Instantaneous Moments and Their Properties

In this section, we first review the HIM and its application in parameter estimation of PPSs in the single antenna case. Then we introduce the SHIM which is a natural extension of the HIM to the multiple antenna case. We will show that the Kth-order SHIM of multiple wideband PPSs of order K is also a multiple wideband PPSs, and that among the components contained in that Kth-order SHIM there are some terms that have nice narrowband structure. These narrowband components are related to the highest-order frequency coefficients and to the DOAs of the source signals. This property provides the basis for our proposed method for estimating parameters of multiple wideband PPSs in sensor arrays.

6.3.1 High-Order Instantaneous Moment

The HIM was originally introduced by Peleg et. al. [70]. The Kth-order HIM of a given sequence $x(t)$ is defined by the following recursive formula

$$x^{(K)}(t;\tau) = \begin{cases} x(t), & K = 1 \\ x^{(K-1)}(t+\tau;\tau)\left(x^{(K-1)}\right)^*(t-\tau;\tau), & K > 1, \end{cases} \tag{6.17}$$

where τ is a time lag (positive number) and $(\cdot)^*$ is the conjugate operator. A closed-form description of the HIM of multi-component PPSs in the single antenna case is

given by the following lemma due to Barbarossa et. al. [8].

Lemma 6.1 *Given the signal $s(t)$ composed of the sum of L PPSs of degree K*

$$s(t) = \sum_{l_1=1}^{L} A_{l_1} \exp\left\{ j \sum_{k=0}^{K} v_{l_1,k} t^K \right\}. \tag{6.18}$$

Its Kth-order HIM is still a multi-component PPSs that is given by

$$s^{(K)}(t;\tau) = \sum_{l_1,\cdots,l_{2K-1}=1}^{L} A_{l_1} \cdots A_{l_{2K-1}} \exp\left\{ j \sum_{k=0}^{K} v^{(K)}_{l_1,\cdots,l_{2K-1};k} t^k \right\}, \tag{6.19}$$

where the coefficients $v^{(K)}_{l_1,\cdots,l_{2K-1};k}$ can be computed using the following iterative rule

$$v^{(1)}_{l_1;k} = v_{l_1,k}, \quad k = 0, \cdots, K, \tag{6.20}$$

$$v^{(2)}_{l_1,l_2;k} = \sum_{r=0}^{K-k} \binom{k+r}{k} \left(v^{(1)}_{l_1;k+r} - (-1)^r v^{(1)}_{l_2;k+r} \right) \tau^r, \tag{6.21}$$

$$\vdots$$

$$v^{(K)}_{l_1,\ldots,l_{2K-1};k} = \sum_{r=0}^{K-k} \binom{k+r}{k} \left(v^{(K-1)}_{l_1,\cdots,l_{2K-2};k+r} - (-1)^r v^{(K-1)}_{l_{2K-2+1},\cdots,l_{2K-1};k+r} \right) \tau^r. \tag{6.22}$$

Proof. see [8].

The terms in (6.19) corresponding to equal indexes ($l_1 = l_2 = \ldots = l_{2K-1} = l$) are called autoterms, whereas all other terms are called crossterms. For the sake of convenience, the coefficients of the autoterms will be written as $v^{(K)}_{l,k}$ instead of $v^{(K)}_{l,\cdots,l;k}$.

The autoterms of the Kth-order HIM in (6.19) are known to be complex sinusoids with frequencies related to the highest-order frequency coefficients. This property is described by the following relationship [8], [71]

$$v^{(K)}_{l,1} = (2\tau)^{K-1} K!\, v_{l,K}, \qquad l = 1, \ldots, L. \tag{6.23}$$

Hence, the Kth-order HIM of $s(t)$ given in (6.19) can be rewritten as follows

$$s^{(K)}(t;\tau) = \sum_{l=1}^{L} A_l^{2^{K-1}} \exp\left\{ j \left(v^{(K)}_{l,0} + v^{(K)}_{l,1} t \right) \right\} + \text{crossterms}, \tag{6.24}$$

where $v_{l,0}^{(K)}$ is the constant phase term. The Fourier transform of $s^{(K)}(t;\tau)$ is called the HAF [76]. Based on the HAF, several algorithms have been reported in the literature for estimating the highest-order frequency coefficients $v_{l,K}$ [7], [71], [76]. The basic idea behind these methods is to estimate $v_{l,1}^{(K)}$ by searching for the highest peak of the HAF, then the coefficients $v_{l,K}$ can be extracted from $v_{l,1}^{(K)}$ using (6.23). Once the highest frequency coefficient is estimated, its contribution can be removed and the process can be repeated for estimating the next to highest frequency coefficient and so on.

6.3.2 Spatial High-Order Instantaneous Moment

As a natural extension to the HIM, we introduce the SHIM which is a new nonlinear transformation that can be applied to vector data. We define the Kth-order SHIM of the data vector $\mathbf{x}(t)$ using the following recursive rule

$$\mathbf{x}^{(K)}(t;\tau) = \begin{cases} \mathbf{x}(t), & K = 1 \\ \mathbf{x}^{(K-1)}(t+\tau;\tau) \odot \left(\mathbf{x}^{(K-1)}\right)^*(t-\tau;\tau), & K > 1, \end{cases} \tag{6.25}$$

We give a closed form description of the SHIM of multiple wideband PPSs in sensor arrays by introducing the following two lemmas.

Lemma 6.2 *Given the data vector* $\mathbf{x}(t)$ *composed of the sum of* L *multiple wideband PPSs of degree* K

$$\mathbf{x}(t) = \sum_{l_1=1}^{L} d_{l_1}(t)\mathbf{a}(\theta_{l_1}, \boldsymbol{\omega}_{l_1}, t), \tag{6.26}$$

where $d_{l_1}(t)$ *and* $\mathbf{a}(\theta_{l_1}, \boldsymbol{\omega}_{l_1}, t)$ *are defined in (6.2) and (6.7) respectively. Then, the* K*th-order SHIM of* $\mathbf{x}(t)$ *is still a multiple wideband PPSs scenario, i.e.,*

$$\mathbf{x}^{(K)}(t;\tau) = \sum_{l_1,\cdots,l_{2K-1}=1}^{L} d_{l_1,\cdots,l_{2K-1}}^{(K)}(t)\mathbf{a}_{l_1,\cdots,l_{2K-1}}^{(K)}(t), \tag{6.27}$$

where

$$d^{(K)}_{l_1,\cdots,l_{2K-1}}(t) = \alpha_{l_1}\cdots\alpha_{l_{2K-1}} \exp\left\{ j \sum_{k=0}^{K} \omega^{(K)}_{l_1,\cdots,l_{2K-1};k} t^k \right\}, \tag{6.28}$$

and

$$\mathbf{a}^{(K)}_{l_1,\cdots,l_{2K-1}}(t) = \begin{bmatrix} 1 \\ \exp\left\{ j \frac{h_1}{c\Delta t} \sum_{k=1}^{K} \Omega^{(K)}_{l_1,\cdots,l_{2K-1};k} t^{k-1} \right\} \\ \vdots \\ \exp\left\{ j \frac{h_{M-1}}{c\Delta t} \sum_{k=1}^{K} \Omega^{(K)}_{l_1,\cdots,l_{2K-1};k} t^{k-1} \right\} \end{bmatrix} \tag{6.29}$$

In (6.28), the frequency coefficients $\omega^{(K)}_{l_1,\cdots,l_{2K-1};k}$ *can be computed using the following iterative rule:*

$$\omega^{(1)}_{l_1;k} = \begin{cases} \omega_{l_1,0}, & k = 0 \\ \frac{1}{k}\omega_{l_1,k}, & k = 1,\ldots,K, \end{cases} \tag{6.30}$$

$$\omega^{(2)}_{l_1,l_2;k} = \sum_{r=0}^{K-k} \binom{k+r}{k} (\omega^{(1)}_{l_1;k+r} - (-1)^r \omega^{(1)}_{l_2;k+r})\tau^r, \tag{6.31}$$

$$\vdots$$

$$\omega^{(K)}_{l_1,\ldots,l_{2K-1};k} = \sum_{r=0}^{K-k} \binom{k+r}{k} (\omega^{(K-1)}_{l_1,\cdots,l_{2K-2};k+r} - (-1)^r \omega^{(K-1)}_{l_{2K-2+1},\cdots,l_{2K-1};k+r})\tau^r, \tag{6.32}$$

and the spatial frequency coefficients $\Omega^{(K)}_{l_1,\cdots,l_{2K-1};k}$ *can be computed using the following*

iterative rule

$$\Omega^{(1)}_{l_1;k} = \omega_{l_1,k} \sin\theta_{l_1}, \quad k = 1, \ldots, K, \tag{6.33}$$

$$\Omega^{(2)}_{l_1,l_2;k} = \sum_{r=0}^{K-k} \binom{r+k-1}{k-1} (\Omega^{(1)}_{l_1;k+r} - (-1)^r \Omega^{(1)}_{l_2;k+r})\tau^r, \tag{6.34}$$

$$\vdots$$

$$\Omega^{(K)}_{l_1,\ldots,l_{2K-1};k} = \sum_{r=0}^{K-k} \binom{r+k-1}{k-1} (\Omega^{(K-1)}_{l_1,\cdots,l_{2K-2};k+r} - (-1)^r \Omega^{(K-1)}_{l_{2K-2+1},\cdots,l_{2K-1};k+r})\tau^r. \tag{6.35}$$

Proof. See Appendix A.

Lemma 6.3 *The autoterms of the Kth-order SHIM given in (6.27) are narrowband with spatial frequencies*

$$\Omega^{(K)}_{l,1} = (2\tau)^{K-1}(K-1)!\ \omega_{l,K} \sin\theta_l, \tag{6.36}$$

and the signal waveform of the lth autoterm is a complex sinusoid with frequency

$$\omega^{(K)}_{l,1} = (2\tau)^{K-1}(K-1)!\ \omega_{l,K}. \tag{6.37}$$

Proof. By setting $l_1 = l_2 = l$ in the 2nd-order SHIM (6.34) we find that

$$\Omega^{(2)}_{l,K} = 0, \tag{6.38}$$

$$\Omega^{(2)}_{l,K-1} = 2\tau(K-1)\omega_{l,K} \sin\theta_l. \tag{6.39}$$

Similarly, by setting $l_1 = l_2 = l_3 = l$ in the 3rd-order SHIM we find that

$$\Omega^{(3)}_{l,K} = \Omega^{(3)}_{l,K-1} = 0, \tag{6.40}$$

$$\Omega^{(3)}_{l,K-2} = (2\tau)^2(K-1)(K-2)\omega_{l,K} \sin\theta_l. \tag{6.41}$$

Repeating the same procedure until reaching the Kth-order SHIM we get

$$\Omega_{l,k}^{(K)} = \begin{cases} (2\tau)^{K-1}(K-1)!\,\omega_{l,K}\sin\theta_l, & k=1, \\ 0, & k=2,\ldots,K \end{cases} \tag{6.42}$$

which proves (6.36). The proof of (6.37) results directly from (6.23) by substituting for $v_{l,k} = \omega_{l,k}/k$. ■

Based on Lemma 6.3, the Kth-order SHIM given in (6.27) can be rewritten in the following form

$$\mathbf{x}^{(K)}(t;\tau) = \sum_{l=1}^{L} d_l^{(K)}(t)\mathbf{a}\left(\omega_{l,1}^{(K)}, \theta_l\right) + \text{crossterms}, \tag{6.43}$$

where

$$d_l^{(K)}(t) = \alpha_l^{2^{K-1}} \exp\left\{j\left(\omega_{l,0}^{(K)} + \omega_{l,1}^{(K)} t\right)\right\} \tag{6.44}$$

is the signal waveform of the lth autoterm and

$$\mathbf{a}\left(\omega_{l,1}^{(K)}, \theta_l\right) = \left[1, \exp\left\{j\frac{\omega_{l,1}^{(K)}}{c\Delta t} h_1 \sin\theta_l\right\}, \ldots, \exp\left\{j\frac{\omega_{l,1}^{(K)}}{c\Delta t} h_{M-1}\sin\theta_l\right\}\right]. \tag{6.45}$$

is the steering vector associated with the lth autoterm.

The fact that the signal waveforms of the autoterms of $\mathbf{x}^{(K)}(t;\tau)$ are sinusoids provides the basis for estimating the highest-order frequency parameters via estimating the frequencies of the autoterms. The HAF that has been widely used for estimating the highest-order frequency coefficients in the single antenna case can be used for estimating the same parameters in the multiple antenna case, i.e., the HAF of the output of each sensor can be used to obtain an estimate of the highest-order frequency coefficients. Hence, in the multiple antenna case, the number of estimates of each frequency parameter that can be obtained is equal to the number of sensors. The M different estimates of each frequency parameter can be incorporated to obtain a better final estimate of that parameter.

More interestingly, Lemma 6.3 provides the basis for estimating the DOAs of the PPSs by computing the Kth-order SHIM and retrieving the spatial frequencies of the autoterms contained in that SHIM. Unfortunately, conventional array processing techniques can not be used to estimate the spatial frequencies of the autoterms due to the existence of wideband crossterms. However, the fact that the time-frequency signatures of the autoterms are localizable and distinguishable from the time-frequency signatures of the crossterms motivates the use of STFD-based methods for estimating the DOAs.

6.4 A New PPS Parameter Estimation Algorithm

In the previous Section, we have shown that the autoterms of the Kth-order SHIM of multiple wideband PPSs of order K are narrowband while the crossterms are, in general, wideband. We have also shown that the waveforms of the autoterms are sinusoids while the waveforms of the crossterms are high-order PPSs. Hence, the SHIM of the array data output vector given in (6.1) can be written as

$$\mathbf{x}^{(K)}(t;\tau) = \mathbf{A}^{(K)}\mathbf{d}^{(K)}(t) + \mathbf{n}^{(K)}(t;\tau) + \text{crossterms}, \tag{6.46}$$

where $\mathbf{d}^{(K)}(t)$ is the vector that contains the waveforms of the autoterms, $\mathbf{n}^{(K)}(t;\tau)$ is the vector that contains all the noise terms contained in the Kth-order SHIM, and $\mathbf{A}^{(K)}$ is the mixing matrix

$$\mathbf{A}^{(K)} = \left[\mathbf{a}\left(\omega_{1,1}^{(K)},\theta_1\right),\ldots,\mathbf{a}\left(\omega_{L,1}^{(K)},\theta_L\right)\right]. \tag{6.47}$$

Note that the mixing matrix $\mathbf{A}^{(K)}$ does not change with time. In what follows we will introduce an algorithm for estimating the frequency parameters $\omega_{l,k}(l=1,\ldots,L;k=1,\ldots,K)$ as well as the DOAs $\{\theta_l\}_{l=1}^{L}$.

The proposed algorithm estimates the required parameters in four basic steps. First, we compute M different estimates of the highest-order frequency parameters $\{\omega_{l,K}\}_{l=1}^{L}$. Next, we compute J different estimates of the DOAs denoted as $\hat{\theta}_l^{(i)}, (l = 1, \ldots, L; i = 1, \ldots, J)$. Then, we compute M different estimates of $\omega_{l,k} (l = 1, \ldots, L; k = 1, \ldots, K-1)$. Finally, we select the best set of estimates from the available sets of estimates as the final estimate. Note that these four basic steps have to be done sequentially because each step incorporates the results obtained in the previous steps in the estimation process. In what follows we will give a detailed explanation of each of the four basic steps.

In the first basic step, we start by computing M different estimates of the frequencies of the autoterms contained in the SHIM of $\mathbf{x}(t)$, i.e., we compute M different estimates of $\{\omega_{l,1}^{(K)}\}_{l=1}^{L}$ where the mth estimate $\{\hat{\omega}_{l,1;m}^{(K)}\}_{l=1}^{L}$ can be obtained by searching for the L highest peaks of the HAF of the mth sensor data output. The HAF of the mth sensor data output can be obtained by simply computing the discrete Fourier transform of the mth row of $\mathbf{x}^{(K)}(t;\tau)$, that is,

$$X_m^{(K)}(\omega) = DFT\left\{x_m^{(K)}(t;\tau)\right\}, \quad m = 1, \ldots, M. \tag{6.48}$$

Then, M different estimates of the highest-order coefficients $\{\omega_{l,K}\}_{l=1}^{L}$ can be retrieved from $\{\hat{\omega}_{l,1;m}^{(K)}\}_{l=1}^{L}$ as follows

$$\hat{\omega}_{l,K;m} = \frac{\hat{\omega}_{l,1;m}^{(K)}}{(2\tau)^{K-1}(K-1)!}, \quad m = 1, \ldots, M. \tag{6.49}$$

An additional processing step is required to combine the M different estimates $\hat{\omega}_{l,K;m}$ in order to obtain a final estimate of $\omega_{l,K}$. An easy way to do so is to choose the mean or the median as the final estimate. Another way to obtain the final estimate is to evaluate the value of the exact ML (c.f. (6.16)) at each of the estimates at hand [91]. Then, the estimate that yields the maximum likelihood can be chosen as the final

estimate. However, this method can not be used unless all the frequency coefficients are estimated. Hence, we will use the mean of $\hat{\omega}_{l,K;m}$ as a temporary estimate of $\omega_{l,K}$. We will incorporate this temporary estimate in subsequent estimation steps while the ML selection criterion will be used at the very last step of the estimation process. In particular we define the mean of the available estimates as

$$\bar{\omega}_{l,K} = \frac{1}{M} \sum_{m=1}^{M} \hat{\omega}_{l,K;m}. \tag{6.50}$$

The second basic step of the algorithm involves estimating the DOAs $\{\theta_l\}_{l=1}^{L}$. The nice structure of autoterms contained in the Kth-order SHIM in (6.46) motivates the use of subspace-based methods for estimating the DOAs. However, conventional subspace-based methods can not be used because the covariance matrix of $\mathbf{x}^{(K)}(t;\tau)$ is full rank due to the existence of wideband crossterms. Fortunately, STFD-based techniques (e.g. time-frequency MUSIC) can be used if the STFD matrices are computed at time-frequency points that belong to the time-frequency signatures of the autoterms. The sample SPWVD matrix of $\mathbf{x}^{(K)}(t)$ is given by

$$\hat{\mathbf{D}}_{\mathbf{x}^{(K)}}(t,f) = \sum_{T=-(N_0-1)/2}^{(N_0-1)/2} \mathbf{x}^{(K)}(t+T) \left(\mathbf{x}^{(K)}\right)^H (t-T) e^{-j4\pi fT}, \tag{6.51}$$

where N_0 is the odd window length. For every time-frequency point that belongs to the signatures of the autoterms, the following holds true

$$\begin{aligned} \mathbf{D}_{\mathbf{x}^{(K)}}(t,f) &= \mathrm{E}\{\hat{\mathbf{D}}_{\mathbf{x}^{(K)}}(t,f)\} \\ &= \mathbf{A}^{(K)} \mathbf{D}_{\mathbf{d}^{(K)}}(t,f) \left\{\mathbf{A}^{(K)}\right\}^H + \sigma^2_{\mathbf{n}^{(K)}} \mathbf{I}, \end{aligned} \tag{6.52}$$

where

$$\mathbf{D}_{\mathbf{d}^{(K)}}(t,f) = \mathrm{E}\{\hat{\mathbf{D}}_{\mathbf{d}^{(K)}}(t,f)\}, \tag{6.53}$$

$$\hat{\mathbf{D}}_{\mathbf{d}^{(K)}}(t,f) = \sum_{T=-(N_0-1)/2}^{(N_0-1)/2} \mathbf{d}^{(K)}(t+T) \left\{\mathbf{d}^{(K)}\right\}^H (t-T) e^{-j4\pi fT}. \tag{6.54}$$

The eigenstructure properties of the STFD matrix (6.52) can be exploited to estimate the autoterms spatial frequencies $\{\Omega_{l,1}^{(K)}\}_{l=1}^{L}$ in a similar way as in the conventional subspace-based array processing techniques. In practical situations, the sample STFD matrices (6.51) are used instead of the exact (statistically expected) matrices (6.52). In order to reduce the effect of the sensor noise and to make sure that the STFD matrix is full rank, an averaging over multiple time-frequency points can be used. In particular, we form the averaged STFD matrices $\tilde{\mathbf{D}}_{\mathbf{x}^{(K)}}^{(i)}(i = 1, \ldots, J)$, where the ith STFD matrix is formed by averaging multiple SPWVD matrices computed at $P_i Q_i$ different time-frequency points that belong to the time-frequency signatures of the autoterms, i.e.,

$$\tilde{\mathbf{D}}_{\mathbf{x}^{(K)}}^{(i)} = \sum_{p_i=1}^{P_i} \sum_{q_i=1}^{Q_i} \hat{\mathbf{D}}_{\mathbf{x}^{(K)}}(t_{p_i}, f_{q_i}), \quad p_i = 1, \ldots, P_i; q_i = 1, \ldots, Q_i. \tag{6.55}$$

Each averaged STFD matrix can be used to obtain an estimate of the DOAs. The signal subspace (or noise subspace) can be obtained from the eigen-decomposition of the matrices $\tilde{\mathbf{D}}_{\mathbf{x}^{(K)}}^{(i)}$, then any subspace-based method (e.g. MUSIC) can be used to compute estimates of $\Omega_{l,1}^{(K)}$. Using (6.36), estimates of $\{\theta_l\}_{l=1}^{L}$ can be retrieved from $\{\hat{\Omega}_{l,1;i}^{(K)}\}_{l=1}^{L}$ as follows

$$\hat{\theta}_l^{(i)} = \arcsin\left\{ \frac{\hat{\Omega}_{l,1;i}^{(K)}}{(2\tau)^{K-1}(K-1)!\omega_{l,K}} \right\}, \quad i = 1, \ldots, J. \tag{6.56}$$

Once again, the final estimate of the DOAs can be obtained using the mean, median, or the ML selection criteria. At the time being, a temporary estimate of θ_l will be computed as the mean of the J available estimates, that is,

$$\bar{\theta}_l = \frac{1}{J} \sum_{i=1}^{J} \hat{\theta}_l^{(i)}. \tag{6.57}$$

The temporary estimate $\bar{\theta}_l$ will be incorporated in subsequent processing steps.

Although one STFD matrix ($J = 1$) is enough to estimate the sources DOAs, we recommend that multiple STFD matrices be used for this purpose. The reason we do that is to obtain a temporary estimate of the DOAs that is as accurate as possible in order to avoid error propagation due to the recursive nature of the algorithm.

In the third basic processing step, we estimate the frequency coefficients $\omega_{l,k}(l = 1,\ldots,L; k = 1,\ldots,K-1)$ in a recursive manner starting with $\omega_{l,K-1}$. At each iteration, we incorporate the temporary estimates that have been obtained in previous processing steps in order to remove the contribution of the already estimated parameters from $\mathbf{x}(t)$. If we consider the iteration at which we estimate $\omega_{l,k}$, assuming that the values of the temporary estimates $\bar{\theta}_l$ and $\{\bar{\omega}_{l,z}\}_{z=k+1}^{K}$ are obtained in previous steps, we can compute the compensating vectors

$$\mathbf{y}_{l,k}(t) = \exp\left\{-j\sum_{z=k+1}^{K}\frac{1}{z}\bar{\omega}_{l,z}t^z\right\}\tilde{\mathbf{a}}_{l,k}, \quad l = 1,\ldots,L, \tag{6.58}$$

where

$$\begin{aligned}\tilde{\mathbf{a}}_{l,k} = \Bigg[&1, \exp\left\{-j\frac{h_1}{c\Delta t}\sum_{z=k+1}^{K}\bar{\omega}_{l,z}t^{z-1}\sin\bar{\theta}_l\right\},\\ &\ldots, \exp\left\{-j\frac{h_{M-1}}{c\Delta t}\sum_{z=k+1}^{K}\bar{\omega}_{l,z}t^{z-1}\sin\bar{\theta}_l\right\}\Bigg]^T.\end{aligned} \tag{6.59}$$

Then, we can compute the compensated data vectors as

$$\tilde{\mathbf{x}}_{l,k}(t) = \mathbf{x}(t)\odot\mathbf{y}_{l,k}(t), \quad l = 1,\ldots,L. \tag{6.60}$$

If the values of the temporary estimates $\bar{\theta}_l$ and $\{\bar{\omega}_{l,z}\}_{z=k+1}^{K}$ are accurately estimated, then the lth signal component contained in $\tilde{\mathbf{x}}_{l,k}(t)$ will be of order k while all other signal components will be of order K, i.e., the compensation reduces the order of the lth signal component by $K-k$. Let $\tilde{\mathbf{x}}_{l,k}^{(k)}(t)$ be the kth-order SHIM of $\tilde{\mathbf{x}}_{l,k}(t)$. Then, the waveform of the lth autoterm contained in $\tilde{\mathbf{x}}_{l,k}^{(k)}(t)$ will be a complex sinusoid with

frequency

$$\omega_{l,1}^{(k)} = (2\tau)^{k-1}(k-1)!\ \omega_{l,k}. \tag{6.61}$$

Moreover, the array response vector associated with this lth autoterm will be narrowband with spatial frequency

$$\Omega_{l,1}^{(k)} = (2\tau)^{k-1}(k-1)!\ \omega_{l,k} \sin\theta_l. \tag{6.62}$$

The above equation showes that the array response vector does not change with time. Hence, we can obtain M different estimates of the frequency coefficient $\omega_{l,1}^{(k)}$, where the mth estimate $\hat{\omega}_{l,1;m}^{(k)}$ can be obtained by searching for the highest peak of the HAF defined as

$$\tilde{X}_{l,k;m}^{(k)}(\omega) = DFT\{x_{l,k;m}^{(k)}(t;\tau)\}, \tag{6.63}$$

where $x_{l,k;m}^{(k)}(t;\tau)$ is the mth-row of $\tilde{\mathbf{x}}_{l,k}^{(k)}(t)$. Then, M different estimates of $\omega_{l,k}$ can be retrieved from the estimates $\hat{\omega}_{l,k;m}^{(k)}$ as follows

$$\hat{\omega}_{l,k;m} = \frac{\hat{\omega}_{l,1;m}^{(k)}}{(2\tau)^{k-1}(k-1)!}, \qquad m = 1, \ldots, M. \tag{6.64}$$

The temporary estimate $\bar{\omega}_{l,k}$ can be computed as the mean of $\hat{\omega}_{l,k;m}$. The process can be repeated until the first order frequency parameters $\{\omega_{l,1}\}_{l=1}^{L}$ are estimated.

The final step in the algorithm involves selecting the best set of estimates from the available sets of estimates $\{\hat{\boldsymbol{\omega}}^{(m)}, \hat{\boldsymbol{\theta}}^{(i)}\}(m = 1, \ldots, M; i = 1, \ldots, J)$ where

$$\hat{\boldsymbol{\theta}}^{(i)} \triangleq \left[\hat{\theta}_1^{(i)}, \ldots, \hat{\theta}_L^{(i)}\right]^T \tag{6.65}$$

and

$$\hat{\boldsymbol{\omega}}^{(m)} \triangleq \begin{bmatrix} \hat{\omega}_{1,1;m} & \hat{\omega}_{2,1;m} & \cdots & \hat{\omega}_{L,1;m} \\ \hat{\omega}_{1,2;m} & \hat{\omega}_{2,2;m} & \cdots & \hat{\omega}_{L,2;m} \\ \vdots & \vdots & \ddots & \vdots \\ \hat{\omega}_{1,K;m} & \hat{\omega}_{2,K;m} & \cdots & \hat{\omega}_{L,K;m} \end{bmatrix}. \tag{6.66}$$

The set that maximizes the ML value will be chosen as the final set of estimates, i.e., we choose the final set of estimates as

$$[\hat{\boldsymbol{\theta}}, \hat{\boldsymbol{\omega}}] = \arg \max_{\boldsymbol{\theta},\boldsymbol{\omega}} L_P(\boldsymbol{\theta}, \boldsymbol{\omega}) \qquad \text{s.t.} \qquad \boldsymbol{\theta} \in \hat{\boldsymbol{\theta}}^{(i)}, \quad i = 1, \ldots, J, \quad \boldsymbol{\omega} \in \hat{\boldsymbol{\omega}}^{(m)}, \quad m = 1, \ldots, M. \tag{6.67}$$

We stress that the proposed algorithm is still applicable when the received PPSs are subject to aliasing in time domain as long as there is no aliasing in the spatial domain. In order to avoid ambiguity in the frequency parameters $\omega_{l,k}, (k = 2, \ldots, K)$, the following condition must hold

$$\left|\omega_{l,k}^{(k)}\right| = (2\tau)^{K-1}(K-1)!\ |\omega_{l,K}| < \pi, \quad k = 2, \ldots, K. \tag{6.68}$$

The above conditions imply that the waveforms of the autoterms are not subject to aliasing in the time domain. Regardless of the values of the true frequency parameters, the above condition can be satisfied by making appropriate choice of time lag τ (which is a user design parameter). The problem will be more complicated if the PPSs suffer from aliasing with respect to the initial frequency parameter $\omega_{l,1}$, i.e., if $\omega_{l,1} > \pi$. Let us assume that $\hat{\omega}_{l,1}$ is an estimate of $\omega_{l,1}$, then

$$\hat{\omega}_{l,1;n} = \hat{\omega}_{l,1} + 2\pi n \tag{6.69}$$

is also an estimate of $\omega_{l,1}$ for values of n that satisfies the following condition

$$\left|\frac{1}{c\Delta t}\hat{\omega}_{l,1;n}\right| < \pi. \tag{6.70}$$

The above condition is a necessary condition for the signals to be non-aliased in the spatial domain. The ML estimator, being a space-time processing technique, is able to select the true estimate from the multiple estimates given in (6.69). Hence, the ML selection criterion allows us to avoid ambiguity about $\omega_{l,1}$.

Now, we can formulate our PPS parameter estimation algorithm as follows

- *Step 1:* Estimating the highest-order frequency coefficients $\{\omega_{l,K}\}_{l=1}^{L}$.

  1.1 Choose a positive value τ and compute $\mathbf{x}^{(K)}(t)$ which is the Kth-order SHIM of $\mathbf{x}(t)$.

  1.2 Compute the M different estimates $\hat{\omega}_{l,1;m}^{(K)}$ by searching for the L highest peaks in $X_m^{(K)}(f), (m = 1, \ldots, M)$, where $X_m^{(K)}(f)$ is given by (6.48).

  1.3 Compute $\hat{\omega}_{l,K;m}$ from $\hat{\omega}_{l,1;m}^{(K)}$ using (6.49).

  1.4 Compute $\bar{\omega}_{l,K}$ from $\hat{\omega}_{l,K;m}$ using (6.50).

- *Step 2:* Estimating the DOAs $\{\theta_l\}_{l=1}^{L}$.

  2.1 Compute the sample SPWVD matrices $\hat{\mathbf{D}}_{\mathbf{x}^{(K)}}(t, f)$ at PQ different time-frequency points that belong to the time-frequency signatures of the autoterms.

  2.2 For each value of $i = 1, \ldots, J$, compute the averaged STFD matrices $\tilde{\mathbf{D}}_{\mathbf{x}^{(K)}}^{(i)}$ by means of involving in the averaging process a subset of the PQ time-frequency points that contains $P_i Q_i$ points.

  2.3 Use the matrices $\tilde{\mathbf{D}}_{\mathbf{x}^{(K)}}^{(i)}$ to obtain estimates of the spatial frequencies $\hat{\Omega}_{l,1;i}^{(K)}$ using any subspace-based method (e.g. MUSIC).

  2.4 Compute the DOA estimates $\hat{\theta}_l^{(i)}$ from $\hat{\Omega}_{l,1;i}^{(K)}$ using (6.56).

  2.5 Compute $\bar{\theta}_l$ as the average of $\hat{\theta}_l^{(i)}$.

- *Step 3:* Estimating the frequency coefficients $\{\omega_{l,k}\}_{l=1}^{L}$, $(k = 1, \ldots, K-1)$.

  3.1 Set $k = K-1$. Compute the compensated data snapshots $\{\tilde{\mathbf{x}}_{l,k}(t)\}_{l=1}^{L}$ using (6.60).

  3.2 Compute the kth-order SHIM $\{\tilde{\mathbf{x}}_{l,k}^{(k)}(t)\}_{l=1}^{L}$, then compute the spectrums $\tilde{X}_{l,k;m}^{(k)}, (l = 1, \ldots, L; m = 1, \ldots, M)$ using (6.63).

3.3 Compute the estimates $\hat{\omega}_{l,1;m}^{(k)}$ by searching for the highest peak of the spectrum $\tilde{X}_{l,k;m}^{(k)}$.

3.4 Compute estimates of $\omega_{l,k}$ as

$$\hat{\omega}_{l,k;m} = \frac{\hat{\omega}_{l,1;m}^{(k)}}{(2\tau)^{k-1}(k-1)!}, \qquad m = 1, \ldots, M \tag{6.71}$$

3.5 Compute $\bar{\omega}_{l,k}$ as the mean of $\hat{\omega}_{l,k;m}$.

3.6 Set $k = k - 1$. If $k \geq 1$ go to step 3.

- *Step 4:* Selecting the final estimates.

4.1 For each set of the estimates $\{\hat{\boldsymbol{\omega}}_l^{(m)}, \hat{\boldsymbol{\theta}}_l^{(i)}\}$ $(i = 1, \ldots, J;\ m = 1, \ldots, M)$, evaluate the ML value (c.f (6.16)).

4.2 Choose the set of estimates that yields the highest ML value as the final set of estimates.

6.5 Simulation Results

In our simulations, we assume a ULA of $M = 10$ omnidirectional sensors. The sonar case [32] is considered with the sound propagation speed $c = 1500$ m/s and the interelement spacing $d = 1.5$ m. The additive noise is modeled as a complex Gaussian zero-mean spatially and temporally white process that have identical variances in each array sensor. We assume that the ULA receives two equi-powered chirp signals impinging on the array from the directions $\theta_1 = 10°$ and $\theta_2 = 20°$ relative to the broadside and having the initial continuous-time frequencies 408 Hz and 401 Hz, respectively, and the continuous-time chirp rates -50 Hz/s and 60 Hz/s, respectively (the latter correspond to the discrete-time chirp rates $\omega_{1,2} = -0.00479$ and $\omega_{2,2} = 0.00575$, respectively). An observation interval of $N_s = 256$ snapshots with

the sampling interval $\Delta t = 1/N_s$ is considered. Note that the signals are subject to aliasing in time as the sampling frequency is smaller than the initial frequencies.

The Wigner-Ville distribution computed for $N_s = 256$ samples of the sampled source waveforms in their baseband representation is shown in Figure 6.1. Note that, the baseband representation corresponds to downconverted waveforms with the downconversion frequency 400 Hz. The second-order SHIM of the received data is computed using the time lag $\tau = 25\Delta t$, i.e., the time lag is chosen to be 25 times of the sampling interval. The WVD of the transformed data computed using the data in the first row of the second-order SHIM is shown in Figure 6.2. As we can see from this figure, the time-frequency signatures of the autoterms are parallel to the time index while the time-frequency signatures of the crossterms have chirp components.

The FFT is used to compute the HAF of the data in each row of the second-order SHIM. The HAF spectrum of the data in the first row is shown in Figure 6.3. The chirp rates are estimated by searching for the two highest peaks in the HAF. The STFD-based estimation techniques are used to estimate the sources DOAs. For each autoterm, 200 SPWVD matrices are computed at 200 different time-frequency points that belong to the autoterm signature, and then these 200 SPWVD matrices are used to compute 20 averaged STFD matrices. The root-MUSIC algorithm is used to obtain estimates of the DOAs using the averaged STFD matrices. A total of 500 independent Monte-Carlo simulation runs have been used to obtain each simulation point. The experimental RMSEs of the DOAs, the initial frequencies, and the chirp rates are shown in Figures 6.4, 6.5, and 6.6 respectively. It is clear from these figures that the proposed method has better performance than the well known CBF.

6.6 Conclusions

A new algorithm for estimating the parameters of multiple wideband PPSs in sensor arrays is proposed. The SHIM which is a nonlinear transformation that can be applied to array data vectors has been introduced. The SHIM of multiple wideband PPSs has been discussed and employed to provide recursive estimates of the PPSs frequency parameters. The time-frequency properties of the SHIM have been exploited for estimating the sources DOAs using STFD-based methods. The proposed algorithm has better performance than the CBF at lower computational load. Simulation results were provided to illustrate the effectiveness of the proposed approach.

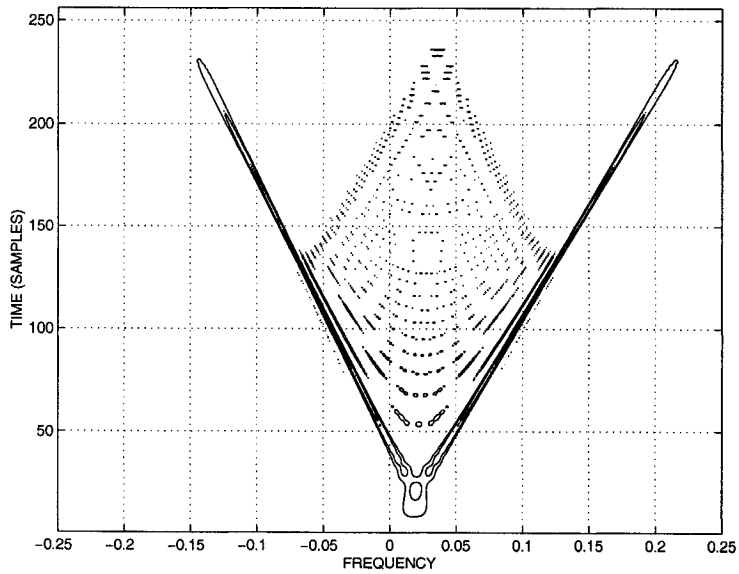

Figure 6.1: WVD of the source waveforms.

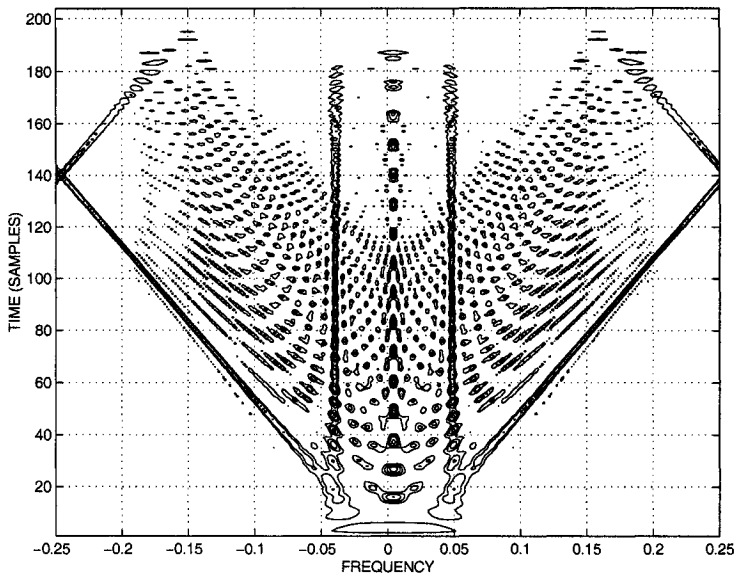

Figure 6.2: WVD of the signal waveforms of the 2nd-order SHIM.

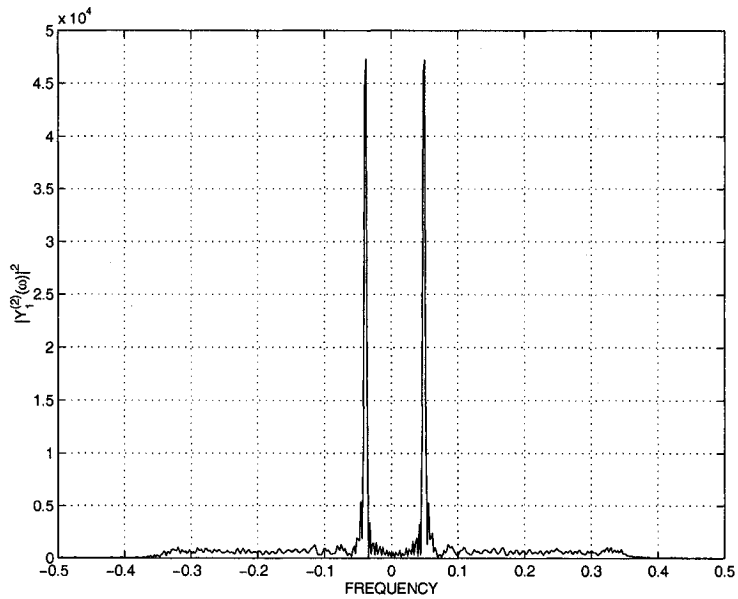

Figure 6.3: Magnitude square of the HAF of the data received at the first sensor.

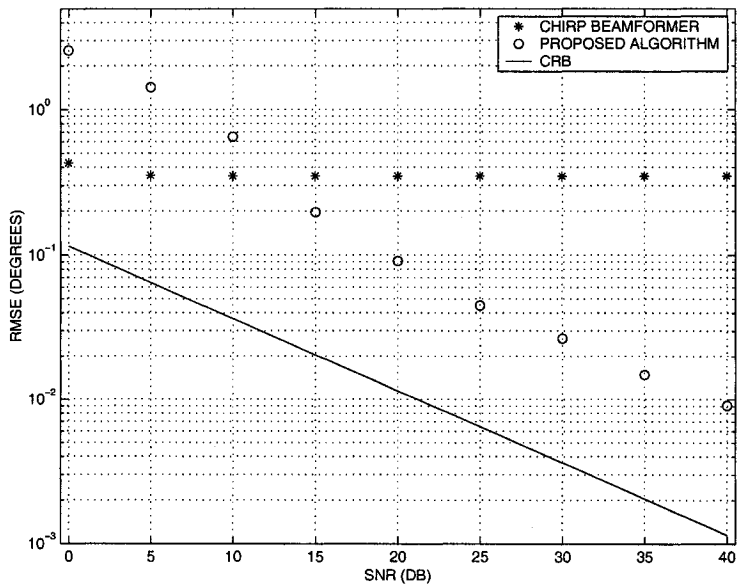

Figure 6.4: DOA estimation RMSEs versus SNR.

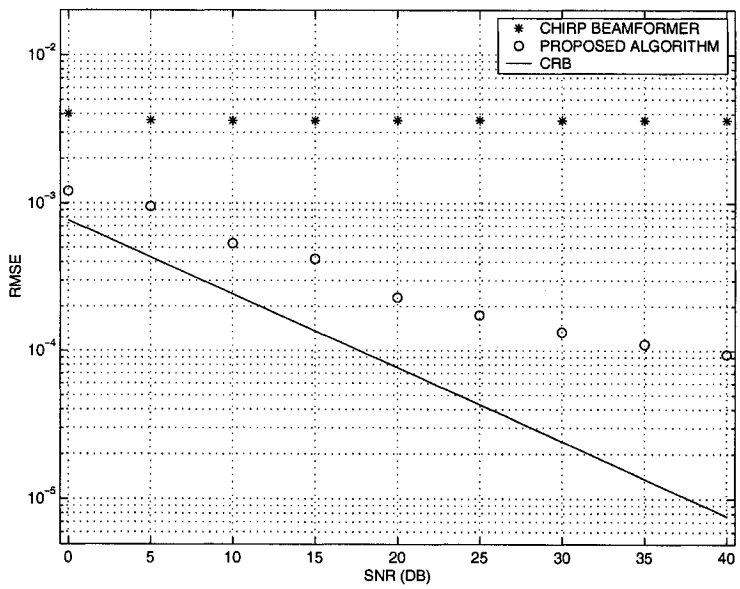

Figure 6.5: Initial frequency estimation RMSEs versus SNR.

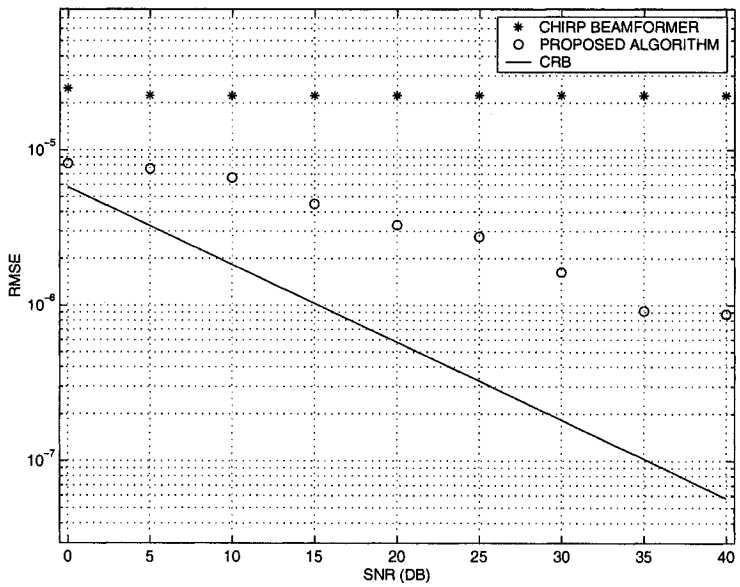

Figure 6.6: Chirp rate estimation RMSEs versus SNR.

Chapter 7

Concluding Remarks and Future Directions

In this chapter we highlight the main contributions in this thesis. We also discuss possible extensions for the future work.

7.1 Conclusions

This thesis has addressed the general problem of array signal processing in the presence of complicated spatio-temporal sources. Several important problems that are encountered in practical applications have been discussed. Novel array processing algorithms and techniques that can efficiently solve these problems have been developed.

The problem of estimating the DOAs of weak desired sources observed in the background of strong interference has been addressed in Chapter 2. A new approach to beamspace preprocessing with a substantially improved robustness against out-of-sector sources has been developed. Our techniques design the beamspace matrix

filter based on proper tradeoffs between the in-sector (passband) source distortion and out-of-sector (stopband) source attenuation. The new concept of *adaptive beamspace* has been introduced. Convex optimization formulations of such robust and adaptive beamspace matrix filter design problems have been proposed using SOC programming. Simulation results have been presented to validate the robustness of the proposed techniques.

Chapter 3 has addressed the problem of parameter estimation of multiple spatially distributed sources. The specific case of ID sources has been considered. A new method for estimating the angular parameters of these ID sources has been developed. The proposed technique is based on the generalization of the well-known Capon estimator. Our method involves a two-dimensional search over the parameter space and shows a substantially improved performance relative to several popular spread source localization techniques. Simulation results have been included in order to verify the effectiveness of the proposed approach.

The problem of DOA estimation of multiple narrowband chirp signals in sensor arrays has been addressed in Chapter 4. For this purpose, a new search-free time-frequency ESPRIT algorithm has been introduced. The proposed algorithm is based on the concept of STFDs. It employs multiple averaged STFD matrices to obtain the estimates of the signal DOAs instead of the covariance matrix (used in conventional array processing methods). Based on computer simulations, it has been shown that in scenarios with chirp signals the proposed technique outperforms the conventional ESPRIT algorithm. The performance improvement is high especially in the case when the SNR is low or the sources are closely spaced.

In Chapter 5, we have approached the problem of estimating the parameters of multiple wideband PPSs in sensor arrays. To solve this problem, a new computationally efficient algorithm has been proposed. The SHIM, which is a nonlinear

transformation, has been introduced. The properties of the SHIM when applied to multiple wideband PPSs have been employed to provide recursive estimates of the PPSs frequency parameters. The time-frequency properties of the SHIM have been also exploited in estimating the sources DOAs using STFD-based methods. The introduced method is computationally efficient as it requires multiple one-dimensional searches instead of multi-dimensional search. It has been shown that the proposed algorithm has better performance than earlier suboptimal techniques. Simulation results have been provided to illustrate the effectiveness of the proposed approach.

7.2 Future Work

Throughout the thesis, the white Gaussian noise assumption has been always used. An interesting extension of the proposed algorithms would be to consider the unknown noise case. Under such a new assumption, all presented algorithms can be further modified.

Several other extensions of our results can be relevant. In what follows, we will describe some of these future research directions.

7.2.1 Robust Beamspace Preprocessing

From our work on robust beamspace preprocessing that has been presented in Chapter 2, several issues arise. Future work could include some of these issues as given below:

- Robust beamspace preprocessing with improved robustness against signal model mismatch. Such a mismatch may result as a consequence of environmental non-stationarity, multipath propagation effects, array manifold errors and perturbations, multiplicative noise and fading effects, and other undesirable phenomena (see [29] and references therein).

- It would be useful if the computational complexity of the adaptive beamspace preprocessing algorithm could be further reduced. Recall that the adaptive beamspace algorithm is implemented via the SOC programming (3.63) which is sparse. It is quite possible that a specially tailored SOC solver for this problem could be developed.

7.2.2 Spatially Spread Sources

More research on the case of spatially distributed sources could be carried out in one of the following two main directions.

- Based on our work in Chapter 3, a future research direction would be the localization of weak desired sources observed in the background of hot clutter. Hot clutter is a terrain-scattered jamming that occurs when a high power jammer transmits its energy into the ground. The ground reflects the energy in a dispersive manner, hence it appears at the receiving array as a distributed source. The scenario becomes quite complicated when the terrain scattered interference impinges on the receiving array within the same spatial domain as the desired source.

- The generalized Capon estimator (4.23) that has been proposed in Chapter 3 for localization of multiple spatially distributed sources requires a two-dimensional search. At each point on the search grid, the eigendecomposition of an $M \times M$ matrix has to be evaluated. The computational complexity could be very high if the two-dimensional search is done over a fine grid. We believe that a computationally efficient adaptive algorithm could be developed for this purpose.

7.2.3 Wideband Polynomial-Phase Signals

Our work on the parameter estimation of multiple wideband PPSs can be considered in several respects that include the following:

- The parameter estimation algorithm that has been developed in Chapter 5 is based on the assumption that the PPSs have a constant amplitude. It would be interesting if our results could be generalized for the case of multiple wideband PPSs with time-varying amplitudes.
- Recall that the SHIM given in (6.25) was exploited by the PPS parameter estimation algorithm. The used SHIM is based on single-lag transformation. The case of SHIM using multi-lag transformation is worth investigating. Also, methods for mitigating the effects of the cross-terms, that appear in the SHIM when applied to multi-component data, are of great demand.
- A further reduction of the computational cost of PPS parameter estimation could be achieved done via developing new search-free algorithms.
- Extension of our approach to the case of moving sources could be made.
- Derivation of the identifiability conditions for parameter estimation of PPSs could be an interesting topic for future research.

Appendix A

Proof of Lemma 6.2

Let $x_m(t)$ be the mth entry in the data vector $\mathbf{x}(t)$

$$\begin{aligned} x_m(t) &= \sum_{l=1}^{L} \alpha_l \exp\left\{ j(\omega_{l,0} + \sum_{k=1}^{K} \frac{1}{k}\omega_{l,k} t^k) \right\} \\ &\quad \cdot \exp\left\{ j\frac{h_m}{c\Delta t} \left(\sum_{k=1}^{K} \omega_{l,k} t^{k-1} \right) \sin\theta_l \right\} \\ &= \sum_{l=1}^{L} d_l(t) a_{l;m}(t), \end{aligned} \tag{A.1}$$

where the sequences $d_l(t)$ and $a_{l;m}(t)$ are defined as follows

$$d_l(t) = \alpha_l \exp\left\{ j(\omega_{l,0} + \sum_{k=1}^{K} \frac{1}{k}\omega_{l,k} t^k) \right\}, \tag{A.2}$$

$$a_{l;m}(t) = \exp\left\{ j\frac{h_m}{c\Delta t} (\sum_{k=1}^{K} \omega_{l,k} t^{k-1}) \sin\theta_l \right\}. \tag{A.3}$$

The 2nd-order HIM of $x_m(t)$ is given by

$$\begin{aligned} x_m^{(2)}(t;\tau) &= x_m(t+\tau)x_m^*(t-\tau) \\ &= \sum_{l_1,l_2=1}^{L} [d_{l_1}(t+\tau)a_{l_1;m}(t+\tau)] \cdot [d_{l_2}(t-\tau)a_{l_2;m}(t-\tau)]^* \\ &= \sum_{l_1,l_2=1}^{L} [d_{l_1}(t+\tau)d_{l_2}^*(t-\tau)] \cdot [a_{l_1;m}(t+\tau)a_{l_2;m}^*(t-\tau)] \\ &= \sum_{l_1,l_2=1}^{L} d_{l_1,l_2}^{(2)}(t;\tau)a_{l_1,l_2;m}^{(2)}(t;\tau), \end{aligned} \tag{A.4}$$

where $d_{l_1,l_2}^{(2)}(t;\tau)$ and $a_{l_1,l_2;m}^{(2)}(t;\tau)$ are the (l_1,l_2)th-terms of the second-order HIM of $d_l(t)$ and $a_{l;m}(t)$ respectively. Repeating this operation $K-1$ times we get

$$x_m^{(K)}(t;\tau) = \sum_{l_1,\ldots,l_2^{K-1}=1}^{L} d_{l_1,\ldots,l_{2K-1}}^{(K)}(t;\tau)a_{l_1,\ldots,l_{2K-1};m}^{(K)}(t;\tau), \tag{A.5}$$

where $d_{l_1,\ldots,l_{2K-1}}^{(K)}(t;\tau)$ and $a_{l_1,\ldots,l_{2K-1};m}^{(K)}(t;\tau)$ are the $(l_1,\ldots,l_{2K-1})$th-terms of the K-order HIM of $d_l(t)$ and $a_{l;m}(t)$ respectively. Making use of Lemma 6.1 we have

$$d_{l_1,\ldots,l_{2K-1}}^{(K)}(t;\tau) = \alpha_{l_1}\cdots\alpha_{l_{2K-1}} \exp\left\{ j\sum_{k=0}^{K} \omega_{l_1,\cdots,l_{2K-1};k}^{(K)} t^k \right\}, \tag{A.6}$$

where the coefficients $\omega_{l_1,\cdots,l_{2K-1};k}^{(K)}$ can be computed using the following iterative rule

$$\omega_{l_1;k}^{(1)} = \begin{cases} \omega_{l_1,0}, & k=0 \\ \frac{1}{k}\omega_{l_1,k}, & k=1,\ldots,K, \end{cases} \tag{A.7}$$

$$\vdots$$

$$\begin{aligned} \omega_{l_1,\ldots,l_{2K-1};k}^{(K)} = &\sum_{r=0}^{K-k} \binom{k+r}{k} \Big(\omega_{l_1,\cdots,l_{2K-2};k+r}^{(K-1)} \\ &-(-1)^r \omega_{l_{2K-2+1},\cdots,l_{2K-1};k+r}^{(K-1)} \Big) \tau^r. \end{aligned} \tag{A.8}$$

Similarly, by making use of Lemma 6.1 we have

$$a_{l_1,\ldots,l_{2K-1};m}^{(K)}(t;\tau) = \exp\left\{ j\frac{h_m}{c\Delta t}\sum_{k=1}^{K} \Omega_{l_1,\cdots,l_{2K-1};k}^{(K)} t^{k-1} \right\}, \tag{A.9}$$

where the coefficients $\Omega^{(K)}_{l_1,\cdots,l_{2K-1};k}$ can be computed using the following iterative rule

$$\Omega^{(1)}_{l_1;k} = \omega_{l_1,k}\sin\theta_{l_1}, \quad k=1,\ldots,K, \tag{A.10}$$

$$\vdots$$

$$\Omega^{(K)}_{l_1,\ldots,l_{2K-1};k} = \sum_{r=0}^{K-k}\binom{r+k-1}{k-1}\left(\Omega^{(K-1)}_{l_1,\cdots,l_{2K-2};k+r} - (-1)^r\Omega^{(K-1)}_{l_{2K-2+1},\cdots,l_{2K-1};k+r}\right)\tau^r. \tag{A.11}$$

Substituting from (A.6) and (A.9) in (A.5), we get

$$x^{(K)}_m(t;\tau) = \sum_{l_1,\ldots,l_2^{K-1}=1}^{L}\alpha_{l_1}\cdots\alpha_{l_{2K-1}}\exp\left\{j\sum_{k=0}^{K}\omega^{(K)}_{l_1,\cdots,l_{2K-1};k}t^k\right\} \cdot\exp\left\{j\frac{h_m}{c\Delta t}\sum_{k=1}^{K}\Omega^{(K)}_{l_1,\cdots,l_{2K-1};k}t^{k-1}\right\}. \tag{A.12}$$

Note that the above equation holds true for all values of $m = 0,\ldots,M-1$. By rearranging the above result in a vector form we get

$$\mathbf{x}^{(K)}(t;\tau) = \sum_{l_1,\ldots,l_2^{K-1}=1}^{L} d^{(K)}_{l_1,\ldots,l_{2K-1}}(t;\tau)\mathbf{a}^{(K)}_{l_1,\ldots,l_{2K-1};m}(t;\tau), \tag{A.13}$$

where

$$\mathbf{a}^{(K)}_{l_1,\ldots,l_{2K-1};m}(t;\tau) = \begin{bmatrix} 1 \\ \exp\left\{j\frac{h_1}{c\Delta t}\sum_{k=1}^{K}\Omega^{(K)}_{l_1,\cdots,l_{2K-1};k}t^{k-1}\right\} \\ \vdots \\ \exp\left\{j\frac{h_{M-1}}{c\Delta t}\sum_{k=1}^{K}\Omega^{(K)}_{l_1,\cdots,l_{2K-1};k}t^{k-1}\right\} \end{bmatrix}. \tag{A.14}$$

Equations (A.13) and (A.14) prove Lemma 6.2. ■

Bibliography

[1] Y. Abramovich, N. Spencer, and S. Anderson, "Stochastic constraints method in nonstationary hot clutter cancellation–part 1: Fundamentals and supervised training applications," *IEEE Transactions on Aerospace and Electronic Systems*, vol. 34, no. 4, pp. 1271–1292, Oct. 1998.

[2] M. G. Amin and Y. Zhang, "Direction finding based on spatial time-frequency distribution matrices," *Digital Signal Processing*, vol. 10, no. 4, pp. 325–339, Oct. 2000.

[3] S. Anderson, "On optimal dimension reduction for sensor array signal processing," *Signal Processing*, vol. 30, no. 2, pp. 245–256, Jan. 1993.

[4] S. Anderson and A. Nehorai, "Optimal dimension reduction for array processing – generalized," *IEEE Transactions on Signal Processing*, vol. 43, no. 8, pp. 2025–2027, Aug. 1995.

[5] A. Baggeroer, W. Kuperman, and P. Mikhalevsky, "An overview of matched field methods in ocean acoustics," *IEEE Journal of Oceanic Engineering*, vol. 18, no. 4, pp. 401 – 424, Oct. 1993.

[6] A. J. Barabell, "Improving the resolution performance of eigenstructure-based direction-finding algorithms," in *Proc. IEEE International Conference*

on Acoustics, Speech, and Signal Processing (ICASSP'83), Boston, MA, Apr. 1983, pp. 336–339.

[7] S. Barbarossa and V. Petrone, "Analysis of polynomial-phase signals by the integrated generalized ambiguity function," *IEEE Transactions on Signal Processing*, vol. 45, no. 2, pp. 316–327, Feb. 1997.

[8] S. Barbarossa, A. Scaglione, and G. B. Giannakis, "Product high-order ambiguity function for multicomponent polynomial-phase signal modeling," *IEEE Transactions on Signal Processing*, vol. 46, no. 3, pp. 691–708, Mar. 1998.

[9] K. L. Bell, H. L. Van Trees, and L. J. Griffiths, "Adaptive beampattern control using quadratic constraints for circular array STAP," in *Proc. 8th Workshop on Adaptive Sensor Array Processing*, MIT Lincoln Laboratory, Lexington, MA, Mar. 2000, pp. 43–48.

[10] A. Belouchrani and M. G. Amin, "Time-frequency MUSIC," *IEEE Signal Processing Letters*, vol. 6, no. 5, pp. 109–110, May 1999.

[11] M. Bengtsson and B. Ottersten, "Low-complexity estimators for distributed sources," *IEEE Transactions on Signal Processing*, vol. 48, no. 8, pp. 2185–2194, Aug. 2001.

[12] O. Besson, M. Ghogho, and A. Swami, "Parameter estimation for random amplitude chirp signals," *IEEE Transactions on Signal Processing*, vol. 47, no. 12, pp. 3208–3219, Dec. 1999.

[13] O. Besson and P. Stoica, "A fast and robust algorithm for DOA estimation of a spatially dispersed source," *Digital Signal Processing*, vol. 9, no. 4, pp. 267–279, Oct. 1999.

[14] ——, "Decoupled estimation of DOA and angular spread for a spatially distributed source," *IEEE Transactions on Signal Processing*, vol. 48, no. 7, pp. 1872–1882, July 2000.

[15] G. Bienvenu and L. Kopp, "Adaptivity to background noise spatial coherence for high resolution passive methods," in *Proc. IEEE International Conference on Acoustics, Speech, and Signal Processing (ICASSP'80)*, Denver, CO, Apr. 1980, pp. 307–310.

[16] J. F. Böhme, "Estimation of spectral parameters of correlated signals in wavefields," *Signal Processing*, vol. 11, no. 4, pp. 329–337, Dec. 1986.

[17] L. Brennan, J. Mallett, and I. Reed, "Adaptive arrays in airborne MTI radar," *IEEE Transactions on Antennas and Propagation*, vol. 24, no. 5, pp. 607–615, Sept. 1976.

[18] J. A. Cadzow, "Direction-of-arrival estimation using signal subspace modeling," *IEEE Transactions on Aerospace and Electronic Systems*, vol. 28, no. 1, pp. 64–79, Jan. 1992.

[19] J. Capon, "High-resolution frequency-wavenumber spectrum analysis," *Proceedings of the IEEE*, vol. 57, no. 8, pp. 1408–1418, Aug. 1969.

[20] J. Chatillon, M. E. Bouhier, and M. E. Zakharia, "Synthetic aperture sonar for seabed imaging: Relative merits of narrow-band and wide-band approaches," *IEEE Journal of Oceanic Engineering*, vol. 17, no. 1, pp. 95–105, Jan. 1992.

[21] C. T. Christou and G. M. Jacyna, "Simulation of the beam response of distributed signals," *IEEE Transactions on Signal Processing*, vol. 53, no. 8, pp. 3023–3031, Aug. 2005.

[22] M. Chryssomomallis, "Smart antennas," *IEEE Antennas and Propagation Magazine*, vol. 42, no. 3, pp. 129–136, June 2000.

[23] L. Cirillo, A. Zoubir, N. Ma, and M. G. Amin, "Automatic classification of auto- and cross-terms of time-frequency distributions in antenna arrays," in *Proc. IEEE International Conference on Acoustics, Speech, and Signal Processing (ICASSP'02)*, Orlando, FL, May 2002, pp. 1445 – 1448.

[24] P. M. Djuric and S. M. Kay, "Parameter estimation of chirp signals," *IEEE Transactions on Acoustics, Speech, and Signal Processing*, vol. 38, no. 12, pp. 2118–2126, Dec. 1990.

[25] G. Fabrizio, A. B. Gershman, and M. Turley, "Robust adaptive beamforming for HF surface wave over-the-horizon radar," *IEEE Transactions on Aerospace and Electronic Systems*, vol. 40, no. 2, pp. 510–525, Apr. 2004.

[26] P. Forster and G. Vezzosi, "Application of spheroidal sequences to array processing," in *Proc. IEEE International Conference on Acoustics, Speech, and Signal Processing (ICASSP'87)*, Dallas, TX, May 1987, pp. 2268–2271.

[27] G. Galati, Ed., *Advanced Radar Techniques and Systems.* London, U.K: IEE, 1993.

[28] A. B. Gershman, "Direction finding using beamspace root estimator banks," *IEEE Transactions on Signal Processing*, vol. 46, no. 11, pp. 3131–3135, Nov. 1998.

[29] ——, "Robust adaptive beamforming in sensor arrays," *International Journal of Electronics and Communications*, vol. 53, no. 6, pp. 305–314, 1999.

[30] A. B. Gershman and M. G. Amin, "Wideband direction-of-arrival estimation of multiple chirp signals using spatial time-frequency distributions," *IEEE Signal Processing Letters*, vol. 7, no. 6, pp. 152–155, June 2000.

[31] A. B. Gershman, M. Pesavento, and M. G. Amin, "Estimating parameters of multiple wideband polynomial-phase sources in sensor arrays," *IEEE Transactions on Signal Processing*, vol. 49, no. 12, pp. 2924–2934, Dec. 2001.

[32] A. B. Gershman, V. I. Turchin, and V. A. Zverev, "Experimental results of localization of moving underwater signal by adaptive beamforming," *IEEE Transactions on Signal Processing*, vol. 43, no. 10, pp. 2249–2257, Oct. 1995.

[33] M. Ghogho, O. Besson, and A. Swami, "Estimation of directions of arrival of multiple scattered sources," *IEEE Transactions on Signal Processing*, vol. 49, no. 11, pp. 2467–2480, Nov. 2001.

[34] F. Gini, F. Lombardini, and M. Montanari, "Layover solution in multibaseline SAR interferometry," *IEEE Transactions on Aerospace and Electronic Systems*, vol. 38, no. 4, pp. 1344–1356, Oct. 2002.

[35] L. C. Godara, "Application of antenna arrays to mobile communications, part I: Performance improvement, feasibility, and system considerations," *Proceedings of the IEEE*, vol. 85, no. 7, pp. 1031–1060, July 1997.

[36] ——, "Application of antenna arrays to mobile communications, part II: Beam-forming and direction-of-arrival considerations," *Proceedings of the IEEE*, vol. 85, no. 8, pp. 1195–1245, Aug. 1997.

[37] G. H. Golub and C. F. Van Loan, *Matrix Computations*. Baltimore, MD: The Johns Hopkins University Press, 1996.

[38] M. Haardt, "Efficient one-, two-, and multidimensional high-resolution array signal processing," Ph.D. dissertation, Technical University of Munich, Germany, 1996.

[39] R. Hamza and K. Buckley, "Multiple cluster beamspace and resolution-enhanced ESPRIT," *IEEE Transactions on Antennas and Propagation*, vol. 42, no. 8, pp. 1041–1052, Feb. 1994.

[40] A. Hassanien, S. Abd Elkader, A. B. Gershman, and K. M. Wong, "Beamspace preprocessing with an improved robustness against out-of-sector sources using second-order cone programming," in *Proc. IEEE Sensor Array and Multichannel Signal Processing Workshop (SAM'04)*, Sitges, Spain, July 2004.

[41] ——, "Convex optimization based beamspace preprocessing with an improved robustness against out-of-sector sources," *IEEE Transactions on Signal Processing*, accepted.

[42] A. Hassanien and A. B. Gershman, "A computationally efficient approach for parameter estimation of multiple wideband polynomial-phase sources in sensor arrays," *IEEE Transactions on Signal Processing*, in preparation.

[43] A. Hassanien, A. B. Gershman, and M. G. Amin, "Time-frequency ESPRIT for direction-of-arrival estimation of chirp signals," in *Proc. IEEE Sensor Array and Multichannel Signal Processing Workshop (SAM'02)*, Rosslyn, VA, Aug. 2002, pp. 337 – 341.

[44] A. Hassanien, S. Shahbazpanahi, and A. B. Gershman, "A generalized Capon estimator for localization of multiple spread sources," *IEEE Transactions on Signal Processing*, vol. 52, no. 1, pp. 280–283, Jan. 2004.

[45] S. Haykin, Ed., *Advances in Spectrum Analysis and Array Processing.* Englewood Cliffs, New Jersey: Prentice Hall, 1991.

[46] R. Hettich and K. O. Kortanek, "Semi-infinite programming: Theory, methods, and applications," *SIAM Review*, vol. 35, no. 3, pp. 380–429, Sept. 1993.

[47] A. G. Jaffer, "Maximum likelihood direction finding of stochastic sources: A separable solution," in *Proc. IEEE International Conference on Acoustics, Speech, and Signal Processing (ICASSP'88)*, New York, Apr. 1988, pp. 2893–2896.

[48] S. Jeng and H. Lin, "Smart antenna system and its application in low-earth-orbit satellite communication systes," *IEE Proceedings - Microwaves, Antennas and Propagation*, vol. 146, no. 2, pp. 125–130, Apr. 1999.

[49] Y. Jin and B. Friedlander, "Detection of distributed sources using sensor arrays," *IEEE Transactions on Signal Processing*, vol. 52, no. 6, pp. 1537–1548, June 2004.

[50] H. Krim and M. Viberg, "Two decades of array signal processing research: The parametric approach," *IEEE Signal Processing Magazine*, vol. 13, no. 4, pp. 67–94, July 1996.

[51] J. Krolik, "The performance of matched-field beamformers with mediterranean vertical array data," *IEEE Transactions on Signal Processing*, vol. 44, no. 10, pp. 2605 – 2611, Oct. 1996.

[52] M. Lang and B. C. Frenzel, "Polynomial root finding," *IEEE Signal Processing Letters*, vol. 1, no. 12, pp. 141–143, Dec. 1994.

[53] H. B. Lee and M. S. Wengrovitz, "Resolution threshold of beamspace MUSIC for two closely spaced emitters," *IEEE Transactions on Acoustics, Speech, and Signal Processing*, vol. 38, no. 9, pp. 1545–1559, Sept. 1990.

[54] Y. Lee, J. Choi, I. Song, and S. Lee, "Distributed source modeling and direction-of-arrival estimation techniques," *IEEE Transactions on Signal Processing*, vol. 45, no. 4, pp. 960–969, Apr. 1997.

[55] S. G. Lemon, "Towed-array history, 1917-2003," *IEEE Journal of Oceanic Engineering*, vol. 29, no. 2, pp. 365–373, Apr. 2004.

[56] W. Li, X. Huang, and H. Leung, "Performance evaluation of digital beamforming strategies for satellite communications," *IEEE Transactions on Aerospace and Electronic Systems*, vol. 40, no. 1, pp. 12–26, Jan. 2004.

[57] S. Lie, A. R. Leyman, and Y. H. Chew, "Wideband chirp parameter estimation in sensor arrays through DPT," *Electronics Letters*, vol. 39, no. 23, Nov. 2003.

[58] J. Liu, A. B. Gershman, Z.-Q. Luo, and K. M. Wong, "Adaptive beamforming with sidelobe control: A second-order cone programming approach," *IEEE Signal Processing Letters*, vol. 10, no. 1, pp. 331–334, Jan. 2003.

[59] M. Lobo, L. Vandenberghe, S. Boyd, and H. Lebret, "Applications of second-order cone programming," *Linear Algebra and its Applications*, vol. 284, pp. 193–228, 1998.

[60] F. Lombardini and H. D. Griffiths, "Optimum and suboptimum estimation performance for multibaseline InSAR," in *Proc. EuSAR*, Munich, Germany, May 2000, pp. 315–318.

[61] F. Lu, E. Milios, S. Stergiopoulos, and A. Dhanantwari, "New towed-array shape-estimation scheme for real-time sonar systems," *IEEE Journal of Oceanic Engineering*, vol. 28, no. 3, pp. 552–563, July 2003.

[62] Y. Meng, "Estimation of directions of arrival of spatially dispersed signals in high resolution array processing," Ph.D. dissertation, McMaster University, Hamilton, ON, Canada, July 1995.

[63] Y. Meng, P. Stoica, and K. M. Wong, "Estimation of the directions of arrival of spatially dispersed signals in array processing," *IEE Proceedings - Radar, Sonar and Navigation*, vol. 143, no. 1, pp. 1–9, Feb. 1996.

[64] P. Moulin, M. Anitescu, K. O. Kortanek, and F. A. Porta, "The role of linear semi-infinite programming in signal adapted QMF bank design," *IEEE Transactions on Signal Processing*, vol. 45, no. 9, pp. 2160–2174, Sept. 1997.

[65] Y. Nesterov and A. Nemirovsky, *Interior-Point Polynomial Methods in Convex Programming.* vol. 13 of *Studies in Applied Mathematics*, SIAM, Philadelphia, PA, 1994.

[66] P. O'Shea, "A fast algorithm for estimating the parameters of a quadratic FM signal," *IEEE Transactions on Signal Processing*, vol. 52, no. 2, pp. 385–393, Feb. 2004.

[67] B. Ottersten, M. Viberg, and T. Kailath, "Performance analysis of the total least squares ESPRIT algorithm," *IEEE Transactions on Signal Processing*, vol. 39, no. 5, pp. 1122–1135, May 1991.

[68] K. I. Pedersen, P. E. Mogensen, and B. H. Fleury, "Spatial channel characteristics in outdoor environments and their impact on BS antenna system performance," in *Proc. IEEE Vehicular Technology Conference (VTC'98)*, vol. 2, Ottawa, Canada, May 1998, pp. 719–723.

[69] ——, "A stochastic model of the temporal and azimuthal dispersion seen at the base station in outdoor propagation environments," *IEEE Transactions on Vehicular Technology*, vol. 49, no. 2, pp. 437–447, Mar. 2000.

[70] S. Peleg and B. Friedlander, "The discrete polynomial-phase transform," *IEEE Transactions on Signal Processing*, vol. 43, no. 8, pp. 1901–1914, Aug. 1995.

[71] ——, "Multicomponent signal analysis using the polynomial-phase transform," *IEEE Transactions on Aerospace and Electronic Systems*, vol. 32, no. 1, pp. 378–387, Jan. 1996.

[72] S. Peleg and B. Porat, "Estimation and classification of polynomial-phase signals," *IEEE Transactions on Information Theory*, vol. 37, no. 3, pp. 422–430, Mar. 1991.

[73] M. Pesavento, "Array processing in complicated environments," Master's thesis, McMaster University, Hamilton, ON., Canada, Dec. 2000.

[74] M. Pesavento, A. B. Gershman, and Z.-Q. Luo, "Robust array interpolation using second-order cone programming," *IEEE Signal Processing Letters*, vol. 9, no. 1, pp. 8–11, Jan. 2002.

[75] V. F. Pisarenko, "The retrieval of harmonics from a covariance function," *Geophysical Journal, Royal Astronomical Society*, vol. 33, pp. 347–366, 1973.

[76] B. Porat, *Processing of Random Signals, Theory and Methods.* Englewood Cliffs, NJ: Prentice-Hall, 1994.

[77] R. Raich, J. Goldberg, and H. Messer, "Bearing estimation for a distributed source: Modeling, inherent accuracy limitations, and algorithms," *IEEE Transactions on Signal Processing*, vol. 48, no. 2, pp. 429–441, Feb. 2000.

[78] E. Rodriguez and J. M. Martin, "Theory and design of interferometric synthetis aperture radars," *IEE Proceedings F, Radar and Signal Processing*, vol. 139, no. 2, pp. 147–159, Apr. 1992.

[79] Y. Rong, S. Vorobyov, A. B. Gershman, and N. D. Sidiropoulos, "Blind spatial signature estimation via time-varying user power loading and parallel factor analysis," *IEEE Transactions on Signal Processing*, vol. 53, no. 5, pp. 1697–1710, May 2005.

[80] R. Roy and T. Kailath, "ESPRIT–estimation of signal parameters via rotational invariance techniques," *IEEE Transactions on Acoustics, Speech, and Signal Processing*, vol. 37, no. 7, pp. 984–995, July 1989.

[81] A. Scaglione and S. Barbarossa, "Statistical analysis of the product high-order ambiguity function," *IEEE Transactions on Information Theory*, vol. 45, no. 1, pp. 343–356, Jan. 1999.

[82] R. O. Schmidt, "Multiple emitter location and signal parameter estimation," in *Proc. RADC Spectral Estimation Workshop*, Rome, NY, Jan. 1979, pp. 243–258.

[83] ——, "Multiple emitter location and signal parameter estimation," *IEEE Transactions on Antennas and Propagation*, vol. 34, no. 3, pp. 276–280, Mar. 1986.

[84] S. G. Schock, "A method for estimating the physical and acoustic properties of the sea bed using chirp sonar data," *IEEE Journal of Oceanic Engineering*, vol. 29, no. 4, pp. 1200–1217, Oct. 2004.

[85] S. Shahbazpanahi, S. Valaee, and M. H. Bastani, "Distributed source localization using ESPRIT algorithm," *IEEE Transactions on Signal Processing*, vol. 49, no. 10, pp. 2169–2178, Oct. 2001.

[86] S. Shahbazpanahi, S. Valaee, and A. B. Gershman, "A covariance fitting approach to parametric localization of multiple incoherently distributed sources," *IEEE Transactions on Signal Processing*, vol. 52, no. 3, pp. 592–600, Mar. 2004.

[87] S. Shamsunder, G. B. Giannakis, and B. Friedlander, "Estimating random-amplitude polynomial phase signals: A cyclostationary approach," *IEEE Transactions on Signal Processing*, vol. 43, no. 2, pp. 492–505, Feb. 1995.

[88] D. V. Sidorovich and A. B. Gershman, "Two-dimensional wideband interpolated root-MUSIC applied to measured seismic data," *IEEE Transactions on Signal Processing*, vol. 46, no. 8, pp. 2263–2267, Aug. 1998.

[89] I. Solomon, D. Gray, Y. Abramovich, and S. Anderson, "Over-the-horizon radar array calibaration using echoes from ionised meteor trails," *IEE Proceedings - Radar, Sonar and Navigation*, vol. 145, no. 3, pp. 173–180, June 1998.

[90] P. Stoica, O. Besson, and A. B. Gershman, "Direction-of-arrival estimation of an amplitude-distorted wavefront," *IEEE Transactions on Signal Processing*, vol. 49, no. 2, pp. 269–276, Feb. 2001.

[91] P. Stoica and A. B. Gershman, "Maximum-likelihood DOA estimation by data-supported grid search," *IEEE Signal Processing Letters*, vol. 6, no. 10, pp. 273–275, Oct. 1999.

[92] P. Stoica, E. G. Larsson, and A. B. Gershman, "The stochastic CRB for array processing: A text book derivation," *IEEE Signal Processing Letters*, vol. 8, no. 5, pp. 148–150, May 2001.

[93] P. Stoica and R. Moses, *Introduction to Spectral Analysis.* Upper Saddle River, NJ: Prentice-Hall, 1997.

[94] P. Stoica and A. Nehorai, "Performance study of conditional and unconditional direction-of-arrival estimation," *IEEE Transactions on Acoustics, Speech, and Signal Processing*, vol. 38, no. 10, pp. 1783–1795, Oct. 1990.

[95] ——, "MUSIC, maximum likelihood, and Cramer-Rao bound," *IEEE Transactions on Acoustics, Speech, and Signal Processing*, vol. 37, no. 5, pp. 720–741, May 1989.

[96] J. F. Sturm, "Using sedumi 1.02, a MATLAB toolbox for optimization over symmetric cones," *Optimzation Methods and Software*, vol. 11-12, Aug. 1999.

[97] R. J. Vaccaro, "The past, present, and futureof underwater acoustic signal processing," *IEEE Signal Processing Magazine*, vol. 15, no. 4, pp. 21–51, July 1998.

[98] S. Valaee, B. Champagne, and P. Kabal, "Parametric localization of distributed source," *IEEE Transactions on Signal Processing*, vol. 43, no. 9, pp. 2144–2153, Sept. 1995.

[99] H. L. Van Trees, *Optimum Array Processing.* New York: Wiley, 2002.

[100] B. Van Veen and B. Williams, "Structured covariance matrices and dimensionality reduction in array processing," in *Proc. 4th Workshop Spectrum Estimation and Modeling*, Aug. 1988, pp. 168–171.

[101] V. Varadarajan and J. Krolik, "Array shape estimation tracking using active sonar reverberation," *IEEE Transactions on Aerospace and Electronic Systems*, vol. 40, no. 3, pp. 1073 – 1086, July 2004.

[102] B. Völcker and B. Ottersten, "Linear chirp parameter estimation from multi channel data," in *Proc. Asilomar Conference on Signals, Systems, and Computers)*, vol. 1, Pacific Grove, CA, Nov. 1999, pp. 24–27.

[103] G. Wang and X.-G. Xia, "Iterative algorithm for direction of arrival estimation with wideband chirp signals," *IEE Proceedings - Radar, Sonar and Navigation*, vol. 147, no. 5, pp. 233–238, Oct. 2000.

[104] J. H. Winters, "Smart antennas for wireless systems," *IEEE Personal Communications Magazine*, vol. 5, no. 1, pp. 23–27, Feb. 1998.

[105] X.-G. Xia, "Discrete chirp-fourier transform and its application to chirp rate estimation," *IEEE Transactions on Signal Processing*, vol. 48, no. 11, pp. 3122–3133, Nov. 2000.

[106] J. Xie, Y. Yuan, and Y. Liu, "Super-resolution processing for HF surface wave radar based on pre-whitened MUSIC," *IEEE Journal of Oceanic Engineering*, vol. 23, no. 4, pp. 313–321, Oct. 1998.

[107] G. Xu, S. D. Silverstein, R. H. Roy, and T. Kailath, "Beamspace ESPRIT," *IEEE Transactions on Signal Processing*, vol. 42, no. 2, pp. 349–356, Feb. 1994.

[108] X. L. Xu and K. M. Buckley, "A comparison of element and beam space spatial-spectrum estimation for multiple source clusters," in *Proc. IEEE International Conference on Acoustics, Speech, and Signal Processing (ICASSP'90)*, May 1990, pp. 2643–2646.

[109] ——, "An analysis of beam-space source localization," *IEEE Transactions on Signal Processing*, vol. 41, no. 1, pp. 501–504, Jan. 1993.

[110] A. Zeira and B. Friedlander, "Direction of arrival estimation using parametric signal models," *IEEE Transactions on Signal Processing*, vol. 44, no. 2, pp. 339–350, Feb. 1996.

[111] ——, "Joint direction finding, signal, and channel response estimation for a polynomial phase signal in a multipath channel," in *Proc. Asilomar Conference on Signals, Systems, Computers*, vol. 1, Pacific Grove, CA, Nov. 1996, pp. 733–737.

[112] P. Zetterberg, "Mobile cellular communications with base station antenna arrays: Spectrum efficiency, algorithms and propagation models," Ph.D. dissertation, Royal Institute of Technology, Stockholm, Sweden, June 1997.

[113] Y. Zhang and M. G. Amin, "Beamspace time-frequency MUSIC with application to airborne antenna array," in *Proc. Asilomar Conference on Signals, Systems, and Computers)*, vol. 1, Pacific Grove, CA, Nov. 1998, pp. 838–841.

[114] Y. Zhang, W. Mu, and M. G. Amin, "Subspace analysis of spatial fime-frequency distribution matrices," *IEEE Transactions on Signal Processing*, vol. 49, no. 4, pp. 747–759, Apr. 2001.

[115] M. Zoltowski, M. Haardt, and C. P. Mathews, "Closed-form 2-D angle estimation with rectangular arrays in element space or beamspace via unitary ESPRIT," *IEEE Transactions on Signal Processing*, vol. 44, no. 2, pp. 316–328, Feb. 1996.

[116] M. D. Zoltowski, G. M. Kautz, and S. D. Silverstein, "Beamspace root-MUSIC," *IEEE Transactions on Signal Processing*, vol. 41, no. 1, pp. 344–364, Jan. 1993.